DESIGN AND PERFORMANCE ANALYSIS OF LARGE HORIZONTAL AXIS OFFSHORE WIND TURBINES

by

Benjamin Chalikosa

Submitted in partial fulfilment of the requirements for the degree
Master of Engineering (Electrical Engineering)

in the

Department of Electrical, Electronic and Computer Engineering
Faculty of Engineering, Built Environment and Information Technology

UNIVERSITY OF PRETORIA

December 2020

SUMMARY

DESIGN AND PERFORMANCE ANALYSIS OF LARGE HORIZONTAL AXIS OFFSHORE WIND TURBINES

by

Benjamin Chalikosa

Supervisor: Prof. Ramesh C. Bansal

Co-supervisor: Dr. Nsilulu T. Mbungu

Department: Electrical, Electronic and Computer Engineering

University: University of Pretoria

Degree: Master of Engineering (Electrical Engineering)

Keywords: Capacity factor, energy production, hub height, large wind turbines, maximum tip speed, rated power output, rotor diameter, system specifications and testing model, wind farms

System specifications and testing model for increasing the rated power output, rotor diameter, hub height, and maximum tip speed of horizontal axis wind turbines is designed and implemented on the system advisor model simulator. Its performance is tested on offshore wind turbine's direct-drive and single stage-low speed generators. Although this simulator produces impressive results, it has some limitations in the operation of wind turbines. The terrain and topography of wind turbines are not considered in the simulation process. It also does not assess the electrical transients and physical stress of wind turbine components. Despite its limitations, four large offshore wind turbines and wind farms have been successfully simulated. It is found that the 9 MW, 10 MW, 11 MW and their respective wind farms generate more energy and better capacity factor on the direct-drive than single stage-low speed generator. Furthermore, a rectangular layout of 20 wind turbines

considerably impacted the excellent performance of this generator on the wind farms. Another notable outcome of the study is that higher system specifications do not always generate feasible results for wind turbines despite favourable weather conditions. For the Vestas 8 MW wind turbine, the viable percentages for increasing the size of its rated power output, rotor diameter, hub height and maximum tip speed is only 12.5%, 25% and 37.5%. The viability of these three upgrades has been confirmed by suitable graphs of power curves and feasible energy production results. Thus, these percentages confirm an 8 MW wind turbine's attainable design limits for generating realistic energy production and capacity factor.

On the contrary, a 50% increase in the above four system specifications yielded unviable capacity factor and energy production results. This is because this upgrade is too high to work successfully on the current wind turbine technology. Furthermore, the shape of the power curve from the 50% specifications is not the typical curve for wind turbines. It has been observed that increasing the value of maximum tip speed beyond 143 m/s and the rotor diameter beyond 246 m give rise to an unusual power curve. Concerning wind speed for high energy production, an average daily minimum and maximum wind speed of 4.58 m/s and 15.08 m/s yielded good results. Given the prevailing trend of designing large wind turbines, findings in this study are particularly helpful in understanding how capacity factor, energy production and energy losses are affected by the size of system specifications. Not only that, but these findings also have fundamental concepts that can be used to optimize the design of large offshore wind turbines. The study is equally valuable for determining suitable weather conditions and wind power potential for large offshore wind farm sites.

ACKNOWLEDGMENT

In the first instance, I wish to express my deepest gratitude to my research supervisors, Prof. Ramesh Bansal and Dr Tresor Mbungu, for their dedicated guidance and advice in every step of this dissertation's research process and writing. I also genuinely appreciate their understanding, patience and support during this study period. On the other part, I must also show my sincere appreciation to Mr Paul Gilman (NREL Consultant), who was very patient with my knowledge gaps as I mastered how to use the system advisor model simulator.

My other appreciation goes to all the Electrical, Electronic and Computer Engineering faculty members for their various support throughout my study. More particularly, I would like to show appreciation to the following lecturers: Prof. Ramesh Bansal (Renewable energy-EGH 732), Dr Lijun Zhang (Energy optimization-ENO 732), Prof. Raj Naidoo (Power distribution engineering-EEV 732), Dr Tebello N.D Mathaba (Energy management-EES 732), and Prof. JAG Malherbe (Introduction to research-EIN 732). Their enthusiasm and teaching style in their respective modules helped me carry positive memories of their lessons and made a powerful impression on my studies. Thus, I would like to recognize the invaluable knowledge they provided during my BEngHons Electrical Engineering degree study. Most of their advice is evident throughout this dissertation. Along with these educators, I am also extremely grateful to Mrs Heleen Gous (Postgraduate Administrator) and Ms Stefanie Steenberg (Administrator–EBIT). Even though they are not part of the lecturers, their outstanding student administration and communication with me during the study is highly and much appreciated.

On the other hand, getting through my research and dissertation writing required more than academic support. For this reason, I sincerely express my gratitude to the Almighty God for the privilege of good health and for generously providing me with the ability, strength and knowledge to do this research. Without these blessings, writing this dissertation would not have been accomplished. On a similar note, my special thanks are extended to my mother (Eva Matipa) and my sister (Maureen Musonda). This dissertation stands as a witness statement and testimony of their encouragement and unconditional love. Even though we experienced some highs and lows during this study period, they did not allow me to quit studying. I am forever grateful for the strong encouragement they provided to me.

LIST OF SYMBOLS

A	A cross-sectional area in m
C_P	Rotor efficiency
C_T	Turbulence thrust coefficient
C_t	Wind turbine coefficient
D	Rotor diameter in m
$F_{adj,j}$	Hourly adjustment factor
$f(V)$	Weibull probability distribution function of wind speed
F_{wsd}	Wind speed deficit factor
H	Height in meters at a wind speed of v m/s
H_0	Reference height of 10 m at a wind speed of V_0 m/s
k	Dimensionless shape parameter
KE	The kinetic energy in J
$\mathcal{M}$	The mass flow rate in kg/s
M	Mass in kg
n	Number of times of upgrading W
P	Power in W
P_b	Power extracted by the blades
$P_{j,n}$	The electrical output of wind turbine n in an hour j in kWh/h
P_m	Rated capacity of the wind farm in kW
$P_{(wf,j)}$	The electrical output of the wind farm in an hour j in kWh/h
Q_{sys}	Adjusted annual electrical energy output in kWh
U	Scaled-up system specification
V	Wind speed in m/s
V_{adj}	Adjusted wind speed in m
V_C	Cut-in wind speed in m/s

V_F	Cut-out wind speed in m/s
V_R	Rated wind speed in m/s
W	First system specification that needs to be upgraded
χ	Crosswind distance between the wind turbines in the rotor radii
α	Friction coefficient
γ	The ratio of downstream to upstream wind speed
ΔU	The difference in wind speed
λ	Scale parameter in m/s
ρ	Air density of 1.225 kg/m^3
σ	Turbulence intensity

LIST OF ABBREVIATIONS

CAWT	Cross axis wind turbine
CMS	Condition monitoring systems
CNC	Computer numerical control
Cp	Power coefficient
CPS	Cyber-physical system
CS	Customer side
CSD	Control system design
DC	Direct current
DFIG	Doubly fed induction generators
DFIM	Doubly fed induction machine
DSDT	Dynamic security decision tree
DSM	Demand-side management
FM	Financial model
HAWT	Horizontal axis wind turbines
HTS	High temperature superconductor
IoE	Internet of energy
kW	Kilowatts
LCOE	Levelized cost of energy
LVRT	Low voltage ride-through requirement
NREL	National renewable energy laboratory
PM	Performance model
PMIG	Permanent magnet induction generators
PMSG	Permanent magnet synchronous generators
REBCO	Rare-earth-barium-copper-oxide
RPM	Revolutions per minute
SADC	Southern African Development Community
SAM	System advisor model
SFCL	Superconductor fault current
SRW	Sam resource wind
SSTM	System specifications and testing model
UD	User-defined
US	Utility side
WECS	Wind energy conversion systems

TABLE OF CONTENTS

LIST OF TABLES

LIST OF FIGURES

CHAPTER 1 INTRODUCTION

1.1 CHAPTER OVERVIEW

This chapter presents the problem statement, research gap, research aim and objectives, and research questions. It also discusses the hypothesis and approach for carrying out the process of research. Furthermore, the research goals and research contributions of the study are equally given in this chapter. Another essential attribute of the chapter is the research outputs of the study. Last but not least is the overview of the study at the end of the chapter.

1.2 PROBLEM STATEMENT

1.2.1 Context of the problem

At present, most countries depend on fossil fuels and hydropower as their main sources of energy. Although hydropower is a good source of renewable energy, it is susceptible to droughts. There is less or no water for generating electricity during persistent drought because rivers tend to dry up. For this reason, electricity prices suddenly increases and power rationing (load shedding) becomes the business of the day. As a consequence, the demand for electricity in many countries has not been showing a declining graph. This means that the overall high demand for electricity in most parts of the world cannot be satisfied only from this source. Therefore, hydropower is unreliable for now, and other additional sustainable sources of electricity are required in many countries [1] - [3]. While fossil fuel sources continue to be the preferred option of generating more electricity to meet the current demand, these fuels create five massive problems.

1.2.1.1 Air pollution

Air pollution from coal-fired power plants is a severe problem in big cities in most countries. This is because they emit carbon monoxide, carbon dioxide, and nitrogen dioxide. In addition, these sources are also known to singlehandedly generate dangerous sulphur dioxide, mercury and soot emissions. On the other side, buses, cars and trucks powered by fossil fuels are key contributors to nitrogen oxides. These poisonous gases can severely affect human health and the natural environment [4].

1.2.1.2 Negative effects on human health

On a similar note, fossil fuel combustion emits toxic elements and greenhouse gases. These gases negatively affect human health and result in severe health complications such as cardiovascular diseases, chronic asthma, chronic bronchitis and low lung functioning. More than just the lungs are affected by these pollutants, and they equally have the potential to cause untimely death at every stage of life [4].

1.2.1.3 Environmental pollution

The process of storing, transporting or processing fossil fuels can have enormous consequences on the environment when something goes wrong. For example, fatal accidents involving oil train derailment and thousands of pipeline accidents occur while transporting these fuels. As a result, water and air are polluted. In other situations, drilling or mining underground oil and coal gives rise to severe land degradation. These operations cause forests and the entire mountain tops to be blasted away and scraped. Sadly, even after the operations have stopped, the once prosperous land in nutrients is forever diminished and does not return to what it was before [4].

1.2.1.4 Global warming

The carbon dioxide given off when burning fossil fuels is one of the major gases that cause global warming. Most of the ultimate effects of global warming are not fully known. However, there is a definite possibility that it is the cause of unbelievable climate change that the world is experiencing now. Thus, if all the energy requirements for the world are to be sourced from fossil fuels, international efforts to reduce the effects of global warming

would undoubtedly be defeated [4].

1.2.1.5 Price fluctuations

Fossil fuels are also more vulnerable to market manipulation and price fluctuations. This is one aspect highly experienced by developing countries that fully depend on importing oil, coal, and gas. Given this dependence, the price volatility of fossil fuels has greatly troubled many less developed countries. In most cases, oil price fluctuations lead to increased production costs and may have inflationary effects on the economy [5].

Although fossil fuels can help meet most countries' electricity demands, these fuels' environmental and health risks must not always be ignored. Above and beyond, fossil fuels are a finite resource that cannot be replaced once harvested. It takes specific conditions and hundreds of years to replenish them [5]. On the basis of environmental and health hazards of fossil fuels, it is an appropriate time for many countries to seriously start investing in sustainable sources of energy such as solar and wind. Wind energy is a free renewable resource, which is very abundant in most countries. Moreover, unlike fossil fuels, no matter how much it is used today, supply will still be the same in the future.

Another thing entirely different about wind energy is that it is a source of non-polluting and clean electricity. As a result, wind energy plants emit no greenhouse gases or air pollutants. Furthermore, wind power plants are relatively faster to build than nuclear or hydropower and other fossil fuel plants. On the bright side, taking the greener path of electricity generation is possible in many developing countries. This is because most of these countries are still in the process of building infrastructure for energy. Thus, they are not yet fully immersed in fossil fuel 'dirty' technology [6].

1.2.2 Research gap

Although the last two decades have seen the rise of wind and solar energy projects in some parts of the world, the largest green energy source for many countries is still hydropower. In contrast, wind energy projects are lagging behind these two technologies of clean power. As

of today, only a few countries have realized the potential of wind energy. Thus, in these countries, many wind turbines are contributing electrical energy to the national grid. However, this technology is only mentioned in generic terms in other countries, while solar energy projects are repeatedly covered in the media. Generally, wind energy opportunities in many countries are still relatively unknown and face several technical challenges. One of the challenges is the lack of suitable models for designing and testing system specifications for large wind turbines. As observed in the trend for designing wind turbines [86] – [90], most researchers have not addressed this issue. In an effort to fill the gap, this study has designed a model that can be used to increase the size of rated power output, rotor diameter, maximum tip speed and a hub height of horizontal axis wind turbines (HAWT).

1.3 RESEARCH AIM

This study aims to design system specifications and testing model for increasing rotor diameter, maximum tip speed, hub height, and rated power output of HAWT.

1.4 RESEARCH OBJECTIVE AND QUESTIONS

This study comprise the following research objectives and questions.

1.4.1 Research objectives

- Design and simulate a model for increasing the rated power output, rotor diameter, hub height and maximum tip speed of HAWT.
- Increase the rated power out, rotor diameter, hub height and maximum tip speed of the 8 MW wind turbine using this model.
- Assess and test the performance of scaled-up specifications on the direct drive and single stage-low speed generator on four offshore wind turbines and wind farms.
- Determine the percentage increase of energy production, capacity factor and system energy losses of scaled-up specifications on the direct drive and single stage-low speed generator.

- Determine the average daily minimum and maximum wind speed required to generate the highest monthly and annual energy from the scaled-up specifications.

1.4.2 Research questions

- What are the feasible limits of increasing rated power output, rotor diameter, hub height and a maximum tip speed of the 8 MW wind turbine?
- What is the percentage contribution of capacity factor, system energy losses, monthly and annual energy of the scaled-up system specifications?
- What drivetrain system generates more energy on the scaled-up specifications between direct drive and single stage-low speed generator?
- What are the average daily minimum and maximum wind speed required to generate the highest monthly and annual energy on the scaled-up specifications?

1.5 APPROACH AND HYPOTHESIS

1.5.1 Approach

A simulation and modelling technique is used in this study. Simulation is an approximate way of imitating a system's operation or process over some time [9]. In any case, simulation models are helpful when attempting to understand how specific processes or systems work. By identifying the main parts or variables of a process or system, it is possible to simulate these variables and subsequently create a representation of the entire system. Although in most cases, simulations are computer models, this approach is fascinating for many studies. It gives results that have sound theoretical and practical implications. However, it should be noted that no model can substitute real-life situations.

Thus, this approach has its limitations and often simplifies reality. Some of these limitations can lead to unexpected variables during the simulation process. As a result, this may complicate modelling and make it difficult for the system to work. On another note, obtaining complete and sufficient data for building and testing models may not be easy.

Furthermore, it is also essential to be careful about the impact of assumptions for a system or process under investigation. This is because some assumptions may oversimplify reality and lead to errors in the model's construction [10]. Despite its limitations, the areas where the simulation approach can be applied are potentially many. These areas include electrical power systems, logistics, wind power systems, industrial and enterprise networking devices, disease transmission and social systems. In most of these applications, successful models have explained many phenomena with remarkably huge theoretical significance. More importantly, the results' practical significance can also be considerable and valuable when one models something accurately. This is because they are always better chances of manipulating or improving what has been well modelled [10].

Concerning this study, suitable simulator software for implementing the designed model is the system advisor model (SAM). It is used to simulate four large offshore wind turbines and wind farms. The primary system specifications of wind turbines important to the study are rotor diameter, hub height, maximum tip speed and rated power output. These four specifications are the key input variables of the model. During the simulation process, system energy losses, capacity factor, power curves, monthly and annual energy production are observed. Thereafter, these results are analyzed and discussed. It should also be pointed out that one of the limitations of SAM is the inability to model electrical transients and the physical stress of wind turbine components. Hence these elements are not considered in this study.

1.5.2 Hypothesis

The hypothesis of this study is as follows: If rated power output, rotor diameter, hub height and a maximum tip speed of HAWT is scaled up by the same increment factor, then the direct-drive generator will produce more energy and better capacity factor than a single stage-low speed generator.

1.6 RESEARCH GOALS

In this line of work for large wind turbines, the following are the research goals.

- Encourage countries that depend on fossil fuels to unlock their wind energy potential and have hydro/wind/solar combination sources of electricity.
- Promote economic cooperation and regional integration among countries through the wind energy industry.
- Encourage countries that rely on fossil fuels to develop their economies through sustainable energy sources such as wind.
- Create awareness of favourable weather conditions required for wind energy projects sites.
- Encourage research and development activities among countries that could improve the performance and reliability of large wind turbines.

1.7 RESEARCH CONTRIBUTION

1.7.1 Power deficit solution for the SADC region

This study's findings are solutions for minimizing the power deficit currently facing most member countries of the Southern African Development Community (SADC) region.

1.7.2 Reference guide for electrical engineers and researchers

For researchers, electrical engineers, and students involved in wind turbine projects or energy planning, this study is a valuable reference guide for understanding how the size of system specifications affects wind turbines' energy production. Similarly, this study is also a practical reference guide for wind turbine engineers and planners for assessing suitable weather conditions for wind turbine and wind farm project sites.

1.7.3 Software simulator for renewable energy projects

Students and researchers in universities often struggle to find suitable software simulators for renewable energy projects. However, as a result of using SAM in this study, a useful experimental research tool is contributed to the electrical engineering field. This simulator can be used as a decision-making tool for energy researchers, policymakers, project developers and financial analysts. It helps simulate photovoltaic energy systems, battery storage, solar power, fuel cell-pv-battery, geothermal, solar water heating, biomass combustion, wind, and marine energy (tidal waves).

1.8 RESEARCH OUTPUTS

The following are the titles for the research papers:

- Exploring the energy potential of large offshore wind turbines.
- Performance of wake models on the energy production of large offshore wind farms.

1.9 OVERVIEW OF STUDY

In this study, four system specifications for large offshore wind turbines and wind farms are designed using system specifications and testing model (SSTM). Then, the energy potential of these specifications is tested on the SAM simulator. This process is guided by the problem statement, hypothesis and approach, research aim, objectives and questions, and research goals given in Chapter 1. Alongside these seven elements are the research outputs and contributions of the study. On the other side, Chapter 2 presents the literature study on the ongoing technology developments of wind turbine components. This chapter also reviews some methods and guidelines for connecting wind turbines to power grids. At the same time, monitoring and control strategies for wind turbines are equally discussed. Adding to this discussion is an explanation of the prevailing trend for the future development of wind turbines. Finally, a suitable wind energy software simulator for the study is also considered at the end of this chapter. On a different note, Chapter 3 describes the process of designing and applying SSTM in SAM. Under this process, two different types of wind turbines and

wind farms are simulated. In the first case, four user-defined (UD) specifications for large offshore wind turbines and wind farms are designed using the SSTM systems. Together with the other eight typical specifications, these UD parameters are then simulated in SAM. The UD parameters result from increasing the size of four system specifications of the Vestas 8 MW wind turbine using the equation $U = 0.125Wn + W$ of the turbine system of SSTM. The four scaled-up specifications include rated power output, rotor diameter, hub height and maximum tip speed.

On a related note, the second case simulates the Vestas 8 MW wind turbine and Vestas 160 MW wind farm using the NREL library system specifications of SAM. Thus, this wind turbine and the wind farm are the baseline system to which UD wind turbines and wind farms' performance are compared. The performance results of both cases are given in Chapter 4 using tables and figures. Next, a performance analysis of these results is given in Chapter 5. In this chapter, the performance of the direct-drive and single stage-low speed generator of four UD wind turbines and wind farms is compared to that of the Vestas 8 MW wind turbine and Vestas 160 MW wind farm. Points of comparison involve capacity factor, power curves, system energy losses, annual and monthly energy production. Apart from these performance metrics, weather conditions for air temperature, wind direction, pressure, and wind speed for the highest monthly and annual energy production are also discussed. Finally, yet significantly, Chapter 6, the final chapter, closes the study's work with the conclusion and future research recommendations.

CHAPTER 2 LITERATURE STUDY ON THE DESIGN TECHNOLOGY FOR WIND TURBINES

2.1 CHAPTER OVERVIEW

This chapter presents an overview of wind power technology's current directions and how it affects wind turbine components' design and performance. Precisely, the chapter analyses recent developments on the design and performance of rotor blades and generators. It also explains ongoing developments for different techniques of grid connections for wind farms. On a similar note, monitoring and control mechanisms for wind turbines are equally revealed. Apart from that, the most current power ratings of commercial wind turbines and wind farms are stated. Furthermore, design considerations for offshore wind farms are also reviewed. Finally, at the end of the chapter is a discussion on the future design of wind turbines and the suitable renewable energy simulator for the study. More notably, a research gap in the existing literature that needs to be filled is identified in this chapter. It involves designing a model for increasing and testing the size of wind turbine system specifications.

2.2 INTRODUCTION

A wind turbine is the heart of any generation system for renewable wind power. It can convert kinetic energy from the wind into mechanical energy and then into electrical power. A block diagram of this energy conversion process is briefly explained in Figure 2.1 [11]. The focus of this chapter is on the last two stages of this process. In particular, Section 2.3 looks at how wind power technology influences wind turbines' design and performance.

Next in order is the impact of component design on the performance of wind turbines in Section 2.4. Similarly, current ratings of wind turbines and wind farms are presented in Section 2.5. On the other hand, Section 2.6 discusses the prevailing trend of designing wind turbines. This trend strives for continuous technology advancements for wind turbines which can lead to cost reductions of wind power and further improve power generation from wind. At the same time, Section 2.7 addresses the design considerations for offshore wind farms. Although these design elements may be used on onshore and offshore wind farms, the latter requires more detailed design, construction and grid connectivity. Finally, a suitable software simulator for the study is discussed in Section 2.8.

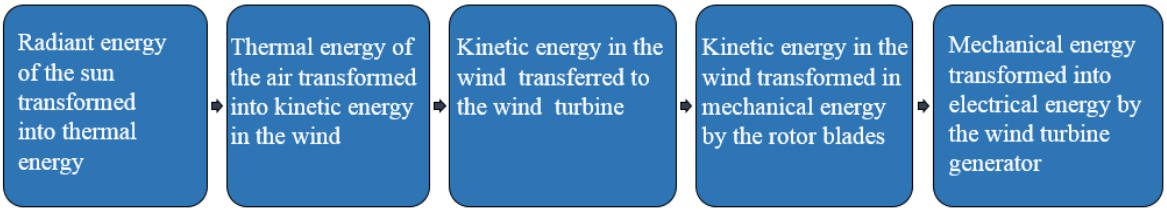

Figure 2.1. Process of transforming kinetic energy into electrical energy.

2.3 THE IMPACT OF WIND POWER TECHNOLOGY ON THE DESIGN AND PERFORMANCE OF WIND TURBINES

A review of how wind power technology affects wind turbines' design and performance is discussed in this section. More particularly, this discussion looks at how the wind power equation, tower height, power curves, maximum rotor efficiency, and tip speed affect wind turbines' design technology and operation.

2.3.1 Design impact of wind power equation

Wind power mainly depends on blade radius, air density, and wind speed [12]. This section explains the relationship between these three elements and how they affect the design and performance of wind turbines. An explanation of this relationship is done by deriving the mathematical equation of power in the wind.

2.3.1.1 Kinetic energy

Given a small packet of air moving at a speed of v m/s with mass m kg, its kinetic energy (KE) can be expressed using (2.1).

$$KE = \frac{1}{2}mv^2 \tag{2.1}$$

2.3.1.2 Mass flow rate

If we consider the mass m of air to be moving in a cross-sectional area A with velocity v m/s, its flow rate $\mathcal{M}$ is the product of speed (v), cross-sectional area (A) and air density (ρ) as explained by (2.2a) and (2.2b).

$$\mathcal{M} = \frac{m}{\Delta t} = \rho vA \tag{2.2a}$$

$$m = \mathcal{M}\Delta t \tag{2.2b}$$

Substituting the mass m of (2.2b) into (2.1) yields

$$KE = \frac{1}{2}\mathcal{M}\Delta t v^2 \tag{2.3}$$

2.3.1.3 Power

We know that power (P) is energy divided by time (Joules/second). This definition can also be expressed by (2.4).

$$P = \frac{KE}{\Delta t} \tag{2.4}$$

In order to derive the equation for power in the wind, the expression for the kinetic energy of (2.3) is substituted into (2.4), as shown in (2.5a), (2.5b) and (2.5c). Thus, the final result is (2.5d), which is the mathematical expression for power in the wind.

$$P = \frac{\frac{1}{2}\mathcal{M}\Delta t v^2}{\Delta t} \tag{2.5a}$$

$$P = \frac{1}{2}\mathcal{M}v^2 \tag{2.5b}$$

$$P = \frac{1}{2}\rho v A v^2 \tag{2.5c}$$

$$P = \frac{1}{2}\rho A v^3 \tag{2.5d}$$

Three critical observations that are key factors in the design and performance of large wind turbines can be deduced from (2.5d). These essential elements are explained below.

- Power in the wind is directly proportional to the cube of wind speed. This means that doubling the speed of the wind increases the power by eight times. Thus, the amount of electricity produced by a wind turbine generator is largely determined by wind speed.
- Wind power is also directly proportional to the swept area (A) of the wind turbine rotor, where $A = \frac{\pi}{4}D^2$ for HAWT. Therefore, doubling the diameter of the rotor blade increases the power by a factor of 4. This is due to the fact that power in the wind is directly proportional to the square of the blade diameter. Therefore, generators produce more electricity when rotor blades spin through a larger area.
- The cost of a wind turbine also increases in proportion to the diameter of the blade. However, because power is proportional to the diameter squared, designing giant wind turbines is more cost-effective.

2.3.2 Design impact of tower height and air friction

The impact of even a modest increase in wind speed can be very significant for wind power. This is related to the fact that wind power is directly proportional to the cube of the wind's speed. For this reason, designing taller towers for wind turbines is one way of getting into higher wind speeds. However, it is also essential to know that wind speeds are slowed down in the first few hundred metres above the ground. This effect results from air experiencing friction as it moves across the surface of the earth. High irregularities such as buildings and forests are one cause of this resistance. On the contrary, smooth surfaces such as the calm oceans and seas offer very little air resistance. Hence, the speed variation with elevation is satisfactory. This explains why many commercial wind turbines are being designed for

offshore technology. One expression that is very useful in characterizing the impact of the roughness of the earth's surface on the wind's speed is given in (2.6) [12].

$$\left(\frac{v}{v_0}\right)=\left(\frac{H}{H_0}\right)^{\alpha} \tag{2.6}$$

where H is the height in metres at a wind speed of v m/s, H_0 is the reference height of 10 m at a wind speed of v_0 m/s and α is the friction coefficient.

2.3.3 Design impact of maximum rotor efficiency

Like other technology for energy systems, the performance of a wind turbine also has certain fundamental constraints. One of these constraints limits its maximum possible conversion efficiency of kinetic energy in the wind to mechanical power. Using Figure 2.2, this study explains this constraint by deriving the theoretical maximum rotor blade efficiency 59.3%. With reference to this diagram, v_1 is the upwind velocity of the uninterrupted wind, v_2 is the downwind velocity, and v_b is the velocity of the wind that passes through the rotor blades. It should also be noted that within the stream tube, the mass flow rate is the same everywhere and is denoted by $\mathcal{M}$ [12].

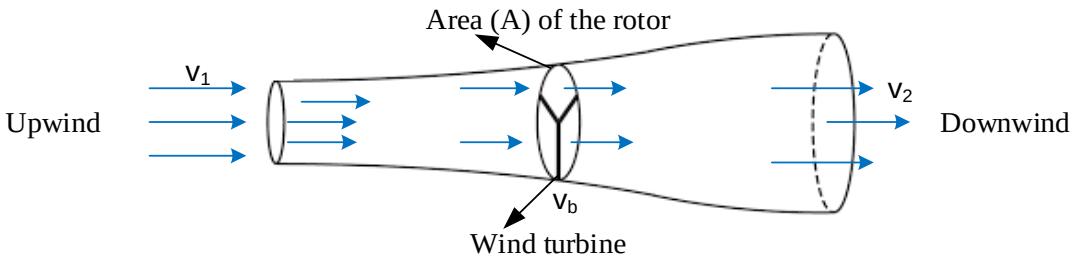

Figure 2.2. Wind stream tube for deriving maximum rotor efficiency [12].

2.3.3.1 Power extracted by the rotor blades

The power extracted by the blades (P_b) is given by (2.7). It is equal to the difference in kinetic energy between the upwind (v_1) and the downwind (v_2) air flows.

$$P_b = \frac{1}{2}\mathcal{M}(v_1^2 - v_2^2) \tag{2.7}$$

2.3.3.2 Mass flow rate

The rotor's swept area (A) is the more comfortable place for determining the mass flow rate $\mathcal{M}$ equation. Therefore, at this point $\mathcal{M}$ is determined, as shown in (2.8).

$$\mathcal{M} = \rho A v_b \tag{2.8}$$

2.3.3.3 Velocity of the wind through the rotor

The wind velocity through the rotor is given by the downwind and upwind speeds average, as shown by (2.9).

$$V_b = \frac{v_1 + v_2}{2} \tag{2.9}$$

Therefore, (2.8) can now be written as

$$\mathcal{M} = \rho A\left(\frac{v_1 + v_2}{2}\right) \tag{2.10}$$

Substituting mass flow rate $\mathcal{M}$ of (2.10) into (2.7) yields (2.11a).

$$P_b = \frac{1}{2}\rho A\left(\frac{v_1 + v_2}{2}\right)\left(v_1^2 - v_2^2\right) \tag{2.11a}$$

$$\text{Let } \gamma = \frac{v_2}{v_1} \tag{2.11b}$$

where, v_2 / v_1 is the ratio of the downstream to upstream wind speed. Using (2.11b), (2.11a) can now be expressed as shown in (2.12a), (2.12b) and (2.12c).

$$P_b = \frac{1}{2}\rho A\left(\frac{v_1 + \gamma v_1}{2}\right)(v_1^2 - \gamma^2 v_1^2) \tag{2.12a}$$

$$= \left[\frac{1}{2}(1+\gamma)(1-\gamma^2)\right] \times \frac{1}{2}\rho A v^3 \tag{2.12b}$$

$$P_b = \textit{Fraction extracted} \times \textit{Power in the wind} \tag{2.12c}$$

Equation (2.12b) shows that the power extracted from the wind is equal to the quantity in the brackets multiplied by the upstream power. Thus, the quantity shown in the brackets is

the fraction of the wind's power extracted by the rotor blades. This is the rotor efficiency and is denoted as C_p.

$$Rotor\ efficiency\left(C_p\right)=\left[\frac{1}{2}\left(1+\gamma\right)\left(1-\gamma^2\right)\right] \tag{2.13}$$

2.3.3.4 Maximum rotor efficiency

The derivative of (2.13) concerning γ is given by (2.14). This equation gives the maximum possible efficiency of the rotor.

$$\frac{dC_p}{d\gamma}=\frac{1}{2}\left[\left(1+\gamma\right)\left(-2\gamma\right)+\left(1-\gamma^2\right)\right]=\frac{1}{2}\left(1+\gamma\right)\left(1-3\gamma\right)=0 \tag{2.14}$$

Solving (2.14) results in $\gamma=\frac{v_2}{v_1}=\frac{1}{3}$ (2.15)

Substituting (2.15) into (2.13) results in the theoretical maximum rotor blade efficiency $0.5926\%\approx 59.3\%$. This percentage is the rotor's maximum theoretical efficiency and is called Betz' law or Betz efficiency. Given the best operating conditions, modern wind turbines can approach 80% of this limit. This is about 45% to 50% efficiency in transforming the wind's power into a rotating generator shaft. However, this efficiency depends on many rotor blade variables such as blade material, blade design, blade angle/pitch, blade length, blade number, and blade shape [12].

2.3.3.5 Tip speed ratio

Given the wind speed, rotor efficiency is usually presented as a function of its tip speed ratio, as shown in (2.16).

$$TSR=\frac{Rotor\ tip\ speed}{Upwind\ wind\ speed}=\frac{rpm\times\pi D}{60v} \tag{2.16}$$

where TSR is tip speed ratio, D is the rotor diameter (metres), v is the upwind wind speed (m/s), and rpm is revolutions per minute of the rotor [12].

2.3.4 Design impact of power curve parameters

Table 2.1 explains important design parameters for the power curve of wind turbines. These four parameters show the relationship between the electrical power expected from the complete system (generator, blades, gearbox) and wind speed. Successful design and performance of wind turbines rely on accurate modelling of power curves. This curve is significant because wind turbines are designed to work in a range of specific wind speeds [13].

Table 2.1 Design parameters for power curves.

Parameters	Description
Rated power	At wind speeds between V_R and V_F, the output is equal to the generator's rated power.
Cut-in wind speed (V_C)	At wind speeds below V_C no power is generated.
Rated wind speed (V_R)	At V_R, the wind turbine is expected to generate electricity at its rated capacity.
Cut-out wind speed (V_F)	Above V_F, the wind turbine is expected to be shut down.

2.4 THE IMPACT OF COMPONENT DESIGN ON PERFORMANCE OF WIND TURBINES

The main components of HAWT include rotor (blades and hub), gearbox, high and low-speed shafts, generator, controller, yaw drive, tower, brakes, wind vane, and anemometer [4]. In addition, the mainframe, nacelle, yaw control (for upwind turbines), bedplate and the wind turbine housing are also part of HAWT subsystems [11]. Furthermore, these wind turbines use electronic power converters, cables, transformers, and switchgear to balance the electrical systems [14], [15]. As can be seen from this list of components, wind power technology is a very complex system. Among the issues resulting from this complexity is the low efficiency of wind energy capture [14]. Improving the efficiency and reliability of

wind turbines can have a significant impact on their performance. This explains why many researchers' primary focus is to address challenges that affect wind turbine components' performance. However, this field of study has a broad scope and requires a concerted effort from different engineering disciplines [16]. This chapter's centre of interest is on some research activities related to the design and performance of rotor blades, generators, grid connections, monitoring, and control mechanisms of HAWT. These activities are discussed in the remaining sections of this chapter.

2.4.1 Design developments for rotor blades

The wind turbine rotor is one of the most significant parts of the wind energy system. It is among those components responsible for converting wind's kinetic energy into mechanical power [4]. Although this component's technology has been improving slowly, notable progress in its design has been attained. This is due to developments in modern wind turbine technology and optimization of its structural elements. Owing to this progression, there is a significant improvement in wind turbines' generated power output efficiency. In terms of cost for wind power systems, rotor blades are within the group of the most expensive components. Despite the cost, a good design of blades based on aerodynamics principles should result in a high lift to drag ratio. Additionally, wind turbine blades must have outstanding mechanical strength and low inertia for reliable and durable operation [18]. This section reviews the recent developments in some key aspects of wind turbine blades in keeping with the above attributes.

2.4.1.1 Aerodynamic and structural zones

In order to extend the fatigue life of rotor blades, it is necessary to alleviate loads on the structural section to achieve better aerodynamic performance [4], [18]. A demonstration of this process on two-dimensional airfoil data for large wind turbines is illustrated [19]. In another aspect of aerodynamics, efficient and economical design of blades can be achieved by maximizing the rotor power's coefficient. An example of this direct design optimization approach of blades for small HAWT is given [20]. This approach combines airfoil and blade design analysis and allows computer numerical control (CNC) manufacturing. It also offers

a seamless link with computational fluid dynamics. The drag effects, Reynolds number effects, hub and tip effects are considered in the optimization design. It is evident from this approach that aerodynamic efficiency (thinner airfoils) and structural capability (thicker airfoils) are two contradictory demands that drive the design of blades. Similarly, two other dominating constraints for blade design include modal analysis that suppresses natural frequencies and maximum deflections that prevent the tower's striking [20]. Given these constraints, the designer must identify the necessity for the system instead of subcomponent level optimization. However, this needs input from the manufacturer iterative design cycles [17].

2.4.1.2 Different optimum design methods and techniques

On the other hand, fluid-structure interaction modelling is very significant for wind turbine technology advancement. These models are necessary to improve blade design and predict wind turbines' life fatigue without complete and expensive tests. Based on this modelling aspect, an assessment of the flow fields' aerodynamics and turbulence models' reliability is presented [21]. According to the results, the blades' flow predictions can be reliably made as long as suitable advanced turbulence models are used. Furthermore, this prediction can also happen in the dominant frequency of the pressure fluctuations and the blades' downstream wake. In another circumstance, a twin wind turbine that does not use the yaw rotation's actuation is illustrated [22]. Compared to wind turbines that use yaw rotation, it is found that when the yaw angle is increased, the thrust and average power of wind turbines decreases.

Furthermore, under the combined effect of fluid-structure interaction and yaw conditions, blades' aerodynamic performance shows more asymmetrical characters [23]. Despite the achievements, few researchers simulate the entire structure of wind turbines using these models. It turns out that most aerodynamic modelling has been highly simplified [24]. In most cases, blade design problems use the blade element momentum, vortex-based and computational fluid dynamics methods. However, some researchers have implemented surrogate models such as response surface models to reduce the computational time of wind turbine design problems [25]. In other situations, designs that include the blade hub's kinetic

analysis and the tower may be used. The kinetic analysis looks at the force and vibration analysis of the tower-blade-hub coupled system. With this design destroying the tower by resonance cannot happen [26].

On a different note, the effects of blade design for HAWT on ice accretion is examined using NREL airfoils families. Based on the numerical prediction of results, there is a 10% to 65% lift coefficient reduction [27]. Nonetheless, this result is largely dependent on the shape of the accredited ice. Under other conditions, an application that uses the inverse finite element method for designing blades is presented [28]. This method's outcome enables the blades to have the required aerodynamic shape even after large deformations due to elasticity. In other cases, the maximum power coefficient of blades is improved by using blade element momentum theory [29] and linearization of twist and chord distribution of blades [30]. Furthermore, the surrogate optimization method for the aerodynamic design of wind turbine rotor blades can also be used [31]. Other findings indicate that optimizing the design of blades should satisfy not only the requirements of structural strength. Instead, it should also prevent collisions between the tower and the blade tip [32].

2.4.1.3 Benefits of increasing the diameter

One of the essential parameters involved in the maximum capture of wind is the diameter and length of the blades. The size and design of these elements are of great importance to the generation of electricity. Based on this reason, the recent general direction is towards using large blades. This benefits the sweeping of wind in a large area and subsequently results in considerable energy output. Ultimately, the main goal of increasing and optimizing the blades is to achieve high output power. But it should be noted that when the blades' size increases, their noise and mass should also be considered essential parameters during the design process [33]. Although this increase in blades' size reduces the levelized cost of energy (LCOE), it introduces remarkable aeroelastic effects. These effects are caused by inertial dynamics, interaction of aerodynamic loads and elastic deflections [34]. Aeroelastic effects may lead to problems of instability, such as flutter and edgewise instability. This problem can be destructive to both the wind turbine and the blades when the turbines' size increases even larger. Thus, it is important to investigate aeroelasticity's characterization

when developing the next generation of large wind turbines. Some of the comprehensive reviews on aeroelastic modelling of blades for wind turbines are explained [34]. The effects of a pitch angle on small-scale wind turbines' blade performance in urban environments are also addressed [35].

2.4.1.4 Impact of airfoils

Wind turbine performance is directly impacted by the operation of airfoils installed along with the blades. While reducing mass and the loads, airfoils specifically tailored to blade requirements also help obtain good rotor performance [36]. A design method for airfoils that maximizes the lift/drag ratio in a fixed and free transition angle of attack is analyzed [37]. This study focuses on the shape and space control of airfoils using the Taylor high order polynomial series. The findings of the investigation show that this method can optimize the aerodynamic performance of wind turbine airfoils. Unfortunately, this method does not consider the entire aerodynamic performance within the angle of attack's continuous design. On a different note, a method that combines the curvature smooth continuous theory and functional integral for wind turbine airfoils is described [38]. This method is different from most current airfoil design methods that use one point of design for the angle of attack to obtain the maximum aerodynamic performance. Thus, this new method has the advantage of considering the continuous angle of attack. It also increases the entire aerodynamic performance and makes the aerodynamic force convergence.

Similarly, a design of airfoils meant for active flow control in HAWT is investigated [39]. This design has the potential to include the effects of actuation in the process of designing airfoils. By doing so, new control strategies for HAWT can be enabled. In another aspect, airfoil design is provided for low-speed horizontal axis micro wind turbine [40]. It is seen from these results [39], [40] that developing and designing new airfoils is a very challenging piece of work due to the requirements of many computations. However, the use of QBlade software helps to make the design of airfoils relatively easy. In another perspective, a valuable integrated method for designing families of airfoils for large wind turbines is revealed [41]. It can be observed that blades operating at a lower Reynolds number have a lower power coefficient, smaller twist angle, and a sharper shape than those operated at a

higher Reynolds number [42]. Another design of an advanced new airfoil for stall-regulated wind turbines is shown [43]. This airfoil can increase the turbine annual energy production in rough and clean conditions compared to the existing geometries. Similarly, a new method for designing medium thickness airfoils for wind turbines is proposed [44]. This method demonstrates that it is feasible to design different wind turbine airfoils with different thicknesses.

2.4.1.5 Benefits of altering the shape of blades

Most traditional designs for wind turbines involve square non-curved blades. One way of achieving maximum efficiency involves altering the shape of the blades. Thus, for better capturing of wind, recent designs are integrating curved blades. Not only do curved blades work in different wind angles due to their versatility, but they also produce less drag. Undoubtedly, the aspect of curvature is very significant in the design of blades. A study that used the shape of insect wings as a source of inspiration for designing blades is demonstrated [45]. In these experiments, insect wing-inspired design of shapes proves to have high revolutions per minute (rpm). The bee, wasp and cicada inspired blades exhibits the highest rpm, followed by the fly and mosquito inspired designs. Although this increase in rpm is relative to the wind speed, these wing-inspired blades have much potential to increase wind turbines' energy efficiency.

The use of backward swept blades for wind turbine passive load alleviation is also assessed [46]. It is found that sweeping blades backwards produce a structural coupling between torsion towards feathering and flapwise bending towards the tower. On a related note, a mechatronic and aerodynamic design model helpful in performing wind tunnel tests for offshore configurations is illustrated [47]. This model shows that the effective aerodynamic performance of wind turbines can be verified. However, to address the unsustainable increases in the blade's cost per length, manufacturers should devise a new process of manufacturing blades. One potential solution is modularity. Modular designs can fuel the continued growth of the wind energy industry. Ultimately, this can boost energy production in very challenging environments, such as offshore sites and areas with low wind resources [17].

In other respects, frequent wind-direction changes, low wind speed and high turbulence are some of the factors responsible for the poor performance of blades. One way of overcoming these challenges is through a cross-axis wind turbine (CAWT). Early development and design of CAWT are demonstrated [48]. It consists of cross-axis blades that extract wind energy from airflows approaching from the vertical and horizontal directions. The CAWT produces higher rotational speed and power output than the conventional straight-bladed vertical axis wind turbine. However, there is a need to examine the performance of CAWT in the proper wind tunnel since the study was done in low wind speed areas. Besides, the effects of the vertical blade pitch angle on aerodynamics and power performance should be examined. Determining the performance loss at a higher pitch angle with no deflectors is also needed [49].

2.4.1.6 Material innovations

Material innovations that can lower the cost of blades are required. In view of their stiffness per dollar basis, composite materials continue to be chosen by manufacturers. However, there is a need for researchers to consider the potential impact of other materials on costs. Carbon fibres are generating much interest. The knowledge gap in this area include residual stresses, effects of imperfections, crack initiation, porosity, associated safety factors and damage evolution. At the same time, research on attaining reliable stiffness at reasonable prices by using recycled carbon fibre as reinforcement for future blades is relevant. Disposal and recyclability are also end-of-life concerns for the wind industry. All these are active topics of research [17].

Some of these challenges can be resolved by using advanced and suitable materials for designing blades. These materials have properties for high strength that can endure the gravitational and wind forces of the blades. Thus, in recent years the effort of most researchers is to focus on defects of manufactured materials. In most cases, defects comprise dry spots, porosity out-of-plane and in-plane wrinkles and waviness. Hence, in order to increase the confidence for designs that result in strong manufactured blades, component testing of data and materials are essential elements [50]. A model that focuses on the optimization of the aerodynamic behavior of the blades, which are made of a reinforced

polymer of glass fibre is suggested [51].

2.4.1.7 Downtime issues

Although wind power is a favourable energy source for the future, wind turbine blade design faces many limitations. Because of unpredictable wind patterns, blades are not very efficient. Other primary downtime issues for the blades involve: icing, edgewise vibrations, rotor imbalance, erosion, trailing edge disbands, lightning and leading-edge cracks. Cracks reduce the output power and are expensive to repair. In other areas, induced manufacturing defects in the spar cap lead to stress amplification that causes premature failure and cracks. Under other conditions, icing is another issue that negatively impacts reliability and performance. Unfortunately, algorithms being used currently to detect icing may sometimes shut down the wind turbines. This result in loss of energy production [17], [45].

2.4.2 Design developments for generators

A generator is one of the primary subsystems of the drivetrain that is required for power generation. It is responsible for converting the mechanical energy of the rotor blades into electrical energy. When generating power, determining the wind turbines capacity selection, size, and configuration is very important. Therefore, in order to improve the reliability of wind turbines, health management systems for generators are highly needed. That being the case, a helpful framework for quantitative evaluation of wind turbines' health and fault conditions that use generator signals is proposed [4]. The pattern of results from this study demonstrates that this framework is able to detect faults and quantify various health conditions for wind turbines [52]. A review of some other developments for different types of wind turbine generators is given in this section.

2.4.3 Diameter and tower mass system design

Some design concepts for the 20 MW wind turbine generator and how they affect the generator diameter and tower mass of the Vestas 8.8 MW wind turbine are shown in Table 2.2 [53]. Results from this table show that the permanent magnet technology can offer the

lightest type of generators.

Table 2.2 Effect of generator design concepts on tower mass.

Design concepts for up scaling the Vestas 8.8 MW wind turbine (Generator is synchronous permanent with a diameter of 8 meters)			
Power ratings	Upscaling techniques	Generator diameter	Tower top mass
20 MW wind turbine	Using conventional technology	14 meters	1730 metric tons
20 MW wind turbine	Magnetic pseudo-direct drive	8.5 meters	1300 metric tons
20 MW wind turbine	Superconducting technology	10.8 meters	1550 metric tons

2.4.3.1 Doubly fed induction generators

The use of doubly-fed induction generators (DFIG) for wind power generation has increased. This increase is due to its ability to control reactive and active power and support variable speed operation with minimal mechanical stress. However, managing grid disturbances and uncertainties in wind speed is a massive challenge for DFIG. Hence, these two challenges should be addressed for this generator to meet modern grid codes' requirements. In an effort to resolve these constraints, the implementation and design of a new control strategy that uses interval type-2 fuzzy sets for grid integration of DFIG are demonstrated [54]. The results' output shows significant robustness against deviations in the operating conditions, which fulfils the standard requirements of the grid codes.

In any case, there are important factors to consider when designing DFIG for wind energy systems. Notable is the insulation system, rotor slots, core, speed, stator and rotor windings of the generator. Alongside this, the mechanical, electrical, magnetic, thermal, and dielectric aspects should also be considered [55]. A design that considers some of these factors for an adaptive DFIG line side converter is illustrated [56]. Simulation results point to this approach's efficiency to enhance and reinforce the controller and power system's stability. Moreover, when integrated with other improvements such as end wind bracing/banding

and rotor coil lead instead of crimped leads, the estimated mean time between failures in the design of DFIG can be greater than 20 years [57].

2.4.3.2 Brushless doubly-fed induction machines

The rapid development of wind technology over the last decades has resulted in the advancement of many opportunities for further research in the operation of wind turbines. An excellent example of this technology advancement is the brushless doubly-fed induction machine (BDFIM). This machine is an excellent substitute for the standard doubly-fed induction machines (DFIM) used in recent wind turbines. Although these two generator systems have comparable operating characteristics, the BDFIM has certain advantages over the DFIM. Some advantages include improved reliability, robustness, and less maintenance because of the absence of slip-ring and brushes. Furthermore, given its improved fault current capabilities and low voltage ride through, the BDFIM has capabilities that comply with the grid codes' current requirements. However, even though modern DFIM have been evolving for more than 100 years (y), these machines have never been commercialized. Thus, to make modern BDFIM economically feasible and practicable for wind turbine applications, the challenges that need to be addressed by future researchers are identified [58].

Until now, nested-loop rotors are being used extensively in different BDFIM. However, this design is not suitable for larger wind turbines. Therefore, a new optimized rotor design for these machines is presented [59]. In this study, one nested-loop and one bar cage optimized rotor are designed based on the optimization method for BDFM, whose frame size is D180. Optimized and conventional rotor characteristics are compared in terms of iron saturation and rotor circuit parameters. This is done using finite element analysis and analytical methods at rated operating conditions. Generally, results show that when brushless doubly-fed induction generators replace DFIG, there is improved system reliability.

2.4.3.3 Synchronous generators

Replacing synchronous generators with variable speed generators in wind turbines is a challenge. First, it decouples the dynamics of wind turbines from the grid frequency. This

happens because of the control system design (CSD) of wind turbines. The CSD requires the rotor to be decoupled from the stator field in order to realize accurate tracking for the extraction of optimal wind power. However, this makes the generator not respond to system frequency changes and even lowers the system inertia. This behaviour is a threat to system stability. Additionally, the intermittent and stochastic nature of wind energy influences the scheduling of the system directly. Eventually, these results in difficulties in estimating sufficient system reserve to ensure that the immediate supply demands are balanced [60].

Thus, to enable the integration of wind power to the primary grid, many countries have implemented grid codes on wind farms. In addition, some other developing technologies for a low-voltage ride-through and regulation capability involving wind energy are reviewed [60]. However, with the increasing requirement of fault ride-through and system reliability, permanent magnet synchronous generators (PMSG) and direct drive systems with full-scale converters are becoming more attractive. In spite of its advantages, one challenge with PMSG is that its weight and size increases with the increase in the rated power of wind turbines. Thus, a system called Multibrid with a single-stage gearbox and PMSG is helpful in reducing the weight and size of PMSG [61].

2.4.3.4 High temperature superconducting generators

High temperature superconductor (HTS) technology can be used with superconducting high-power distribution and transmission, generators, motors, and fault current limiting devices such as transformers and cables. This technology provides substantial electromotive force in a small area. In most cases, this is due to its vast current density compared to that of a regular conductor. Moreover, compared to conventional machines' characteristics, this technology also reduces generators' loss and weight. Furthermore, the challenge of cooling the windings in massive scale generators can be settled when the conductors of HTS have stabilized. Given these advantages, this technology has been applied to the 10 MW class superconductor generator for wind turbines [62]. In comparison to the conventional permanent and copper-based generators, the HTS technology enabled a considerable reduction of weight and size of the 10 MW class generator for direct-drive systems of wind turbines. Similarly, recent studies focus on using HTS generators to achieve this purpose

when minimizing large-scale gearless generators' size and weight. However, large-scale HTS generators have problems related to the high electromagnetic force because of their high magnetic field and current density. One way of addressing this problem for a 12 MW class of HTS generator of a wind turbine is through a module coil's structural design [63]. Performance assessment shows that support for pole-type is the most suitable for this generator.

Under other circumstances, the optimum design of a 10 MW HTS synchronous generator for wind conversion systems is discussed [64]. It is found that the total cost of the generator, remarkably the price of the HTS materials, has a significant influence on the optimum generator structure. Thus, this factor should be considered in the design procedures. In the other case, a design of 15 MW and 20 MW fully superconducting generators to reduce LCOE is reported [65], [66]. Based on the outcome, a significant part of the losses in fully superconducting generators results from AC losses induced in the windings of the armature. But with the adoption of scribed rare-earth-barium-copper-oxide (REBCO) tapes into the multifilamentary structure, there is an increase in efficiency of about 97% to 99%. Furthermore, in comparison to conventional generators, the synchronous impedance in fully superconducting generators is minimal.

2.4.4 Design developments for grid connections

One of the most challenging problems in modern power grids is transient stability evaluation. This challenge is attributable to the utilization and installation of wind farms in newly interconnected power networks. This is precisely why wind turbine generators' impact on the assessment of transient stability is now the focus of most researchers. A sensitivity-based approach for real-time transient stability and evaluation of wind turbines interconnected to power grids is one way of addressing this challenge [67]. According to the simulation results, this method can quickly estimate unstable equilibrium points in real-time and have fewer computational burdens. Another challenge of grid connections involves maintaining grid reliability and intermittency of wind energy conversion (WEC) systems. One way of addressing this challenge is provided [68]. In this experiment, the configuration of generators

with improvement in the control of power electronics is discussed.

2.4.4.1 Fault ride through capability and low voltage ride-through requirements

The exponential increase in wind power generation makes power systems even more sensitive to different grid faults. Thus, to ensure the stable operation of these systems, new grid codes have been established. Given these codes, wind turbines need to remain connected to the grid and comply with reactive power requirements throughout the faults and post faults periods. This is termed as fault ride through capability. However, connecting the DFIG stator directly to the grid makes it susceptible to grid disturbances (especially the grid faults). These grid faults at the stator terminals of the DFIG induce a sizeable electromotive force in the circuit of the rotor. As long as this force exceeds the rotor-side converter's maximum voltage, it results in rotor overcurrent, rotor over speed, DC-link overvoltage and torque oscillations.

Consequently, this may lead to the destruction of the rotor-side converter, mechanical parts and DC-link capacitor. Therefore, in the absence of specific protection, the DFIG cannot ride through the grid faults. An improved strategy for fault ride-through of DFIG is presented for asymmetrical and symmetrical grid faults [69]. This strategy is achieved through passive and active fault ride through compensators. Performance results show that this method significantly decreases rotor and stator currents, DC-link overvoltage and electromagnetic torque oscillations. Besides, this strategy contributes to grid voltage by supplying reactive power into the grid.

On the contrary, disconnecting wind turbines from the main grid results in other generators' overloading. This state of affairs causes cascading generator failure and subsequent instability of the entire power system. Many countries have instituted grid codes that help stabilize power systems' operations on account of this challenge. Included in the grid codes is the low voltage ride-through (LVRT) requirements. The LVRT requires wind turbines to remain connected to the grid over some specified range of voltage sags. In certain circumstances, LVRT requirements for wind turbines and some grid connections can be severe. To efficiently manage wind turbines, it is essential to understand LVRT requirements

incorporating voltage sags. A practical method for quality voltage assessment that considers LVRT requirements for wind turbines are given [70].

2.4.4.2 Direct current micro and smart grids

By reason of the inherent advantages of direct current (DC) systems, integrating DC microgrids with PMSG wind turbines has created much interest and attention. Nonetheless, in the state of fault conditions, excessive energy is reflected in the rotating parts of PMSG. This results in fast-ageing, mechanical stress and over-speed of the system. Furthermore, substantial fault currents force the generator-side converter to disconnect. This fault makes it not comply with the grid codes. To enhance DC microgrids' performance with PMSG wind turbines during fault conditions, superconductor fault current (SFCL) limiters can be used [71]. It is shown that SFCL can successfully decrease the DC voltage drop and limit DC's resistance. Hence, making the system comply with different grid codes. In other different situations, hybrid renewable energy sources may be integrated with smart grids as well. This is because smart-grid technology improves distributed energy and renewable energy sources efficiently and effectively. Besides, this technology enables renewable energy systems to be reliable, cost-effective and improves the power quality. It also facilitates real-time interaction between the consumers and the power systems [4].

2.4.5 Design developments for monitoring and control mechanisms

Wind power's intermittency nature results in the high cost of maintenance, grid integration, and power distribution issues. Given these challenges, one of the high-priority problems for the wind industry is reducing wind energy production costs. Among the best-emerging methods for achieving cost reduction are advanced control, condition and deployment monitoring of wind turbines [17], [72]. Some of the techniques for achieving this purpose are discussed in this section.

2.4.5.1 Wake control approaches

At the wind farm level, control techniques concentrate on extending the lifetime of wind turbines by minimizing the fatigue load and maximizing the capture of power. Reduction of

fatigue loads can extend the lifetime of wind turbines while capturing more power improves wind farms' operation. These two objectives are associated with the wakes' control, which constitutes field changes of wind when it passes through wind turbines. At the downwind wind turbines, these wakes reduce wind velocity and increase its turbulence even more. Ultimately, the turbulence increases fatigue loads and cause loss of captured power. Thus, in order to reduce the wake effects, more advanced wind farm control strategies are needed. For now, two types of wake control approaches can be used. The first one is the wake redirection approach. With this approach, the wakes of the upwind wind turbines are redirected in order to reduce or avoid effects on downwind turbines. It can be realised by yawing, independent pitch control or pitching [16]. The second approach deals with axial reduction factor based control. It adjusts the upwind wind turbines' captured power to increase the total captured power in the wind farms. A detailed analysis of the axial reduction factor-based approach is given in [73].

2.4.5.2 Condition monitoring systems

Condition monitoring systems (CMS) are usually used to monitor rotating machinery such as the generator and drivetrain components (gearbox or main bearings). This technique uses accelerometers and temperature sensors to assess vibrations and monitor generators and transformers. Though not very common in the industries, gearbox oil CMS measures particle contamination in lubricant fluids. In other cases, internal visual inspection of the blades and gearboxes is performed using borescopes. However, among CMS's primary challenges are the significant number of components required to monitor, given the multiple and complicated failure modes. For example, approximately 17% of failures are because of gears, and 76% of gearbox failures are bearings. A dominant mechanism for failure for many bearings is mainly due to white etching cracks [74].

One good thing is that many hypotheses for the root causes have been developed. However, none of these has been verified thoroughly [17]. On another note, a review of possible solutions for monitoring conditions and challenges of wind turbines is presented [74]. One of the notable findings of this discussion is the need to monitor wind turbine bearings. This is because bearings have a higher impact on component replacement and downtime. For that

matter, most of the generators and gearbox faults are a result of bearing failures. Additionally, the replacement costs for bearings are much lower than the generator or gearbox replacement and the cost of downtime. Thus, it is much profitable to discover and substitute faulty bearings.

2.4.5.3 Multi-objective control techniques

The scaling up of wind turbines in power rating and size help meet the increasing demand for wind energy. However, when the wind turbines' size is increased, the structural loads became even more prominent. As a result, there is more fatigue stress on the wind turbine components, which can cause untimely failure [75]. This is especially true for offshore wind turbines, which are expected to continue increasing in size. Consequently, this development can result in higher costs of manufacturing, design, maintenance and stochastic uncertainty. That is why there is a need for more efficient and reliable systems of monitoring and control. One way of resolving these challenges is given [74]. In this approach, a research overview for monitoring and controlling grid-friendly wind turbines is analyzed. It is anticipated that grid-friendly wind power systems will be a dominant solution for the next generation of large-scale offshore wind farms.

Another way of resolving these challenges is proposed [75]. In this case, the control mechanism involves operating the wind turbine near the optimum power efficiency in the partial load regime. Other measures given in this study include regulating the generated power to its rated value during the high wind regime period. It is also suggested that fatigue loads be reduced during high-speed winds to guarantee the system's reliability. In light of the above findings, one can see that it is not easy to find a control algorithm that can guarantee reliability and efficiency. This is due to the fact that these two aspects have objectives that are conflicting. Therefore, this implies that methods of control that can manage multi-objective problems are still required. Nevertheless, these methods should reduce wind energy production costs to have a competitive edge over other power sources [75]. Moreover, developing more effective and efficient monitoring and control techniques is still a new research area.

2.4.5.4 Variable control strategies

The efficiency of wind power generation can be increased by controlling the variable speed of wind turbines. One variable control strategy for the variable speed of wind turbines is discussed [76]. This method can achieve satisfactory tracking of the rotor speed as per the simulation results. Generally, given the intermittency of wind, considerable power generating systems with variable speed wind turbines are more controllable and efficient. A popular generator for this type of wind turbine is the DFIG. Thus, a modelling of the grid connection of this generator is demonstrated [77]. It can be perceived from the simulation results that significant disturbances in the electrical system create edgewise vibrations in the tower and blades.

The frequency of these vibrations can also be identified. Hence, this study's results provide a sound understanding of the wind system's intrinsic structural mechanical-electro dynamics. More importantly, these results can help in designing future control schemes for frequency components. Another study investigates a controller design and modelling of a front-end speed regulation wind turbine [78]. This controller possesses a differential variable ratio gearbox. For this purpose, it is anticipated that this front-end speed regulation wind turbine will dominate most solutions for the next generation of offshore and large scale wind farms. With that in mind, related advanced technologies of monitoring and control should be further studied.

2.4.5.5 Virtual synchronous generator control

Nowadays, most wind turbines are controlled to produce maximum power without reacting to grid disturbances (other than severe faults). In many cases, the fluctuation of power is balanced using conventional synchronous generators. However, with the replacement of more traditional synchronous generators in wind turbines, the situations can be handled differently. The decrease in system inertia and loss of system controllability may result in frequency and grid voltage fluctuations. Additionally, the variations and uncertainty of the wind may also cause challenges to system operators. Therefore, control functions that can support wind turbines need to be integrated into future grids. Although full converter wind

turbines may achieve this purpose, system operators cannot dispatch and regulate them. Therefore, a virtual synchronous generator control of full converter wind turbines with short term energy storage is unveiled [79]. Experimental results have demonstrated the effectiveness and feasibility of this control method. In another situation, a control strategy for large offshore wind turbines is analysed [80]. The concepts in this design are to prove the possibility of a wind turbine controlling itself optimally [4].

2.4.5.6 Envelope riding

In order to ensure the safe operation of wind turbines and prolong their lifetime, it is crucial to avoid excessive loading through some algorithms. One way of achieving this purpose is illustrated [81]. This approach is based on the concept called envelope riding. It uses online numerical optimization to forecast the extreme winds that may damage the wind turbine. With this method, it is possible to keep the wind turbine within its safe envelope for the whole period of operation (rated and cut-out conditions). Furthermore, results show that this approach is able to improve power output and reduce loads. It should also be stressed that many modern variable speed wind turbines are operated amidst wide-ranging wind speeds (high and low wind speeds).

Therefore, a wind turbine is controlled to switch between these two modes, depending on the wind's prevailing speed. However, this switching of modes can cause vibrations in blades, tower and drivetrain. Such vibrations may lead to performance deterioration in capturing energy, premature failures, and fatigue loads of wind turbines. One way of addressing this problem is through performance improvement of switching control [82]. The simulations results show that this control design is helpful under different wind speeds and improves switching control performance. On another note, a review on the control mechanisms similar to envelop riding and their associated methods is discussed [83].

2.4.5.7 Wireless sensors

Data related to the gearbox, kinetic losses, stress, temperature of the bearings, electrical and environmental conditions can be obtained by placing different sensors on the wind turbines' structures. The sensors can then be wirelessly connected to some central monitoring device

(station). Data obtained from the sensors may then be utilized to develop and design wind turbine systems optimally. Wireless sensor networks can also be used to monitor the health status of wind turbines. Factors such as lightning strikes, moisture absorption, wind gust and any damages to the wind turbines can be monitored. One other advantage of these sensors is the prompt and quick response taken from the central controlling stations [4]. Given this benefit, a suitable wireless sensor routing protocol for wind turbine structure monitoring is developed [84]. This protocol is called ubiquitous mobile gradient. Under simulator results, this protocol successfully monitors sizeable offshore wind turbine structures for different rotor speeds, traffic, and noise conditions.

2.5 CURRENT RATINGS OF WIND TURBINES AND WIND FARMS

A comparison of power ratings of commercial models of wind turbines and wind farms currently operational and available today on the market is given [85], [86]. The analysis omits the designs on the drawing boards, the test-bed prototypes not yet made, and the discontinued wind turbine models. It is noticeable from this information that the power ratings and rotor diameters for wind turbines and wind farms' capacity have been steadily increasing. As of 2019, the world's largest wind turbine reached a power rating capacity of 9.5 MW. The other massive wind turbines installed for commercial and testing usage have the following rating capacity: Samsung S7.0 171 7 MW, Vestas V164 8 MW and Enercon E126 7.5 MW. By 2020 or 2030, wind turbines rated 10 MW and 20 MW are expected to be designed and tested. Similarly, the largest offshore wind farm globally, the Walney wind farm of the UK, had a capacity of 659 MW by 2018. By 2012, China's Gansu wind farm was the largest onshore wind farm with a capacity of 6000 MW. This wind farm had a target of increasing this capacity to 20 GW by the end of 2020. Furthermore, most wind farms use offshore wind turbines with more wind power than onshore ones. This trend is likely to continue even in the future.

2.6 THE TREND FOR FUTURE DESIGN OF WIND TURBINES

As shown in Figures 2.3 and 2.4, the general direction in which wind power technology is

developing is towards powerful and large wind turbines. It is also possible to see from these figures that the hub height, rotor diameter, and power ratings significantly impact wind turbines' growth. This is because, for the past 30 y, these three parameters have been continuously increasing in size. For instance, in 1990, wind turbines' average capacity was below 1 MW with hub heights of about 20 m and rotor diameters of 17 m. Currently, it is more than 3 MW with hub heights of more than 80 m and rotor diameters of more than 100 m. This upsizing of wind turbines is anticipated to increase even further in the future [86].

However, there is little agreement concerning the exact future size of large wind turbines. Some experts recommend a rotor diameter of 120 m to 150 m and a tower height of 120 m to 200 m with a power range of 3 MW to 10 MW [87]. Other recent wind turbine technology developments also show a trend of more giant wind turbines rated 5 MW or more. While onshore wind turbines may be limited by erection equipment and transportation infrastructure, offshore wind turbines experience lesser issues. Therefore, these wind turbines are likely to keep increasing the size of power ratings, hub heights and rotor diameters.

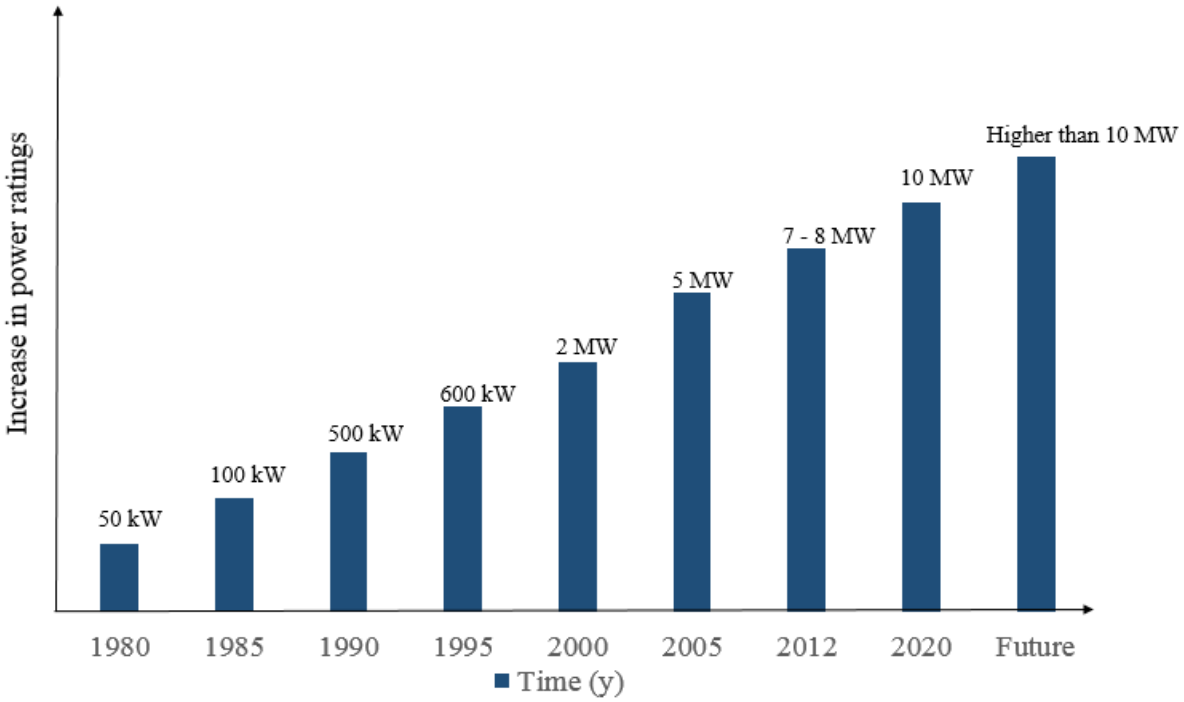

Figure 2.3. The trend in growth size of power ratings for wind turbines [88].

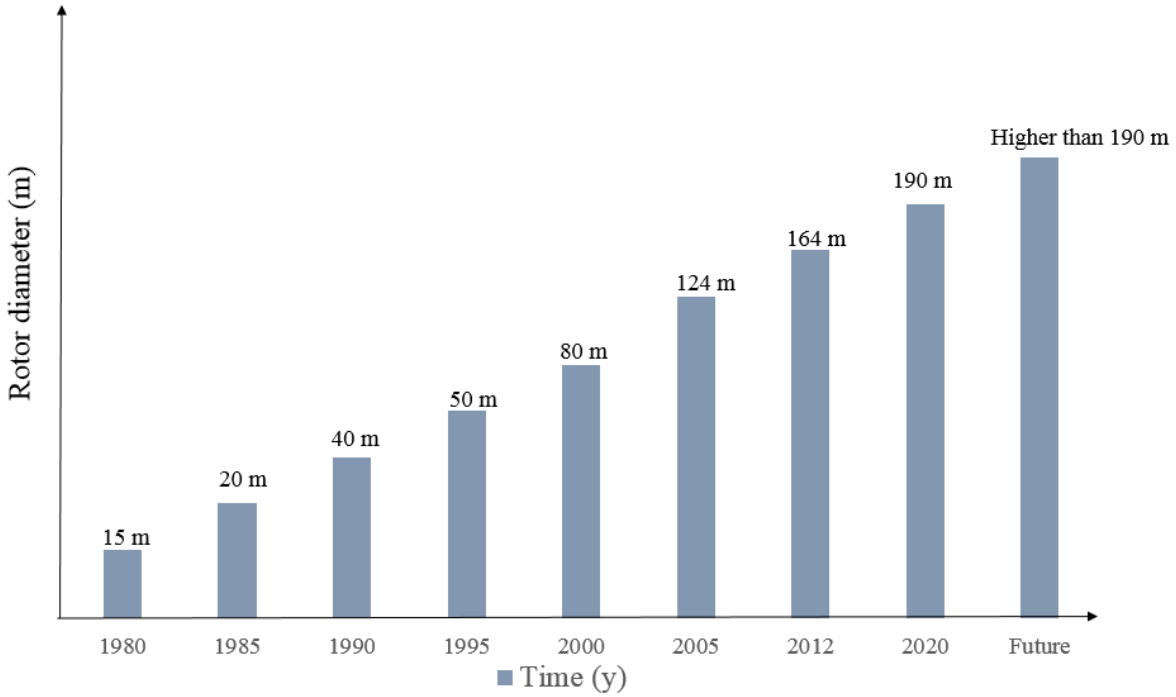

Figure 2.4. The trend in growth size of rotor diameters for wind turbines [88].

2.6.1 Downwind design for offshore wind turbines

The growth size of traditional upwind wind turbines [89] comes with technological challenges that require researchers' attention. Some of these challenges include blade to tower clearance, manufacturing technology, increased loading on nacelle and gearbox, higher weight induced structural loads, and higher aerodynamic loads on blades. Fortunately, a downwind configuration of wind turbines presents opportunities to alleviate some of these issues. The idea involving the implementation of downwind configuration for offshore wind turbines may lower the cost of energy. Besides, a downwind rotor may also alleviate technical challenges such as higher loads on the gearbox, rotor and structure, and tower to blade clearance issues. Moreover, a downwind configuration presents new blade and tower design possibilities, such as full height lattice towers, flexible blades, tower fairing, and high-speed rotors [90]. The design commitment perceived in this study shows many potential opportunities in the design of wind turbines. This is especially the case for offshore weather conditions. Nonetheless, there is a need to study the whole system design optimization and

cost analysis for downwind offshore wind turbines. This is important as a means to quantify the potential of cost savings.

2.6.2 Upscaling design techniques

Several technological challenges should be addressed for the successful development of large wind turbines. To begin with, a detailed study on the tower shadow effects on the blades is required. Secondly, the wind turbine simulation codes should improve accuracy in representing the nacelle effect and tower shadow. It should also be mentioned that the implementation and development of advanced control algorithms to alleviate tower shadow effects is still a key challenge for researchers. This is necessary to ensure the safe operation of downwind rotors [86]. A multidisciplinary design optimization of large wind turbines that addresses some of these technical design and economic challenges is examined [14]. Assessment of results shows that upscaling wind turbines without changing technology concepts and materials is not viable. Furthermore, upscaling techniques should be performed in smaller scaling steps to mitigate the negative impact of wind turbines' design and technology advancement. Otherwise, if not done correctly, upscaling using the existing designs and materials can result in wind turbines that are more expensive than the existing ones.

2.7 DESIGN CONSIDERATIONS FOR OFFSHORE WIND FARMS

Other than being installed individually, wind turbines can also be put in groups called wind farms (also called wind parks). The primary purpose of these sites is to generate electricity in bulky. Some of the reasons offshore wind farms are more desirable than onshore ones include: limited onshore space for installation, lower interference with habitats and high average wind speed. Besides, the market for offshore wind turbines is developing much faster than the onshore wind turbines [4]. It should also be noted that the installation of offshore wind turbines is often done in dense clusters. This is because of the need to minimize the cost of maintenance and transmission. Another reason for the clusters is to have a limited number of quality sites. Other design considerations for wind farms are further

discussed below.

2.7.1 Farm layout

Because of higher energy capacity, offshore wind farms have continued to attract more attention recently. However, investments in wind farms are very high. One way of making them cost-effective is to optimize the wind farm layout. A new way of positioning offshore wind turbines is suggested [91]. In comparison to other layout design methods, this one is more beneficial to wind farms. Nevertheless, one of its limitations is the control strategy. It is only applicable to the exact model used to predict wind speed for each wind turbine. In another vein, improving the efficient production of electrical energy on wind farms requires a good layout design of network cables [92]. In this case, cable networks' optimal design aims to reduce the cost of power lost in cables and the total infrastructure cost over 20 years of expected lifetime. This design shows that energy lost in the cables is a significant component that should be included in the wind farms' layout.

In other instances, maximizing the availability of offshore wind turbines is essential. This can increase annual energy production and subsequently minimize the LCOE. Thus, a design for the high availability of parallel wind turbine power trains is revealed [93]. This design's benefit depends on the type of power train technology and the wind turbine used. Even then, results show that increasing the number of parallel systems does not automatically result in higher power train availability for wind turbines. However, good improvement is seen when repair and failure rates scale with the modules' power ratings.

2.7.2 Hybrid combination of power

The output of power from wind energy systems is variable and not stable. This output depends on the weather conditions of the wind. Therefore, to enhance and improve system design for wind farms, wind power systems should be integrated with other renewable energy sources such as geothermal, biomass or solar. Alternatively, wind farms may also be connected to utility power grids. Not only does this hybrid combination maximize the

generation of power, but it also reduces transmission losses and alleviates peak demands when connected to the grid. Thus, with this approach, the cost of generating electricity can be reduced. Furthermore, in the interest of hybrid power reliability, a system for wind farm dynamic security decision tree (DSDT) is constructed [94]. This system can predict trip-off and over-voltage situations for wind turbines. Not only that, in comparison to the standard simulation transient method, the DSDT can cover more anticipated sets of accidents and effectively lessen the time of simulations.

More importantly, this method can supply decision-making references and intuitive trip-off risk indexes for power grid dispatchers. These acquired indexes of disturbance measures are very useful for designing suitable preventive control strategies for large scale wind farms [94]. On the contrary, off-grid wind power systems are suitable in remote areas where distribution systems are challenging to implement or are inefficient. For example, these systems can work well in developing countries for remote rural area electrification of houses, offices and schools. For maximum efficiency, off-grid wind power systems may be combined with photovoltaic or diesel systems [4].

2.7.3 Internet of energy

One of the most significant market shares of renewable energy around the world is wind energy. The rapid development and growth of this energy have resulted in a considerable increase in the scale and complexity of WEC systems. Hence, there is a need to upgrade strategies and methods for implementing and designing these systems. One of the ways of designing this system is to enable wind energy for the internet of energy (IoE) or energy internet. IoE is a cloud-based network of power sources with distributed and embedded intelligence. It is interfaced with smart grids and mass consumption devices such as electric vehicles, smart buildings and appliances [95]. In light of IoE, WEC mechanisms can be considered as a cyber-physical system (CPS).

On the contrary, in most research trends, CPS for energy applications focuses mainly on the smart grids and energy systems for smart buildings and demand-side management. In so

doing, there is little attention given to systems of generation. On account of this, the state of the art technologies and advances for enabling IoE with WEC is discussed [95]. One unique technology in this discussion is the potential of integrating next-generation WEC systems with CPS. On a similar note, new requirements and challenges of future CPS and WEC such as social components, abstraction, security, networking, safety, sustainability and control are also analysed.

2.7.4 Performance issues

Some of the challenges associated with the design and performance of wind farms are described in this section.

2.7.4.1 Wake effects

Grouping the wind turbines in clusters put most of them in the wake of the upstream ones. This results in the following issues: decrease in the harvested energy due to the loss of the available kinetic energy in the airflow, decrease in the service life of the wind turbine because of the increase in the intensity of the turbulence in the incoming flow, and increase in noise emission as a result of blade vortex interaction. Alongside these issues, the other dominant factor that causes energy losses is the wake effects. Wake effects are also known to cause severe challenges for control systems in advanced wind plants. Therefore, to minimize the wake effects forced upon the downstream wind turbines, upwind rows of wind turbines on a farm are compelled to function at a reduced efficiency [96]. In other situations, it has also been found that offshore wind turbines have the following constraints: difficulties in foundation construction, maintenance, and grid connections [97].

2.7.4.2 Foundations and towers

Towers and foundations have various issues that affect the performance of wind farms. One of these issues includes the effect of unpredictable waves and wind conditions on the towers. In such situations, floating foundations can solve the mooring and anchoring of towers [98]. The influence of technology on how towers can be improved to capture the wind in low wind speed wind farms is also explained [99]. Additionally, higher annual capacity factors and

smooth output can be achieved using a larger swept area and taller towers per rated capacity [100]. Furthermore, the effect of weather on towers and foundations is examined [101], [102]. Finally, it is found that if the systems are to operate as expected in different circumstances, formal validation and verification procedures should be considered [103].

2.8 SYSTEM ADVISOR MODEL SIMULATOR

Researchers and manufacturers use different specialised computer modelling and software simulation tools when designing and developing wind turbines. This research is using the SAM simulator because of its considerable relevance to the objectives of the study. SAM is a desktop application specifically designed to help facilitate techno-economic analysis of projects for renewable energy. It is a decision-making tool for energy researchers, project developers, policymakers, and financial analysts. More importantly, SAM can model grid-connected power systems that use geothermal, photovoltaic, biopower, solar hot water, or wind electricity generation technologies. Its advanced simulation options can facilitate statistical, parametric, and sensitivity studies that comprise many different simulations. Besides, its scripting language, a built-in programming language, can automate complex or repetitive modelling tasks [104].

Another advantage of SAM is its capability to model both central and distributed generation projects. It is also worth mentioning that performance models in SAM are meant for project pre-feasibility level analysis. In terms of wind energy projects, the performance model can produce preliminary estimates of the expected capacity factor and electricity production for large wind farms, small wind projects or a single wind turbine for over one year. These projects can be on the utility side (US) or the meter's customer side (CS). US projects involve selling electricity at prices negotiated through a power purchase agreement, while CS projects require buying and selling electricity at retail rates. Although SAM can give insights on the effects of seasonal and daily wind resource variations, it cannot offer detailed engineering design modelling for electrical transients or physical stresses for wind turbine components. It is equally important to note that every simulation and modelling work in SAM is referred to as a project [104]. Hence, this study is also using the term project in the

same context.

2.9 SUMMARY

This chapter reviews how wind power technology affects the design and performance of wind turbine components, such as rotor blades and generators. Other than that, different design methods of connecting wind turbines to power grids are provided as well. At the same time, monitoring and control strategies are equally reviewed. Another significant aspect of wind power technology discussed is the impact of power curves on wind turbines' design and performance. On a similar note, the chapter discusses how power in the wind, maximum rotor efficiency, and tip speed ratio affect wind turbines' performance. On the other hand, the chapter addresses the benefits of using large rotor diameters, curved shapes, backward sweeping blades, modular blades, and cross-axis blades. Material innovations that can lower the cost of blades are equally described, together with manufactured materials' defects. Similarly, the impact of aeroelastic effects, airfoils and Reynolds number on blades is also examined. On top of this, optimization and downtime issues of blades are explained as well.

Another most essential part of the wind turbine that has been considered is the generator. Concerning this component, different types of generators used in the design of wind turbines are stated. In the other part of the chapter, techniques for improving grid connections' performance using the strategy of a faulty ride through capability and low voltage ride-through requirements of wind turbines are given. Furthermore, monitoring and control mechanisms for enhancing the performance of wind turbines are specified. As for wind farms, the chapter highlights their challenges and how wind turbine design layout, IoE and a hybrid combination of power can resolve some of these issues. Adding to these strategies, the chapter also identifies constraints caused by unpredictable waves and wind conditions on foundations and towers. But more importantly, the chapter suggests how to obtain a higher annual capacity factor using taller towers. On the other side, current power ratings for commercial wind turbines and wind farms are presented. Adding to these ratings, future design developments of wind turbines are also disclosed. Finally, a suitable renewable energy simulator for this study is revealed at the end of the chapter.

CHAPTER 3 DESIGN AND APPLICATION OF SYSTEM SPECIFICATIONS AND TESTING MODEL

3.1 CHAPTER OVERVIEW

An SSTM for wind turbines is designed in this chapter. Its purpose is to increase the size of only four system specifications of wind turbines and test the impact of this change on energy production, capacity factor and system energy losses. This model uses a linear equation to scale up the rated power output, hub height, maximum tip speed, and rotor diameter of HAWT. Although SSTM can work with any suitable wind energy simulator, this study uses SAM simulator for its implementation. With reference to a baseline wind turbine and wind farm, this model's performance is assessed on four large offshore wind turbines and wind farms with different system specifications.

3.2 INTRODUCTION

When it comes to wind turbines' size, their mathematics is relatively easy; bigger and taller is better. These two attributes are two ways of producing more power from wind in some specific areas. With more giant blades and rotors, a wider area of wind is covered, leading to an increase in the total potential production of energy. On the one hand, more steady and high wind speeds are accessed when the blades are taller (high up in the atmosphere). As a result, the capacity factor of wind turbines is increased. However, as can be seen in the growth trend of wind turbines [86] – [88], there is no specific model for increasing the size

of system specifications of wind turbines. Thus, in this chapter, an SSTM for large wind turbines is developed. In terms of operation, this model has two options for modelling system specifications of wind turbines. One can choose to use either user-defined (UD) or the library method. This chapter's primary focus is to simulate two different system specifications of offshore wind turbines and wind farms using these two options. For this purpose, this chapter has two significant simulations to perform. In the first one, different specifications for four offshore wind turbines and wind farms are derived from SSTM and subsequently simulated using the UD technique. On a similar note, a baseline wind turbine and a wind farm based on the NREL library specifications are simulated in the second case. The performance metrics for comparing these two cases are capacity factor, system energy losses, and energy production. In terms of work presented for this chapter, a design and generic explanation of how SSTM works is given first, followed by its implementation in the SAM simulator.

3.3 DESIGN FOR SYSTEM SPECIFICATIONS AND TESTING MODEL

The SSTM design for scaling up and testing system specifications for large wind turbines is shown in Figure 3.1. It consists of four basic operations levels: data input system, turbine system, wind farm system and simulator system. Its intended purpose is to increase the size of four system specifications of wind turbines and estimate the energy production, capacity factor and system energy losses resulting from this increase. SSTM can be implemented in any suitable simulator which supports its four systems. For this study, the simulator that is used to implement it is SAM. An explanation of how SSTM works is discussed in this section according to the functions of each system.

3.3.1 Data input system

A primary source of information for the data input system is key specifications of commercial wind turbines, test-bed prototypes, or discontinued wind turbines, which need to be tested or scaled up in size. This system's input parameters comprise rated power output, rotor diameter, maximum tip speed, hub height, and other typical system specifications of wind turbines. Given the importance of these parameters in the design of SSTM, a brief

description of each parameter is provided.

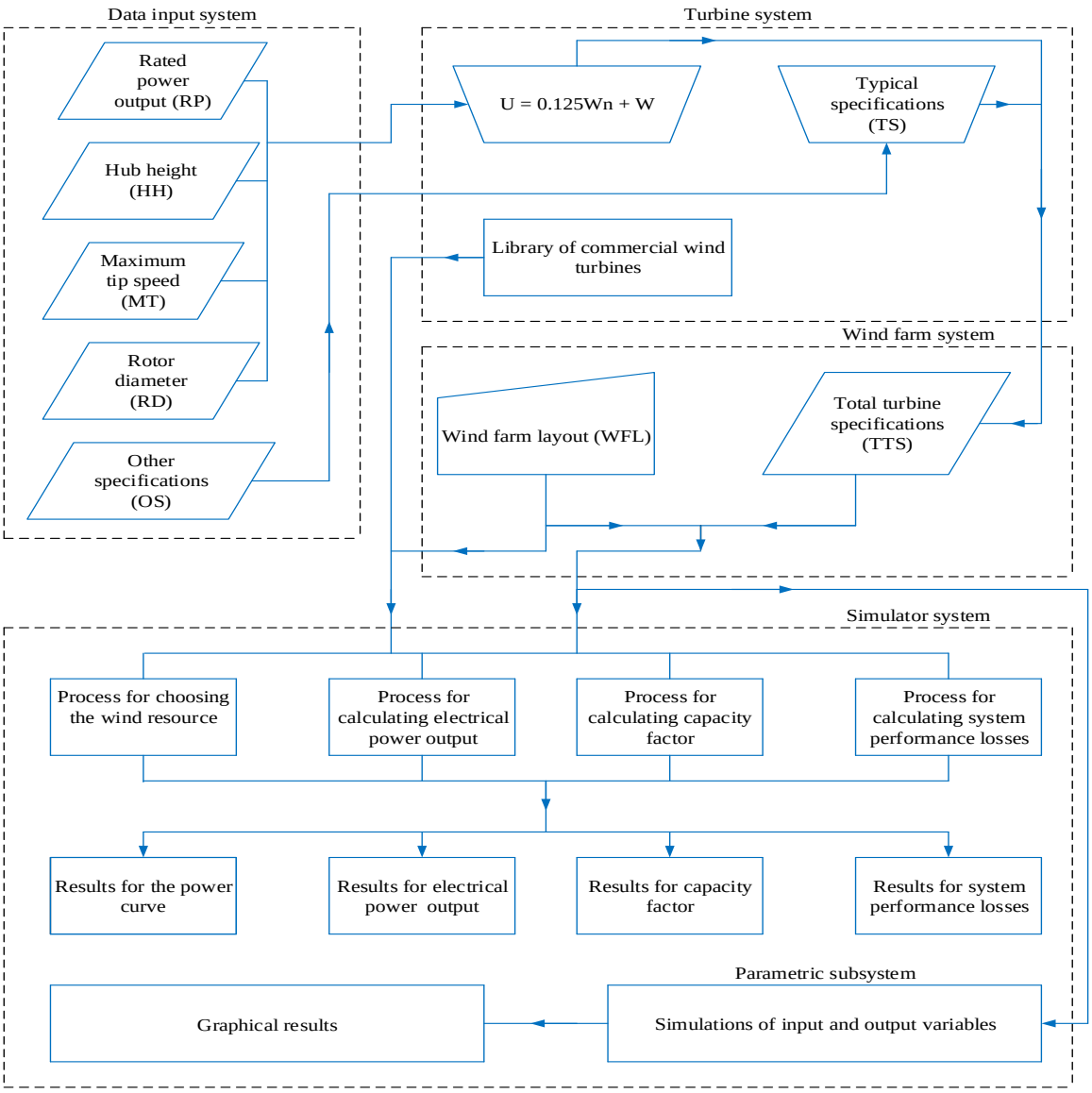

Figure 3.1. Design for system specifications and testing model.

3.3.1.1 Rated power output

The electrical power output of wind turbines increases fast as the speed of wind rises higher and above the cut-in wind speed. However, this increase in power always reaches a limit that the electrical generator cannot manage. This output limit of the generator is referred to as rated power output. In other words, this limit is the nameplate capacity of the wind turbine in kilowatts (kW).

3.3.1.2 Rotor diameter

Rotor diameter is one of the essential variables in the design process of large wind turbines. It is the diameter of a circle that is created when the blades are rotating in the wind. Therefore, increasing rotor diameters makes a significant contribution to the power output of wind turbines. This trend is particularly relevant to the rotor blade diameters of offshore wind turbines.

3.3.1.3 Maximum tip speed

Maximum tip speed is the maximum velocity of the blade tip of the wind turbine. Thus, tip speed is a measurement of how fast the ends of the tip of the blades are moving. Higher tip speed can be advantageous for a given power output because torque on the drivetrain minimizes the drivetrain's mass and cost reduction.

3.3.1.4 Hub height

The hub height of the wind turbine is the rotor's height at a level above the ground. Increasing this height above the ground also tends to increase the wind speeds. Therefore, almost all large wind turbines have hub heights that are above 100 m.

3.3.1.5 Typical system specifications

In total, twelve system specifications are required for the data input system. But for all that number, eight of them are typical specifications common to most large wind turbines. These specifications consist of power coefficient, maximum tip speed ratio, drivetrain design, shear coefficient, tower design, number of blades, cut-in and cut-out wind speeds.

3.3.1.5.1 Power coefficient

Power coefficient (Cp) is the power efficiency of the rotor. It represents the fraction of the rotor's total available power, which the blades can convert to mechanical power. Cp incorporates the efficiency of different wind power systems, such as shaft bearings, generators, turbine blades, power electronics and gear trains. In most cases, modern large wind turbines with good design have Cp values ranging from 0.45 to 0.50. This range of values is approximately 75% to 85% of the Betz limit's theoretical maximum efficiency. In

the design of SSTM, any value that falls in this range can be used.

3.3.1.5.2 Maximum tip speed ratio

The maximum tip speed ratio is the maximum ratio of the blade tip speed to the wind speed. It is a significant number that let us know how fast the blades are turning to the wind's speed. In any case, if the rotor of the wind turbine moves at prolonged speeds, most of the wind would pass through the gaps between the rotor blades without affecting them. In contrast, the blurred blades seem like a rigid wall to the wind speed if the rotor moves too fast. On account of this rotor behaviour, wind turbines should be designed with the most suitable tip speed ratio to extract considerable wind power. In a like manner, when one rotor blade passes through the wind, it causes turbulence in its wake.

While the wind is still turbulent, if the next blade on the spinning rotor reaches this point, it cannot efficiently extract power from the wind. That being so, the rotor should spin a bit more slowly to ensure that the wind striking each blade is not turbulent. For this reason, the tip speed ratio should also be selected in such a way that the three blades do not experience an intolerable turbulent wind. Furthermore, when designing wind turbine generators, this number must be carefully considered as well. For a good design, typical values for the tip speed ratio of HAWT should start from 5 to 8. A tip speed ratio in this range is equally appropriate for the design of SSTM.

3.3.1.5.3 Drivetrain design

A wind turbine's drivetrain comprises the generator and the gearbox. These two components are essential for generating electricity. The gearbox connects the high-speed shaft that attaches to the generator to the low-speed shaft that connects to the wind turbine's blades. With a series of gears of different sizes, the gearbox changes the blades' slow rotation (typically 30 to 60 rpm) to high speed (approximately 1000 to 1800 rpm). It is the latter speed that enables the generator to produce electricity. The following design options for the drivetrain may be used on SSTM: three-stage planetary, single stage-low speed generator, multi-generator or direct drive.

3.3.1.5.4 Number of blades

Nearly all large wind turbines with a specific purpose of producing electricity comprise two or three blades that rotate on the wind turbine's horizontal axis. The SSTM is designed to work with three-bladed wind turbines.

3.3.1.5.5 Tower

The rotor and nacelle are carried and supported by the tower of the wind turbine. Therefore, increasing the height of the tower improves the quality of wind resources above the ground significantly. Different types of tower designs may be used in SSTM depending on the type of simulator system used.

3.3.1.5.6 Shear Coefficient

The shear coefficient measures the wind speed variation to the height above the ground at the wind turbines' installation site. Subject to terrain type, the shear coefficient ranges from 0.1 for open water to about 0.3 for mountains or hills. For wind resource studies on land, the common assumption is the default value of 1/7 (0.14). Conversely, 0.11 may be used for offshore wind turbines over water. In keeping with the simulator system being used, any of the above shear coefficients may be used in SSTM to estimate wind speed at the specified hub height.

3.3.1.5.7 Cut-in and cut-out wind speeds

Cut-in wind speed is the lowest wind speed at which a wind turbine generates power. In contrast, the wind speed at which a wind turbine shuts down to prevent its damage is called cut-out wind speed. Typical SSTM cut-in wind speed values are about 3 m/s to 4 m/s, while the cut-out wind speed is around 25 m/s.

3.3.2 Turbine system

The turbine system is one of the most significant components of the model. It has the primary function of processing the information from the data input system and prepare it for the wind farm system. This system process UD, typical and library system specifications.

UD specifications are derived from the data input system, while the library specifications are for commercially available wind turbines inherent to the turbine system of any renewable energy simulator. Before being processed in the wind farm system, UD specifications are scaled up using a linear equation $U = 0.125Wn + W$. In this equation, U is the scaled-up specification, 0.125 is the increment factor, W is the first specification that needs to be upgraded, and n is the number of times of upgrading W. The only system specifications processed by this equation are the hub height, rated power output, rotor diameter and maximum tip speed.

However, the total turbine specifications (TTS) for determining the power curve in SSTM are four UD parameters and eight typical specifications. These are used as input data for the wind farm system. On the other hand, library system specifications are for existing commercial wind turbines, and they are the reference for comparing the performance of UD specifications. They can also be used as sources of information for the data input system for scaling up purposes. Unlike the UD specifications, rated power output, rotor diameter, hub height and shear coefficient are the only input variables that can be modified on the library system specifications.

3.3.3 Wind farm system

Wind farm layout (WFL) and TTS are the two main design components of the wind farm system. Though these two components are determined separately, both serve as valuable input data to the simulator system. WFL is determined using three parameters: system sizing, type of wake model and wind turbine layout.

3.3.3.1 System sizing

For system sizing of wind farms, the model has three methods that can be utilized: single turbine, wind farm size in terms of capacity (kW) or farm size based on the number of wind turbines. For the latter option, the layout of the wind turbines must also be considered.

3.3.3.2 Type of wake model

Three different wake models can be used on the wind farm system to estimate the effect of upwind wind turbines on downwind turbines' performance. These options include eddy-viscosity, park (WAsP), and simple wake models. The first two models are provided to allow comparison with other modelling software. However, for wake effect calculations on the SSTM wind farm system, simple wake model (SWM) is suitable and sufficient. SWM uses the wind speed deficit factor when estimating the reduction in wind speed at a downwind turbine. Equations (3.1) and (3.2) shows how this model calculates the turbulence intensity and wind speed deficit factor [105].

$$\sigma = \sqrt{\left[\frac{C_T}{7}\times\left(1-\frac{2}{3}\times\log 2x\right)\right]^2 + C_t^2} \tag{3.1}$$

where σ is the turbulence intensity, C_t is wind turbine coefficient, x is crosswind distance between the wind turbines in the rotor radii, and C_T is turbulence thrust coefficient. Wind speed deficit factor (f_{wsd}) is defined in (3.2).

$$f_{wsd} = \frac{C_T}{4\sigma^2 x^2} e^{\left(\frac{-r^2}{2\sigma^2 \mathrm{x}^2}\right)} \tag{3.2}$$

where f_{wsd} is wind speed deficit factor, r is crosswind distance between wind turbines in the number of rotor radii, χ is downwind distance between wind turbines in the number of rotor radii, C_T is wind turbine power coefficient, σ is transverse turbulence intensity. The adjusted wind speed $\left(V_{adj}\right)$ at the downwind turbines is then calculated using (3.3) [105].

$$V_{adj} = V\times\left(1-f_{wsd}\right) \tag{3.3}$$

where f_{wsd} is the wind speed deficit factor of (3.2), V is the wind speed at the neighbouring upwind turbine. The wake effect model uses the wind direction from the wind data to calculate the distance between neighbouring crosswind turbines and neighbouring turbines downwind. It also uses information about the relative position of turbines from the inputs that have been specified on the wind farm system. With this information, a set of coefficients (power coefficient, thrust coefficient and turbulence coefficient) representing

the turbine's effects on wind speed are then calculated. SWM uses a thrust coefficient to calculate the wind speed deficit at each wind turbine due to the upwind turbines' wake effects. The difference in wind speed (ΔU) between an upwind and downwind wind turbine is given by (3.4) [105].

$$\Delta U = \frac{C_t}{4\sigma^2 x^2} . e^{\left(\frac{-r^2}{2\sigma^2 x^2}\right)} \tag{3.4}$$

where σ is the local turbulence coefficient at the wind turbine, x and r, are respectively, the downwind and crosswind distance between wind turbines expressed as some rotor radii.

3.3.3.3 Turbulence coefficient

The turbulence and speed characteristics of wind change as the wind pass through a wind turbine rotor. This ambient turbulence intensity is caused by local thermal effects or terrain as air passes across the wind farm. When modelling the wake effect losses in a wind farm, the model uses the turbulence coefficient value to represent this wind speed variation. A typical value of 0.1 may be used for a smooth terrain with low turbulence and little vegetation, such as a flat plane. This value may be even less for offshore wind farms over water. Alternatively, for projects in an area or a forest with air mixings caused by thermal effects with high turbulence, 0.5 is a typical value to use. It is important to note that wake effects are more significant for a wind farm with a lower turbulence coefficient than a higher one.

3.3.3.4 Wind turbine layout

A wind turbine layout is a diagram showing the locations of the turbines on the wind farm field. On this diagram, a wind turbine is represented by a symbol. Eight design parameters are used to determine the layout of the farm. These parameters include turbines per row, number of rows, turbine shape, turbine spacing, row spacing, row orientation, offset for rows, and offset type. Note that the turbine per row defines the turbines in each row. Turbine spacing is the distance in meters between turbines in each row, while row spacing is the distance in meters between the rows. The distance between a line drawn through a turbine perpendicular to its row and a similar line drawn through a turbine in the nearest

neighbouring row is offset for rows. The offset for rows determines how turbines are aligned between rows. There are two different types of offset for rows in this model: every other row and each row. The former applies the offset distance to alternating rows, while the latter applies the distance to every row.

3.3.4 Simulator system

The data input system, turbine system, wind farm system, and subsystems are linked together in the simulator system. Thus, the simulator system is responsible for simulating data from the turbine and wind farm systems based on the chosen wind resource data file. The results of these simulations are presented as electrical power output, capacity factor, and system energy losses of the wind turbines or wind farms. Another important activity in the simulator is the parametric simulations of input variables and output metrics.

3.3.4.1 Process for choosing wind resource data

The wind resource data provides information concerning the kinetic energy available in the wind at some specified hub height and wind turbine location. In this data, the amount of energy available varies with time and depends on air density and wind speed. There are two main options for selecting the wind resource data in the model: wind speed Weibull distribution and weather files by locations.

3.3.4.1.1 Data from Weibull distribution

The Weibull distribution is appropriate for studies that do not need details of a time series of wind resource data. This option is relevant for representing wind resources as a statistical distribution. The probability that a given wind speed value will happen over a given period is determined by the Weibull probability distribution function shown in (3.5) [105].

$$f(V) = \frac{k}{\lambda^k} \times (V)^{k-1} \times e^{-\left(\frac{v}{\lambda}\right)k} \tag{3.5}$$

where $f(V)$ is the Weibull probability distribution function of wind speed, λ is a scale parameter in m/s, k is dimensionless shape parameter, and v is the wind speed in m/s. Weibull distribution is characterized by a Weibull shape factor and a single average annual

wind speed. Thus, it helps analyze parametric studies on the annual average value of wind speed and the shape of wind speed distribution beyond a year. It is also relevant for preliminary feasibility project studies whose time series data is not yet available. Nevertheless, this type of data does not provide information about the wind direction that the simulator system requires to determine wake effect losses for wind farms.

3.3.4.1.2 Data by location

This wind resource data is obtained from the weather files of the simulator system's folder settings. Each weather file may have wind speed at one or more data heights. If one of the data heights in the weather file is the same as the wind turbine hub height, that wind speed is used. If it is not, the data height nearest the hub height is determined, and the shear coefficient is used to estimate the wind speed at the hub height using (3.6) [105].

$$V_{h,j} = V_{o,j} \times \left(\frac{h}{h_0} \right)^{\alpha} \tag{3.6}$$

where α is wind shear factor, h_0 is data height nearest the wind turbine hub height, h is wind turbine height, $V_{0,j}$ is wind speed from weather file at data height nearest the wind turbine hub height for an hour j, and $V_{h,j}$ is the wind speed at wind turbine height h for an hour j.

3.3.4.2 Process for calculating electrical power

In this model, the wind farm's electrical power output or a single wind turbine is calculated using the 8760 hourly values for one year. These values are then added together and reported as monthly or annual energy.

3.3.4.2.1 Hourly output

The hourly electrical output of a wind farm is the sum of all the wind turbine's electrical output after considering the energy losses of the wind farm. Equation (3.7) shows how this output is calculated [105].

$$P_{(wf,j)} = \frac{L}{100\%} \times \sum_{n=1}^{N} P_{j,n} \tag{3.7}$$

where $P_{j,n}$ is the electrical power output of wind turbine n in the hour j in kWh/h, N is the number of wind turbines in the wind farm, L is a loss factor (wind farm losses on the wind farm), $P_{(wf,j)}$ is the electrical power output of wind farm in an hour j in kWh/h.

3.3.4.2.2 Annual energy

Equation (3.8) explains how the system's annual electrical power output is calculated in the model. This calculation involves the sum of the wind turbine's output adjusted by the performance adjustment factors [105].

$$Q_{sys} = \sum_{n=1}^{8760} \left(P_{wf,j} \times F_{adj,j} \right) \tag{3.8}$$

where $F_{adj,j}$ is the hourly adjustment factor, $P_{wf,j}$ is the electrical power output of the wind farm in hour j in kWh/h, Q_{sys} is adjusted annual electrical energy output of the system in kWh.

3.3.4.3 Process for calculating capacity factor

The system capacity factor in this model is calculated using (3.9). This factor is the ratio of the system's annual electrical power output to its potential power output at the wind farm or wind turbine's rated capacity [105].

$$K = \frac{Q_{sys}}{P_m \times 8760} \tag{3.9}$$

where 8760 is the number of hours in one year, P_m is rated capacity of the wind farm in kW, Q_{sys} is the total annual electrical output of the system in kWh after performance adjustments, K is system capacity factor.

3.3.4.4 Process for calculating system energy losses

System energy losses in the simulator system of SSTM are calculated as a percentage of the gross annual energy production. Six primary sources of these losses are wake, availability,

electrical, turbine performance, environmental, and curtailment losses.

3.3.4.4.1 Wake losses

When a wind turbine uses the kinetic energy in turning the blades, the space at the back of the wind turbine is characterized by reduced wind power capacity, called wake loss. As the wind continues flowing downstream, the wake even spreads out further and only recovers when free stream conditions are approached. The accumulated influence of the wake on energy production on wind farms is referred to as wake effects. Considering wake effects from neighbouring wind farms and their impact on future wind farms is also very important. Thus, this model has a percentage input for the internal wake, external wake and future wake calculations.

3.3.4.4.2 Availability losses

Availability refers to the average expected wind turbine functionality on the wind farm over the whole project life. Thus, availability losses refer to energy loss related to the time wind turbines are unavailable to generate electricity. This factor is represented as a percentage of the gross energy produced. Types of availability losses accounted for in this model include turbine, the balance of plant and grid losses.

3.3.4.4.3 Electrical losses

Electrical losses are an inherent part of the energy transmission process between site equipment, transformers, collector lines and the revenue metering points. These losses are experienced when wind farms are in an operational state. Electrical losses also happen on connection points and low voltage terminals of wind turbines. On the other hand, when the wind farm is not operating, it is also advisable to account for the power consumed by the wind farm. The percentage inputs for electrical losses in this model are referred to as efficiency and facility parasitic consumption.

3.3.4.4.4 Wind turbine performance losses

A power curve provided by the original equipment manufacturer (OEM) can analyse energy production calculations. When the wind speed is above a specific limit, most wind turbines

are shut down. However, significant fatigue loading is caused by high-speed shutdown events. Thus, hysteresis is often introduced into the wind turbine's control algorithm to avoid repeatedly starting the start-up and shutdown process when the winds are near the threshold shutdown. But when given a detailed description of the cut-in and cut-out wind turbine parameters, these values can be used to estimate the loss of production due to high wind hysteresis. This estimation is done by a repeated process of analyzing the power with a minimized cut-out wind speed. Adjusting for site-specific or any generic issues is equally necessary. This adjustment means that the wind turbine's performance may not be according to OEM power curves for a particular site. Therefore, wind turbine performance losses signify the energy produced by the wind turbine at a given wind speed compared to OEM power curves. In the simulator system, the percentage inputs of these losses are represented as sub-optimal performance, generic power adjustment, site-specific power curve adjustment and high wind hysteresis.

3.3.4.4.5 Environmental losses

Several environmental circumstances or conditions affect the energy production of wind turbines. These include surface deterioration of the blades, dirty forming over time on the blades, extreme weather conditions such as ice accumulating on the wind turbines, felling or growth of nearby trees, forests, or other areas of trees close to wind farm sites. In these sites, the flow of wind is affected by how trees change with time. Therefore, if known, the impact assessment of future felling of trees should be assessed. In the model, the above conditions are represented as environmental conditions. The input percentages for these losses are expressed as icing, degradation, environmental and exposure changes.

3.3.4.4.6 Curtailment losses

Planned management of a wind farm minimizes the amount of energy produced compared to what may be available from the wind turbines. For instance, some wind turbines may require to be shut down to alleviate challenges related to planning work conditions and export to the grid or wind turbine loading. Thus, the simulator system gives input percentages for these losses as load curtailment, operational strategies, permit and environmental curtailment.

3.3.5 Parametric subsystem

A parametric subsystem is part of the simulator system whose input data is processed separately from the data input system, turbine system and wind farm system. Parametric simulations are used to explore further the graphical relationship between the input and output variables of SSTM. In other words, this subsystem helps explore the dependence of output results on the input variables.

3.4 USER-DEFINED METHOD OF IMPLEMENTING SYSTEM SPECIFICATIONS AND TESTING MODEL IN SAM SIMULATOR

The UD process of implementing SSTM in SAM is demonstrated on four offshore wind turbines and wind farms using four different system specifications. This section explains the source of information for the data input system and how it is processed in the turbine system, wind farm system, and simulator system of SAM.

3.4.1 Source of parameters for the data input system

The Vestas 8 MW wind turbine is chosen as the source of parameters for the data input system. It is currently one of the largest offshore HAWT on the market and the largest in SAM's NREL library of wind turbines. The reason for choosing this wind turbine is that it is a good starting point for exploring the energy potential of large wind turbines higher than 8 MW. Table 3.1 shows four specifications of the Vestas 8 MW wind turbine that are of primary interest to SSTM. On the other side, eight typical specifications common to large wind turbines are also shown in Table 3.2. The drivetrain, tower and blades are based on the design of SAM. All twelve specifications are useful input parameters for the data input system.

Table 3.1 User-defined specifications for the data input system.

System parameters	Specifications
Rated power output	8 MW
Rotor diameter	164 m
Maximum tip speed	104 m/s
Hub height	105 m

Table 3.2 Typical specifications for the data input system.

System parameters	Typical specifications
Cut-in wind speed	4 m/s
Cut-out wind speed	25 m/s
Power coefficient	0.45
Shear coefficient	0.14
Maximum tip speed ratio	8
Drive train design	Direct drive and single stage-low speed generator
Tower design	Advanced design
Blade design	Advanced design

3.4.2 Processing of parameters in the turbine system

The linear equation $U = 0.125Wn + W$ is responsible for increasing the specifications for rated power output, rotor diameter, hub height and a maximum tip speed of the Vestas 8 MW wind turbine. In other terms, this equation increases each size of these specifications by a factor of 12.5%. Each specification is scaled up four times to effectively assess this change's impact on energy production, capacity factor, and system energy losses. That is to say, each one of them is scaled up by 12.5%, 25%, 37.5% and 50%. The results of these upgrades are shown in Table 3.3.

Table 3.3 Upscaled system specifications of Vestas 8 MW wind turbine.

System parameters	Initial values	12.5% system specifications	25% system specifications	37.5% system specifications	50% system specifications
Rated output	8 MW	9 MW	10 MW	11 MW	12 MW
Rotor diameter	164 m	184.5 m	205 m	225.5 m	246 m
Maximum tip speed	104 m/s	117 m/s	130 m/s	143 m/s	156 m/s
Hub height	105 m	118.125 m	131.25 m	144.375 m	157.5 m

3.4.3 Design parameters for the wind farm system

For this model, the wind farm system is responsible for processing four parameters. These parameters involve system sizing, turbine layout, type of wake model and layout map of the farm. Table 3.4 shows the design specifications for the first three sets of parameters, while the layout map for each wind farm is illustrated in Figure 3.2. A blue symbol on this map represents the wind turbines' locations on the wind farm field. Although the four wind farms have different power rating capacities, the layout of the wind turbines is the same for all.

Table 3.4 Wind farm layout parameters.

Wind farm parameters	Specifications
System sizing:	
Number of wind turbines on each farm	20
Nameplate capacity of each wind turbine	9 MW, 10 MW, 11 MW, 12 MW
Nameplate capacity of each wind farm	180 MW, 200 MW, 220 MW, 240 MW
Wind turbine layout:	
Turbines per row	5
Number of rows	4
Shape	Rectangle
Turbine spacing for rotor diameters	8 rotor diameters
Row spacing for rotor diameters	8 rotor diameters
Offset for rows for rotor diameters	4 rotor diameters
Offset type	Every other row
Row orientation	0 degrees
Wake effects:	
Type of wake model	Simple wake model
Turbulence coefficient	0.1

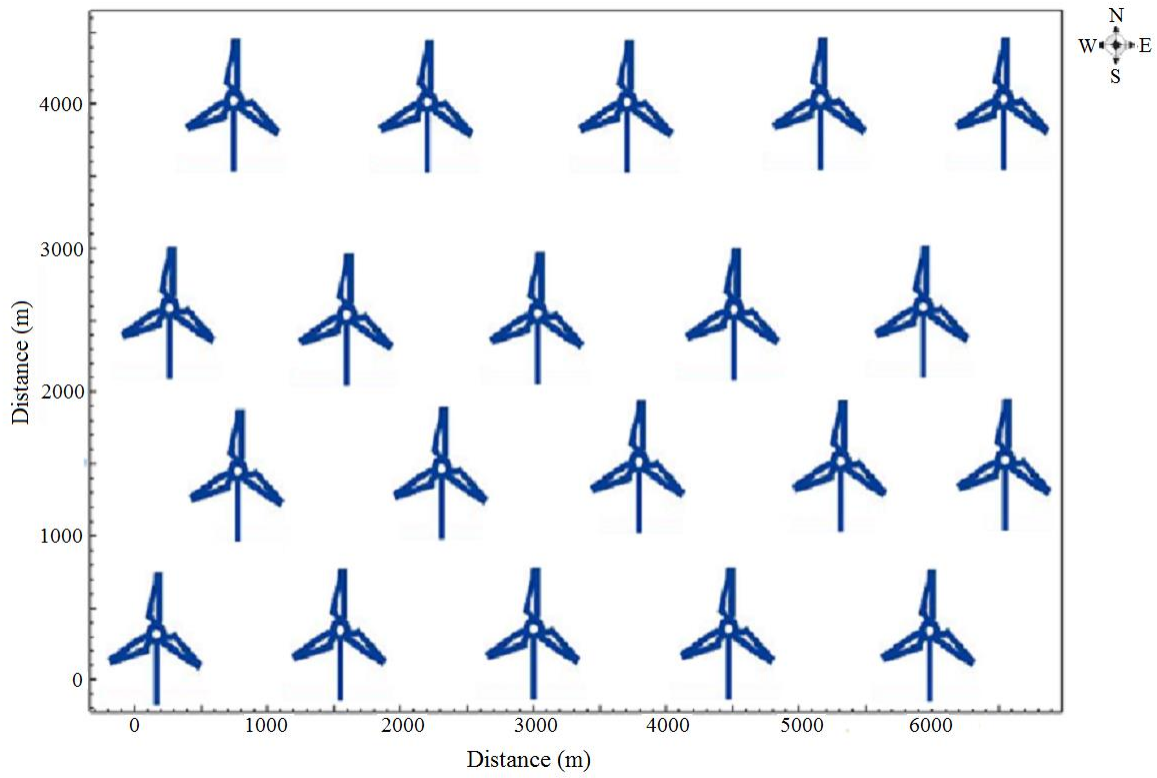

Figure 3.2. Layout map of wind turbines on wind farm fields.

3.4.4 Processing of turbine and wind farm parameters in the simulator system

This section discusses the procedure of simulating parameters from the turbine and wind farm systems using the UD method of SAM. These parameters are for four single wind turbines and wind farms. As the name implies, this method helps simulate and test newly designed parameters for wind turbines.

3.4.4.1 Process of simulating single wind turbines

The required steps for simulating single wind turbines using the TTS of the turbine system are illustrated in Figure 3.3. All the input parameters for the wind turbines are those shown in Tables 3.2 and 3.3. Six significant steps are covered in this process, as described briefly below.

- The first step starts the process of SAM.
- The second step creates and prepares a project file for the work that is to be done.

- The third step relates to choosing the wind performance technology model.
- The fourth step is to characterize (choose) the wind resource data from an hourly data file of a desired specific location.
- The fifth step involves the processing of UD and typical system specifications for the wind turbines.
- The sixth step processes power curves, electrical power output, system energy losses, and wind turbines' capacity factor.

These steps are also beneficial for assessing the performance of existing industrial wind turbines when their system specifications are changed or upgraded.

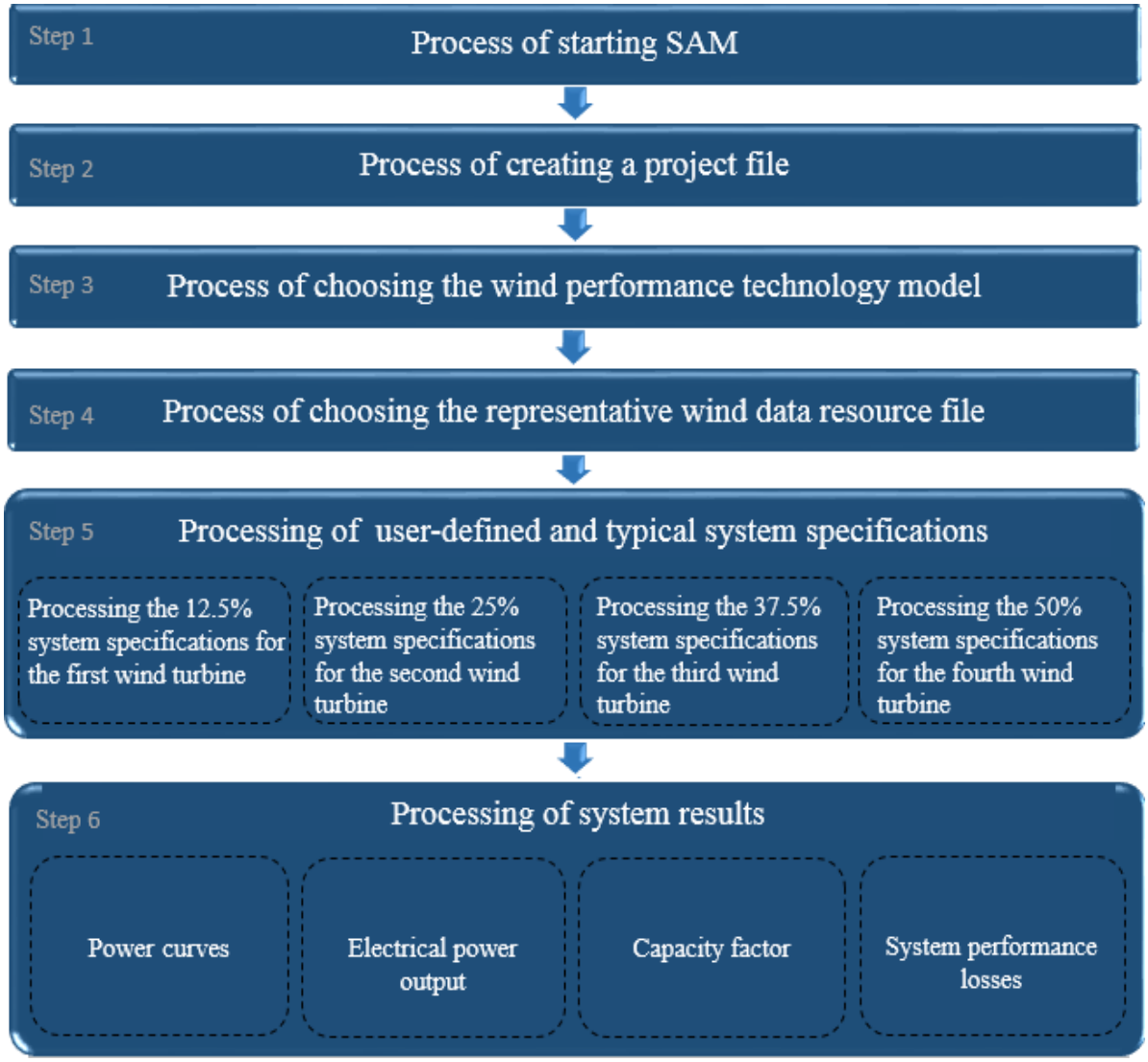

Figure 3.3. User-defined method of simulating single wind turbines.

3.4.4.1.1 Process of starting SAM

Step 1 starts the home screen page of SAM and displays the version of SAM running on the computer. For this study version 2020.2.29, revision three is used. It is the latest version at the time of doing this study. Although SAM can be operated on Windows 7/8/10, it runs on Windows 7 Professional with a 64-bit operating system for this study.

3.4.4.1.2 Process of creating a project file

At step 2, SAM has fully started, and it displays the options to start the work sessions (projects). During this stage, a new project is created and given the name of Project 1.

3.4.4.1.3 Process of choosing a performance model

The technology for the wind performance model is selected at step 3 using the model input page. Much like other performance models in SAM, this model may be used with several financing options. But for this particular study, it is used together with the no financial model.

3.4.4.1.4 Process of choosing a representative wind resource file

A wind resource file for project 1 is chosen at step 4 using the wind resource input page of SAM shown in B.1 of addendum B. This project's representative and typical wind resource file is the Northern CA-offshore NREL AWS Truepower representative file. This study assumes that this wind data file mainly represents the wind situation needed to assess large offshore wind turbines' performance, with a greater than 8 MW power rating.

3.4.4.1.5 Process of determining power curve characteristics

At step 5, typical system specifications and each set of UD specifications shown in Tables 3.2 and 3.3 are entered on the define turbine input page of SAM as illustrated in section B.2 of addendum B. Though this process shows the 12.5% system specifications, the same procedure is done for the 25%, 37.5% and 50% system specifications. The power curves of the wind turbines are determined using these system specifications.

3.4.4.1.6 Process of calculating system performance results

After processing the UD and typical specifications entered in SAM, each wind turbine's system electrical power output is calculated using (3.7) and (3.8). However, in this case, the number of wind turbines (N) in the equations is taken to be 1. At the same time, the capacity factor is calculated using (3.9). Finally, the system energy losses are calculated as percentages of the annual gross energy output. Percentage allocation for the different types of energy losses is shown in Table 3.5.

Table 3.5 Percentage allocation for system energy losses.

Types of system energy losses	Percentage (%) of gross energy output
Wake losses	
Internal wake	0.00
External wake	1.10
Future wake	0.00
Availability losses	
Turbine	3.58
Balance of plant	0.50
Grid	1.50
Electrical losses	
Efficiency	1.91
Parasitic consumption	0.10
Turbine performance losses	
Sub-optimal performance	1.10
Generic power curve adjustment	1.70
Site-specific power curve adjustment	0.81
High wind hysteresis	0.40
Environmental losses	
Icing	0.21
Environmental	0.40
Degradation	1.80
Exposure changes	0.00
Curtailment losses	
Load curtailment	0.99
Grid curtailment	0.84
Operational strategies	0.00
Environmental permit curtailment	1.00

3.4.4.2 Process of simulating wind farms

The process for simulating the 180 MW, 200 MW, 220 MW and 240 MW wind farms using the UD and typical specifications from SSTM is described in this section. Each wind farm has 20 wind turbines, with typical specifications of Table 3.2 and UD system specifications of Table 3.6. Furthermore, all four wind farms are designed with the same layout parameters shown in Table 3.4. Figure 3.4 shows the processing of all these parameters on the wind farm input page of SAM. The procedure for starting SAM, creating a project file, choosing the wind performance model and wind resource file for wind farms is the same as explained in Section 3.4.1.1 to 3.4.1.5. Therefore, this section focuses on steps 6 and 7 only. These two steps describe the processing of wind farm layout parameters, UD, and typical specifications for each farm's wind turbine. For the sake of assessing the performance of single wind turbines without the impact of wake effects, processing of wind farm layout parameters is missing in Figure 3.3.

Table 3.6 User-defined system specifications for wind farms.

Wind farm capacity	Number of wind turbines	User-defined specifications
180MW	20	12.5% system specifications
200MW	20	25% system specifications
220MW	20	37.5% system specifications
240MW	20	50% system specifications

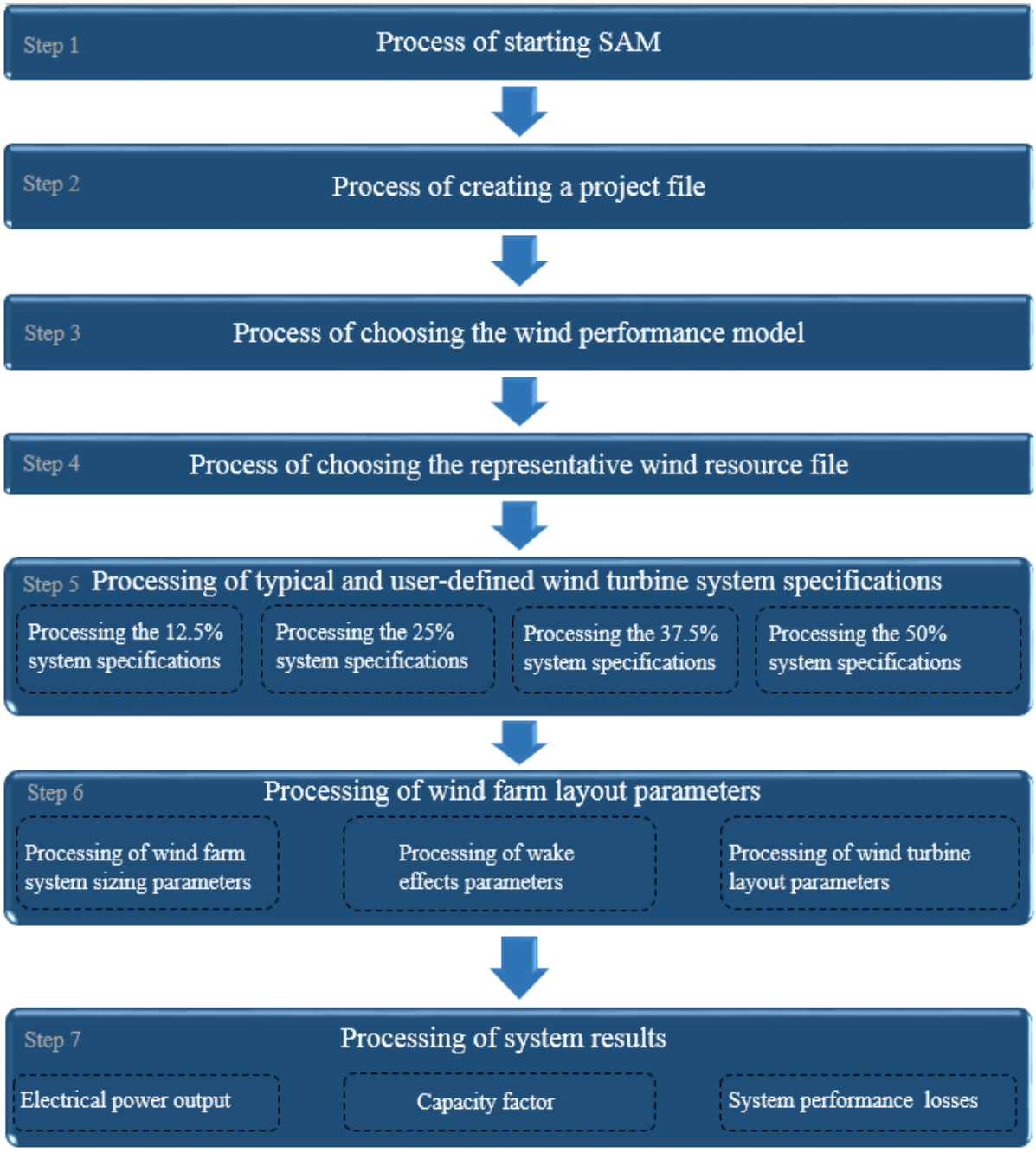

Figure 3.4. User-defined method of simulating wind farms.

3.4.4.2.1 Processing of parameters for wind farm layout

Processing system sizing, wind turbine layout and wake effect input parameters for the wind farms are demonstrated in B.3 of addendum B. Although this process is illustrated for the 180 MW wind farm, the same procedure is used even for the 200 MW, 220 MW and 240 MW wind farms.

3.4.4.2.2 Processing of system performance results

The expected results of the wind farms cover the electrical power output, capacity factor and system energy losses. The electrical power output is calculated using (3.7) and (3.8), whereas the capacity factor is calculated based on (3.8). All the system energy losses are calculated as a percentage of annual gross energy, according to the percentage allocation shown in Table 3.5.

3.5 LIBRARY METHOD OF IMPLEMENTING SYSTEM SPECIFICATIONS AND TESTING MODEL IN SAM SIMULATOR

The library method of SAM is used to simulate the baseline wind turbine and wind farm using the NREL system specifications of the Vestas 8 MW wind turbine. Thus, this wind turbine is a reference to which the performance of UD specifications is compared. The process of simulating the Vestas 8 MW wind turbine and the Vestas 160 MW wind farm is described in this section.

3.5.1 Process of simulating the Vestas 8 MW wind turbine

The first four steps required to simulate the Vestas 8 MW wind turbine are similar to those shown in Section 3.4.1.1 to 3.4.1.4 for UD specifications. Hence, this section does not repeat them. However, the project file's name is Project 2, and the central concern of this section is on steps 5 and 6 of Figure 3.5.

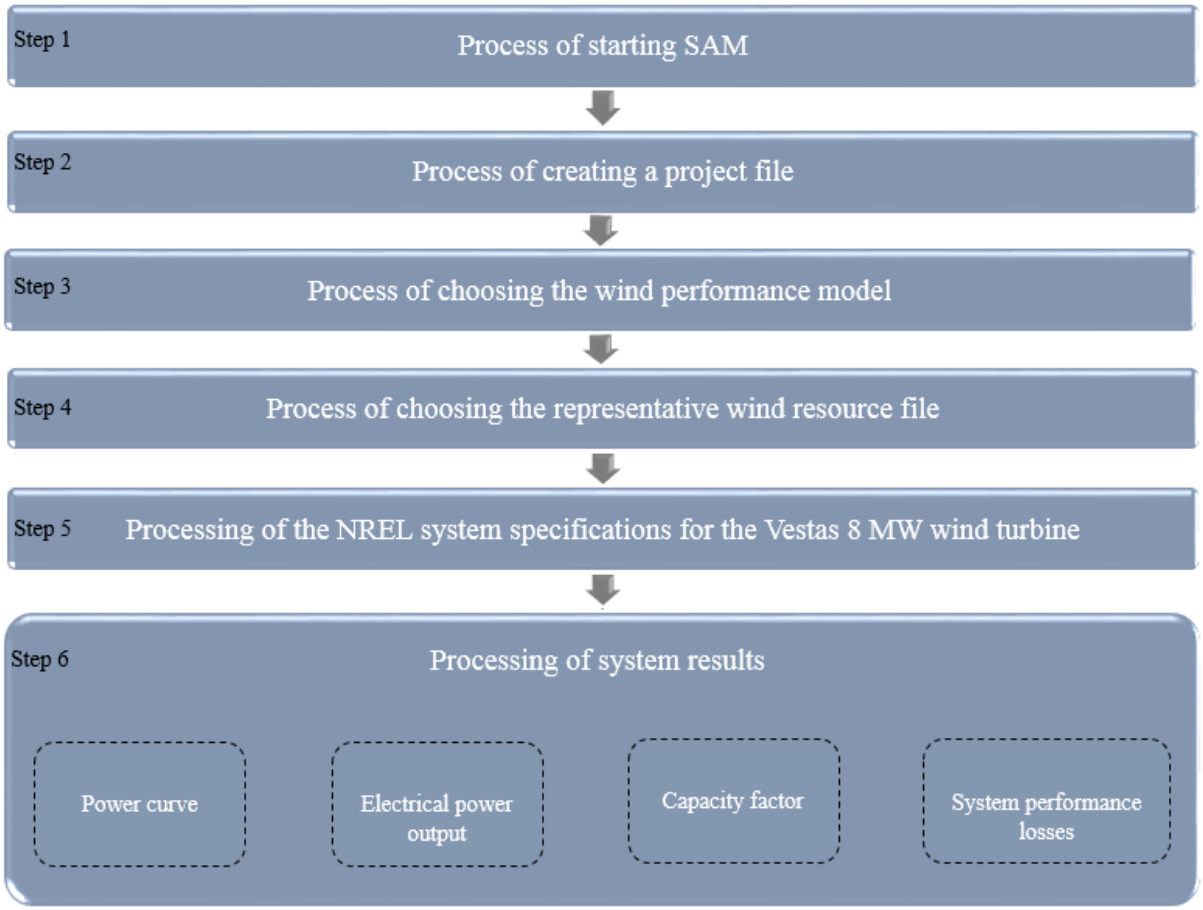

Figure 3.5. Library method of simulating Vestas 8 MW wind turbine.

3.5.1.1 Processing of NREL system specifications

Step 5 involves processing the NREL system specifications of the Vestas 8 MW wind turbine from the turbine library of SAM. Note that when this wind turbine is selected from the library, the following default values are automatically populated on the turbine input page: the rated output of 8000 kW, rotor diameter of 164 m, the hub height of 80 m and shear coefficient of 0.14. However, the hub height of 80 m is too low for the rotor diameter of 164 m. Thus, it is changed to a typical value of 140 m. Most hub heights of modern sizeable offshore wind turbines are above 100 m. The shape of the power curve is determined by these input parameters and other system specifications shown in addendum A.

3.5.1.2 Processing of system results

Processing system results for the power curve, capacity factor, electrical power output, and

system energy losses for this wind turbine is done using the same equations as the UD method. The calculations for electrical power output are based on (3.7) and (3.8), while the capacity factor is calculated by (3.9). On a similar note, the system energy losses are calculated using the percentage allocation of Table 3.5.

3.5.2 Process of simulating the Vestas 160MW wind farm

The Vestas 160 MW wind farm consists of 20 Vestas 8 MW wind turbines. Each wind turbine has the NREL system specifications from the library of SAM. Figure 3.6 explains the process of simulating this wind farm. Note that the processes involved in steps 1 to 4 have been discussed in Section 3.4.1.1 to 3.4.1.4. Similarly, the process for step 5 is also the same, as explained in Section 3.5.1.1. With that in mind, this section only shows the process required in steps 6 and 7 of Figure 3.6.

3.5.2.1 Processing of parameters for the wind farm layout

Apart from the system nameplate capacity, the Vestas 160 MW wind farm's layout parameters are the same as those for UD wind farms, shown in Table 3.4. The processing of these parameters on the SAM wind farm input page is similar to the 180MW wind farm, illustrated in B.3 of addendum B.

3.5.2.2 Processing of system results

The system electrical power output of the Vestas 160 MW wind farm is calculated using (3.7) and (3.8), whereas the capacity factor is determined by (3.9). System energy losses are computed as a percentage of annual gross energy, based on the percentage allocation of energy losses shown in Table 3.5.

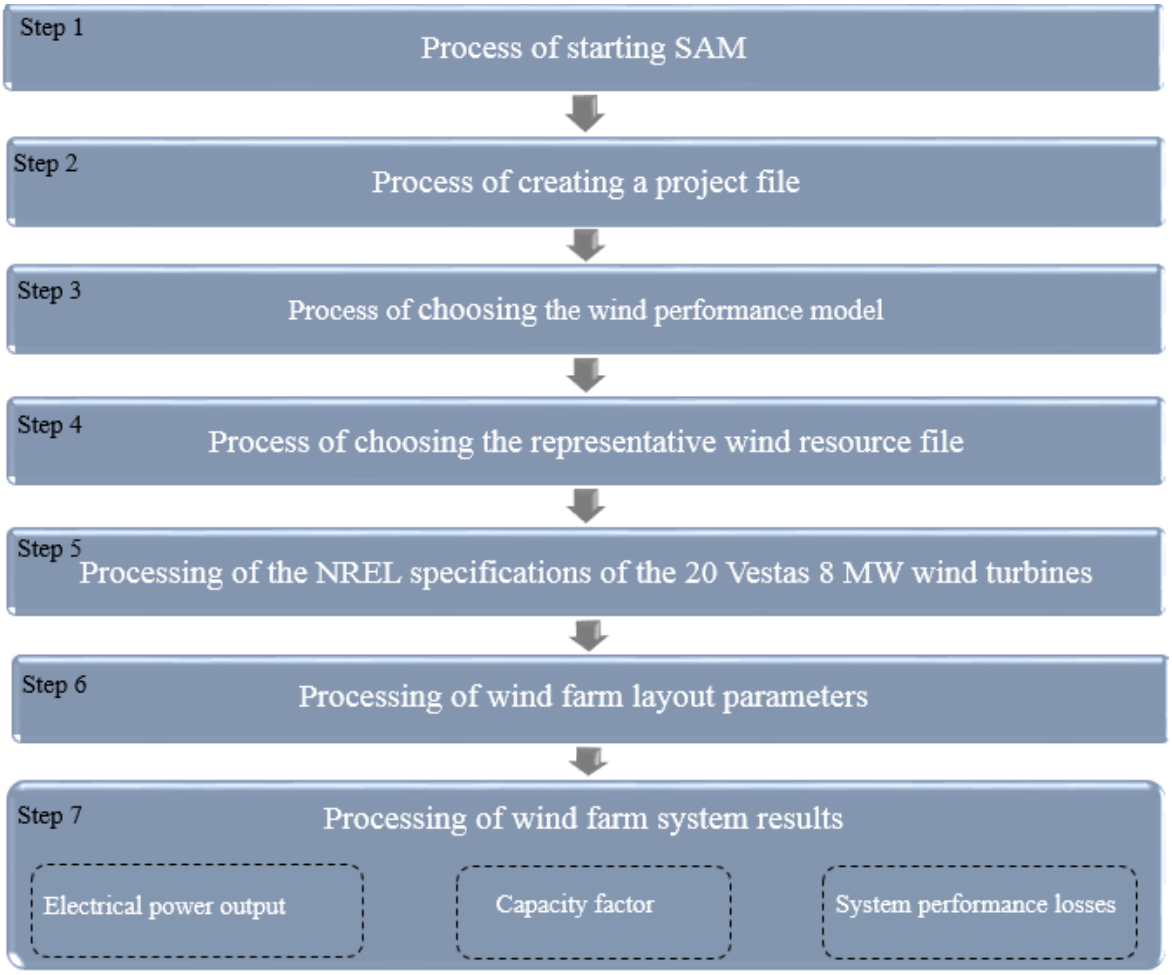

Figure 3.6. Library method of simulating Vestas 160 MW wind farm.

3.6 PARAMETRICS METHOD OF IMPLEMENTING SYSTEM SPECIFICATIONS AND TESTING MODEL IN SAM SIMULATOR

The dependence of output variables (energy production, capacity factor, system energy losses) on the input variables (rotor diameter, hub height, maximum tip speed, rated power output) is further explored using parametric simulations. This process assigns more than one value to one or more input variables to create graphs that show the relationship between the outputs (results) and the input variables. Figure 3.7 shows the procedure of performing parametric simulations. The input system for setting up variables is shown in B.5 of addendum B.

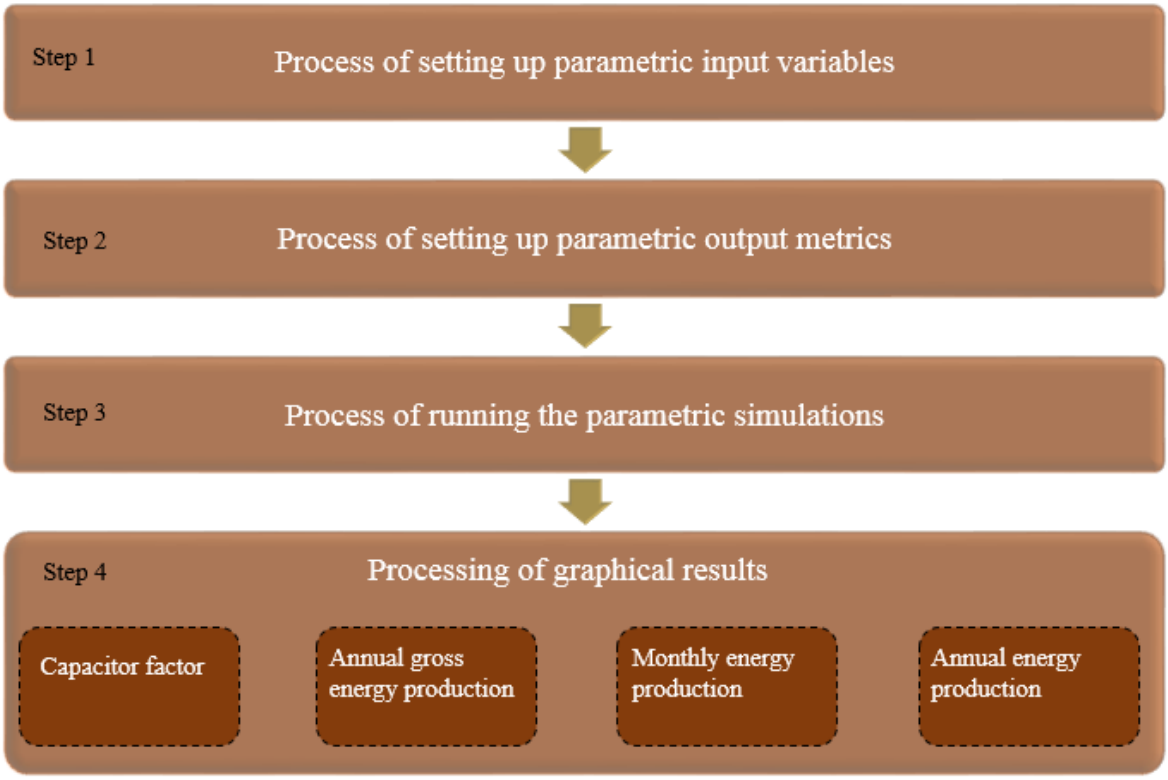

Figure 3.7. Parametric method of simulating input and output variables.

3.6.1 Process of setting up input variables

The chosen parametric input variables include rotor diameter, rated power output, hub height and maximum tip speed. Table 3.7 shows the values assigned to these variables. An increment factor of 12.5% is used on all the variables.

Table 3.7 Input variables for parametric simulations.

Hub height	Maximum tip speed	Rated power output	Rotor diameter
105 m	104 m/s	8000 kW	164 m
118.125 m	117 m/s	9000 kW	184.5 m
131.25 m	130 m/s	10000 kW	205 m
144.375 m	143 m/s	11000 kW	225.5 m
157.5 m	156 m/s	12000 kW	246 m

3.6.2 Process of setting up output metrics

The following variables are chosen as output metrics on the input page for parametric simulations: capacity factor, annual gross energy, monthly and annual energy production. The results for these metrics appear after running the parametric simulations for the input variables.

3.6.3 Process of running the simulations

An example of running the parametric simulations for the input variable of hub height is shown in B.5 of addendum B. A similar procedure is done even for the other three input variables. The graphical results of the simulations are shown in Section 4.6 of Chapter 4.

3.7 SUMMARY

An SSTM for increasing the size and testing performance of specifications for wind turbines is designed in this chapter. This model has four operations levels: data input system, turbine system, wind farm system and simulator system. The data input system is responsible for processing UD and typical specifications for wind turbines. For this study, the source of UD system specifications is the Vestas 8 MW wind turbine. The rated power output, hub height, maximum tip speed and rotor diameter of this wind turbine are increased in the turbine system using the linear equation $U = 0.125Wn + W$. On a different note, the wind farm system determines the system size, wind turbine layout, and the control of wake effects on the wind farm.

At the other end of the model, the simulator system bears the responsibility of simulating all the processed parameters from the turbine and wind farm systems. The viability of SSTM is tested in a SAM simulator using two methods: UD and library techniques. In the UD method, specifications of four wind turbines and wind farms are derived from the turbine and wind farm systems of SSTM and then simulated. The library method involves the simulation of a baseline wind turbine and wind farm using NREL library specifications of SAM.

Performance metrics between these two methods involve capacity factor, system energy losses, and energy production. The relationship between these performance metrics and the input variables are further analyzed with parametric simulations.

CHAPTER 4 PERFORMANCE ANALYSIS OF SYSTEM SPECIFICATIONS AND TESTING MODEL

4.1 CHAPTER OVERVIEW

A practical realization of results that measure the performance of SSTM in the SAM simulator is given in this chapter. These findings are presented as UD, baseline and parametric results. UD results show the performance of four offshore wind turbines and wind farms whose system specifications are determined by the turbine and wind farm systems. On a different note, baseline results describe the Vestas 8 MW wind turbine and Vestas 160 MW wind farm's performance, whose system specifications are from the library of SAM. Both UD and baseline results are given in terms of annual gross energy, power curves, monthly energy, system energy losses, and annual energy after losses. Besides, the dependence of output metrics on crucial input variables is given as graphical results.

4.2 INTRODUCTION

After running the simulations for each wind turbine and wind farm, SAM made a series of 8760 hour by hour calculations. These calculations compute an estimate of the power curve, capacitor factor and the anticipated hourly electricity production. Concerning this production, the computed system results are presented as annual gross energy, system energy losses, annual energy and monthly energy reports. Unlike the annual gross energy results,

annual energy presents the total electricity generated after considering system energy losses. The energy losses consist of wake losses, availability losses, electrical losses, turbine losses, environmental losses and curtailment losses. All of the above results are presented according to their source of system specifications in SSTM. Thus, they are classified as UD, baseline and parametric results. UD results are from four different wind turbines and wind farms, whose specifications are derived from the equation $U = 0.125Wn + W$. For this reason, these results are given according to 12.5%, 25%, 37.5% and 50% system specifications.

Similarly, baseline results refer to the Vestas 8 MW wind turbine and Vestas 160 MW wind farm's performance. The source of specifications for this wind turbine and the wind farm is the NREL library of SAM. These specifications are the reference points for the performance of UD results. On the other hand, the graphical relationship between UD input variables and output metrics of SSTM is provided as parametric results. About their significance, UD results are beneficial to researchers and designers. They can optimize the design and operation of large wind turbines whose rated power output is higher than 8 MW. Additionally, they are valuable for understanding the impact of scaling up system specifications on large wind turbines' energy production.

4.3 PERFORMANCE RESULTS OF USER-DEFINED WIND TURBINES

Performance results of UD specifications for the 9 MW, 10 MW, 11 MW and 12 MW wind turbines are presented in this section using tables and figures. For each wind turbine, results are shown in terms of annual gross energy, system energy losses, annual energy, capacity factor, power curves and monthly energy. The drivetrain design for these results is a single stage-low speed generator and direct drive systems. Based on these generator systems, the capacity factor, monthly energy and annual energy are calculated using (4.1), (4.2) and (4.3), respectively.

$$Capacity\ factor = \frac{Net\ annual\ energy\left(kWh/yr\right)}{System\ capacity\left(kW\right)/8760\left(h/yr\right)} \tag{4.1}$$

$$Monthly\ energy = Sum\ of\ hourly\ energy\ delivered\ for\ a\ month \tag{4.2}$$

$$Annual\ energy = Sum\ of\ hourly\ energy\ delivered\ for\ 1\ year \tag{4.3}$$

On the one hand, all system energy losses are calculated as percentages of the annual gross energy. The percentage allocation is graphically shown in Figure 4.1.

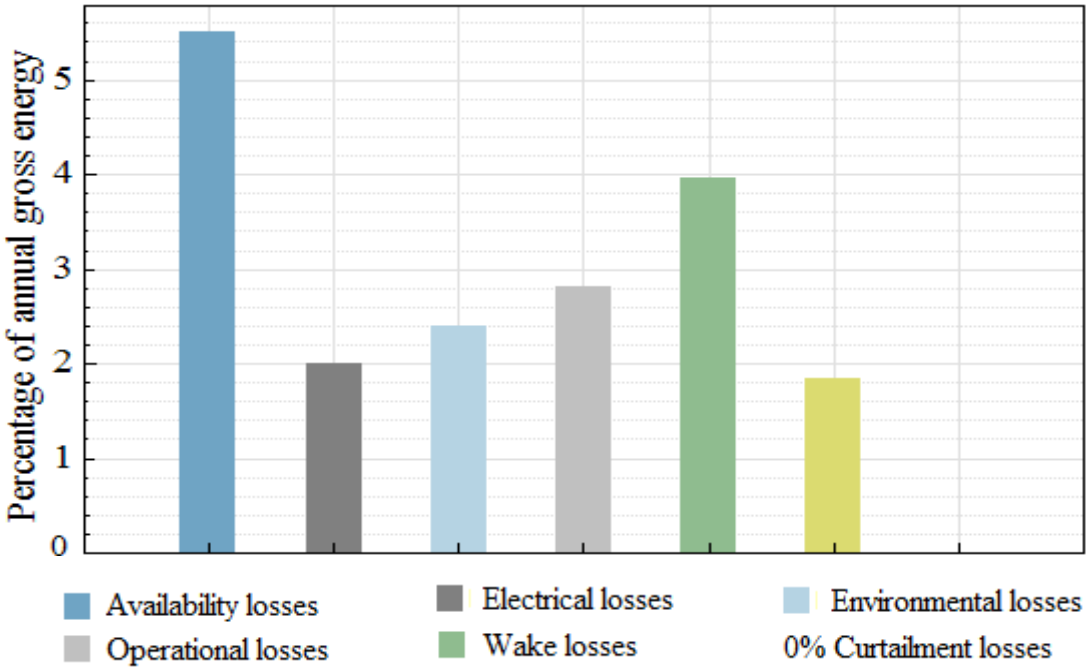

Figure 4.1. Percentage allocation of system energy losses.

4.3.1 Performance results of the 9 MW wind turbine

In the first year of operation, the performance results of the 12.5% system specifications of the 9 MW wind turbine are shown in Tables 4.1, 4.2 and Figure 4.2. Table 4.1 presents the annual gross energy, capacity factor, annual energy after losses, and system energy losses. On a similar note, Table 4.2 gives results for monthly energy production. All the results from these tables are generated from the direct-drive and single stage-low speed generators. Furthermore, the power curve for this wind turbine is given in Figure 4.2. Finally, Table 4.3 shows the average daily minimum and maximum values of wind direction, air temperature, wind speed, and pressure under which the results are produced. The weather conditions for December produced the highest monthly energy production.

Table 4.1 Annual energy, capacity factor and energy losses for 9 MW wind turbine.

Performance metrics (year 1)	Single stage-low speed generator	Direct drive
Annual gross energy (GWh)	36.265	36.598
Annual energy after losses (GWh)	30.261	30.539
Capacity factor (%)	38.4	38.7
System energy losses (GWh)		
Availability losses	1.995	2.013
Electrical losses	0.725	0.732
Environmental losses	0.870	0.878
Operational losses	1.015	1.025
Turbine losses	1.432	1.446
Wake losses	0.675	0.681
Curtailment losses	0.000	0.000

Table 4.2 Monthly energy production of the 9 MW wind turbine.

Month	Monthly energy production (MWh)	
	Single stage-low speed generator	Direct drive
January	2809.820	2831.350
February	2140.920	2164.110
March	2785.410	2806.290
April	2256.420	2280.020
May	2263.790	2288.240
June	3000.620	3024.020
July	2633.790	2660.410
August	2488.360	2516.200
September	2034.020	2055.630
October	2417.220	2441.680
November	2274740	2294.800
December	3155.990	3176.490

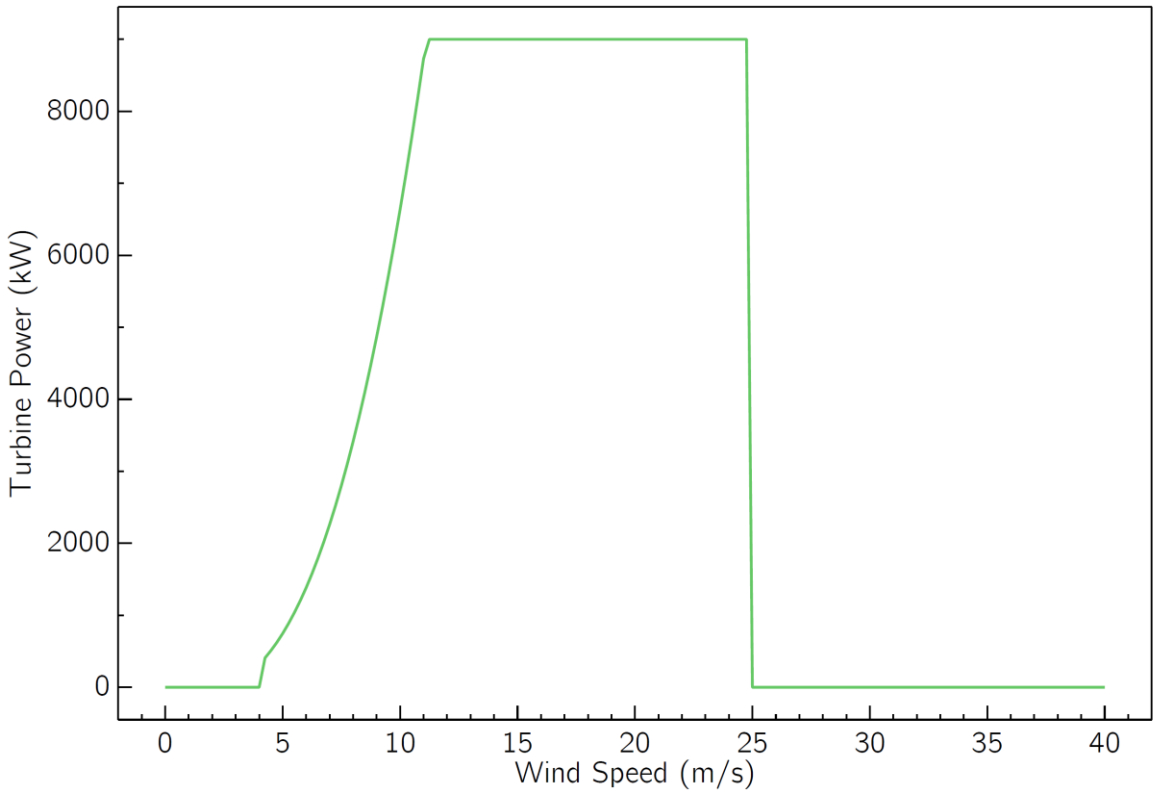

Figure 4.2. The power curve of a 9 MW wind turbine.

Table 4.3 Weather conditions for the 9 MW wind turbine.

Weather conditions	Average daily minimum values		Average daily maximum values	
	December	Annual	December	Annual
Wind direction (°)	64.387	88.921	299.193	327.836
Air temperature (°C)	8.684	9.872	11.326	12.572
Wind speed (m/s)	5.351	4.579	14.501	12.210
Pressure (atm)	0.985	0.987	0.995	0.995

4.3.2 Performance results of the 10 MW wind turbine

Tables 4.4, 4.5, and Figure 4.3 show how the 25% system specifications of the 10 MW wind turbine performed on the direct drive and single stage-low speed generator. Table 4.4 states the annual energy production, capacity factor and system energy losses of this wind turbine. On the other hand, monthly energy production is given in Table 4.5, whereas its power curve is depicted in Figure 4.3. These results are for the first year of operation and are generated

under the weather conditions shown in Table 4.6. This table shows the average daily minimum and maximum values for air temperature, wind direction, pressure, and wind speed. The highest monthly energy production occurred under the December weather conditions.

Table 4.4 Annual energy, capacity factor and energy losses for 10 MW wind turbine.

Performance metrics (year 1)	Single stage-low speed generator	Direct drive
Annual gross energy (GWh)	42.599	42.938
Annual energy after losses (GWh)	35.546	35.829
Capacity factor (%)	40.6	40.9
System energy losses (GWh)		
Availability losses	2.343	2.362
Electrical losses	0.852	0.859
Environmental losses	1.022	1.031
Operational losses	1.193	1.202
Turbine losses	1.683	1.696
Wake losses	0.792	0.799
Curtailment losses	0.000	0.000

Table 4.5 Monthly energy production of the 10 MW wind turbine.

Month	Monthly energy production (MWh)	
	Single stage-low speed generator	Direct drive
January	3241.730	3264.510
February	2516.180	2540.190
March	3229.280	3250.600
April	2647.190	2671.430
May	2678.780	2704.880
June	3547.890	3572.430
July	3128.750	3153.280
August	3019.900	3047.470
September	2413.610	2435.470
October	2861.400	2885.410
November	2639.900	2661.070
December	3621.680	3642.310

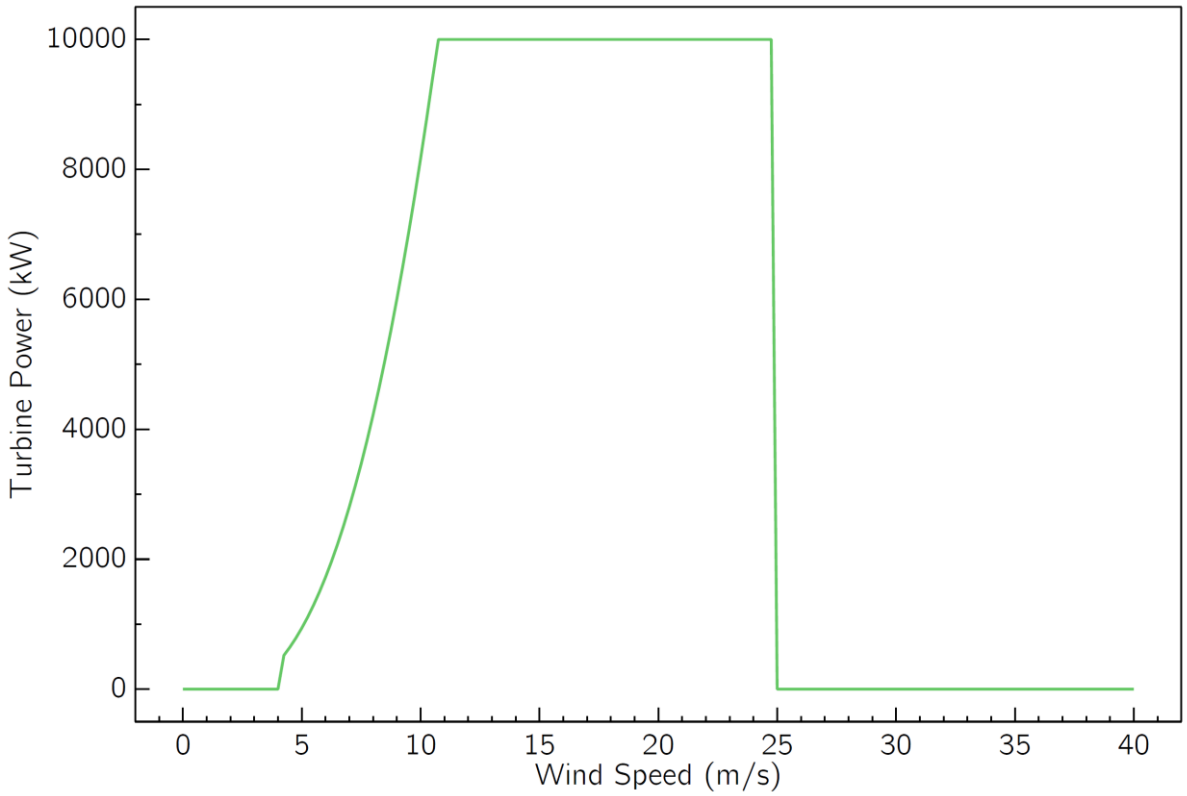

Figure 4.3. The power curve of a 10 MW wind turbine.

Table 4.6 Weather conditions for the 10 MW wind turbine.

Weather conditions	Average daily minimum values		Average daily maximum values	
	December	Annual	December	Annual
Wind direction (^{o})	64.387	88.9205	299.193	327.836
Air temperature (^{o}C)	8.652	9.8582	11.306	12.645
Wind speed (m/s)	5.406	4.6305	14.688	12.393
Pressure (atm)	0.983	0.9858	0.994	0.993

4.3.3 Performance results of the 11 MW wind turbine

The 37.5% system specifications of the 11 MW wind turbine give rise to the performance results shown in Tables 4.7, 4.8 and Figure 4.4. The capacity factor, system energy losses and annual energy production in the first year of operation are shown in Table 4.7. Monthly energy production is provided in Table 4.8. Also, the power curve for this wind turbine is

illustrated in Figure 4.4. All the results are obtained on direct drive and single stage-low speed generators under the weather conditions of Table 4.9. June's air temperature, wind direction, pressure, and wind speed produced the highest monthly energy production.

Table 4.7 Annual energy, capacity factor and energy losses for 11 MW wind turbine.

Performance metrics (year 1)	Single stage-low speed generator	Direct drive
Annual gross energy (GWh)	49.051	49.405
Annual energy after losses (GWh)	40.930	41.226
Capacity factor (%)	42.5	42.8
System energy losses (GWh)		
Availability losses	2.698	2.717
Electrical losses	0.981	0.988
Environmental losses	1.177	1.186
Operational losses	1.373	1.383
Turbine losses	1.937	1.952
Wake losses	0.912	0.919
Curtailment losses	0.000	0.000

Table 4.8 Monthly energy production of the 11 MW wind turbine.

Month	Monthly energy production (MWh)	
	Single stage-low speed generator	Direct drive
January	3687.710	3712.680
February	2910.980	2936.480
March	3680.970	3703.050
April	3052.970	3077.540
May	3115.010	3143.480
June	4103.000	4128.750
July	3610.800	3636.180
August	3547.390	3575.230
September	2797.640	2820.680
October	3304.920	3328.920
November	3027.790	3051.250
December	4090.870	4112.030

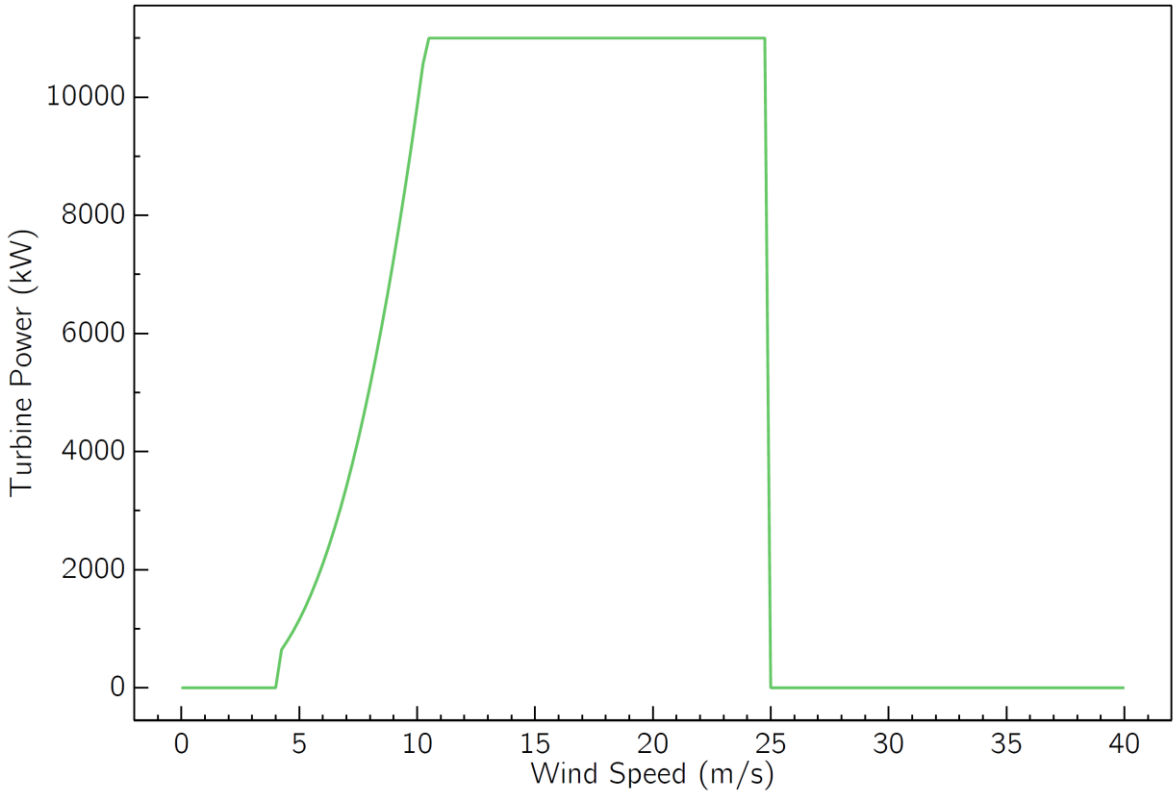

Figure 4.4. The power curve of an 11 MW wind turbine.

Table 4.9 Annual weather conditions for the 11 MW wind turbine.

Weather conditions	Average daily minimum values		Average daily maximum values	
	June	Annual	June	Annual
Wind direction (°)	178.194	92.660	356.710	328.118
Air temperature (°C)	10.609	9.848	12.705	12.700
Wind speed (m/s)	6.501	4.675	12.956	12.576
Pressure (atm)	0.984	0.985	0.990	0.992

4.3.4 Performance results of the 12 MW wind turbine

Results for the performance of the 50% system specifications of the 12 MW wind turbine are provided in Tables 4.10, 4.11 and Figure 4.5. The annual energy production, capacity factor and system energy losses for the first year of operation are shown in Table 4.10. At the same time, monthly energy production is reported in Table 4.11. Figure 4.5 shows the power curve for the wind turbine. The weather conditions of these results are shown in Table

4.12. This table gives the average daily minimum and maximum values of pressure, wind speed, air temperature, and wind direction under which the results are obtained. The highest monthly energy production is generated under the December weather conditions.

Table 4.10 Annual energy, capacity factor and energy losses for 12 MW wind turbine.

Performance metrics (year 1)	Single stage-low speed generator	Direct drive
Annual gross energy (GWh)	80.831	80.831
Annual energy after losses (GWh)	67.449	67.449
Capacity factor (%)	64.2	64.2
System energy losses (GWh)		
Availability losses	4.446	4.446
Electrical losses	1.617	1.617
Environmental losses	1.940	1.940
Operational losses	2.263	2.263
Turbine losses	3.193	3.193
Wake losses	1.503	1.503
Curtailment losses	0.000	0.000

Table 4.11 Monthly energy production of the 12 MW wind turbine.

Month	Monthly energy production (MWh)	
	Single stage-low speed generator	Direct drive
January	6062.240	6062.240
February	4849.680	4849.680
March	5775.010	5775.010
April	5175.010	5175.010
May	5609.220	5609.220
June	6107.290	6107.290
July	5907.910	5907.910
August	5706.810	5706.810
September	5162.400	5162.400
October	5417.990	5417.990
November	5482.530	5482.530
December	6193.030	6193.030

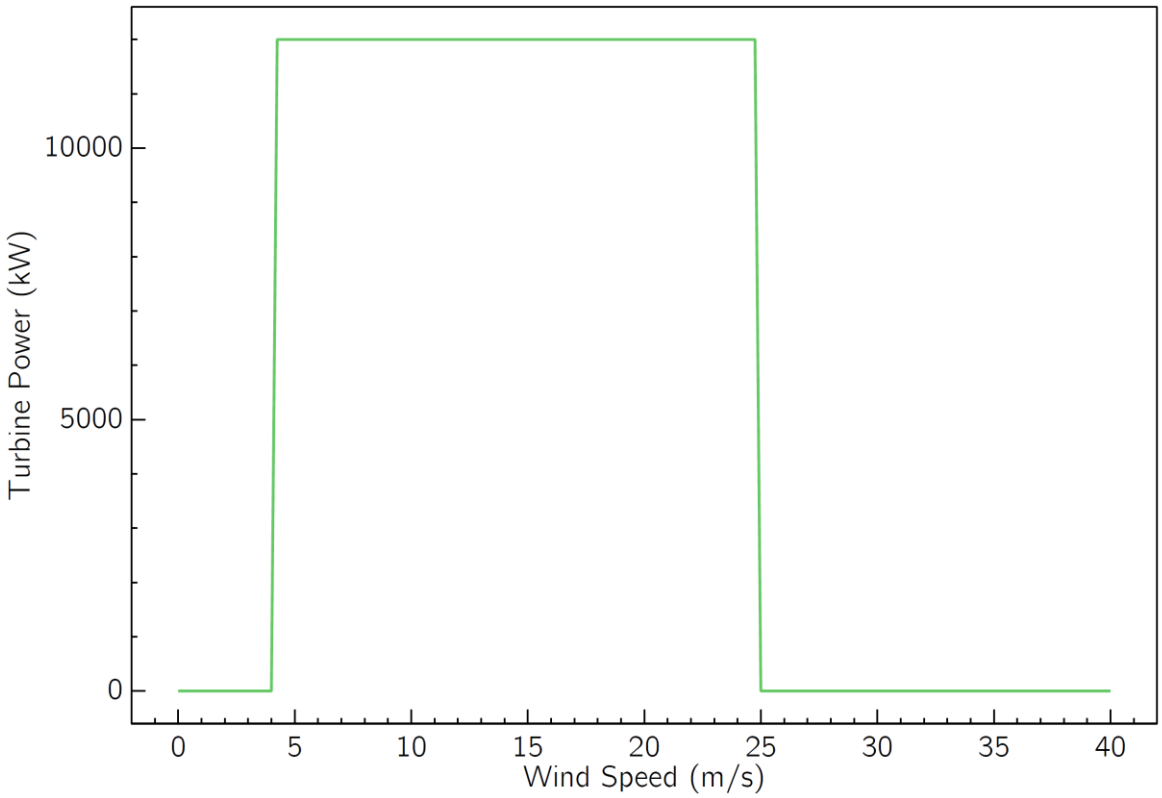

Figure 4.5. The power curve of a 12 MW wind turbine.

Table 4.12 Weather conditions for the 12 MW wind turbine.

Weather conditions	Average daily minimum values		Average daily maximum values	
	December	Annual	December	Annual
Wind direction (°)	64.645	92.660	299.645	328.118
Air temperature (°C)	8.628	9.848	11.302	12.700
Wind speed (m/s)	5.528	4.732	15.071	12.730
Pressure (atm)	0.982	0.985	0.993	0.992

4.4 PERFORMANCE RESULTS OF USER-DEFINED WIND FARMS

This section provides the outcome of using 12.5%, 25%, 37.5% and 50% UD system specifications on offshore wind farms. The performance metrics for these wind farms are equally obtained using (4.1), (4.2), (4.3) and Figure 4.1. Equation (4.1) is used to calculate the capacity factor. Monthly and annual energy production is calculated using 4.2 and 4.3, respectively. The wind farms' system energy losses are obtained using the percentage

allocations shown in Figure 4.1. Moreover, just like the UD wind turbines results, the wind farm results are also obtained on the direct drive and single stage-low speed generators.

4.4.1 Performance results of the 180 MW wind farm

Tables 4.13 and 4.14 are the 12.5% system specifications' performance results on the 180 MW wind farm. Capacity factor, system energy losses and annual energy production is shown in Table 4.13. Similarly, monthly energy production for this wind turbine is indicated in Table 4.14. The weather conditions of these results for air temperature, wind direction, pressure, and wind speed are revealed in Table 4.3. December weather conditions generated the highest energy production for this wind farm.

Table 4.13 Annual energy, capacity factor and energy losses for 180 MW wind farm.

Performance metrics (year 1)	Single stage-low speed generator	Direct drive
Annual gross energy (GWh)	725.297	731.964
Annual energy after losses (GWh)	600.709	606.172
Capacity factor (%)	38.1	38.4
System energy losses (GWh)		
Availability losses	39.891	40.258
Electrical losses	14.506	14.639
Environmental losses	17.407	17.567
Operational losses	20.308	20.495
Turbine losses	28.649	28.913
Wake losses	13.491	13.615
Curtailment losses	00.000	00.000

Table 4.14 Monthly energy production of the 180 MW wind farm.

Month	Monthly energy production (MWh)	
	Single stage-low speed generator	Direct drive
January	55.805	56.226
February	42.464	42.919
March	55.315	55.728
April	44.778	45.241
May	44.862	45.340
June	59.542	59.997
July	52.295	52.819
August	49.299	49.845
September	40.411	40.835
October	47.979	48.464
November	45.212	45.603
December	62.750	63.156

4.4.2 Performance results of the 200 MW wind farm

The performance results of using the 25% system specifications on the direct drive and single stage-low speed generators for the 200 MW wind farm are described in Tables 4.15 and 4.16. Capacity factor, system energy losses and annual energy production are provided in Table 4.15. Monthly energy production is shown in Table 4.16, while the weather conditions for monthly and annual results are stated in Table 4.6. The highest monthly energy production is produced under the December weather conditions.

Table 4.15 Annual energy, capacity factor and energy losses for 200 MW wind farm.

Performance metrics (year 1)	Single stage-low speed generator	Direct drive
Annual gross energy (GWh)	851.973	858.750
Annual energy after losses (GWh)	706.072	711.627
Capacity factor (%)	40.3	40.6%
System energy losses		
Availability losses	46.859	47.231
Electrical losses	17.040	17.175
Environmental losses	20.447	20.610
Operational losses	23.855	24.045
Turbine losses	33.653	33.921
Wake losses	15.847	15.973
Curtailment losses	00.000	00.000

Table 4.16 Monthly energy production of the 200 MW wind farm.

Month	Monthly energy production (MWh)	
	Single stage-low speed generator	Direct drive
January	64.400	64.844
February	49.937	50.409
March	64.200	64.621
April	52.547	53.026
May	53.107	53.616
June	70.416	70.898
July	62.197	62.680
August	59.904	60.447
September	47.974	48.402
October	56.855	57.329
November	52.478	52.892
December	72.056	72.465

4.4.3 Performance results of the 220 MW wind farm

Tables 4.17 and 4.18 presents the performance results of the 37.5% system specifications on the direct drive and single stage-low speed generators for the 220 MW wind farm. System energy losses, capacity factor and annual energy production are presented in Table 4.17. At the same time, monthly energy production is shown in Table 4.18. Weather conditions for the results are presented in Table 4.9. It is observed that the highest monthly energy production occurred during the December weather conditions.

Table 4.17 Annual energy, capacity factor and energy losses for 220 MW wind farm.

Performance metrics (year 1)	Single stage-low speed generator	Direct drive
Annual gross energy (GWh)	981.010	988.110
Annual energy after losses (GWh)	813.397	819.238
Capacity factor (%)	42.2	42.5%
System energy losses (GWh)		
Availability losses	53.956	54.346
Electrical losses	19.620	19.762
Environmental losses	23.544	23.715
Operational losses	27.468	27.667
Turbine losses	38.750	39.030
Wake losses	18.247	18.379
Curtailment losses	00.000	00.000

Table 4.18 Monthly energy production of the 220 MW wind farm.

Month	Monthly energy production (MWh)	
	Single stage-low speed generator	Direct drive
January	73.256	73.745
February	57.793	58.299
March	73.223	73.659
April	60.653	61.141
May	61.758	62.317
June	81.468	81.973
July	71.827	72.326
August	70.436	70.990
September	55.633	56.086
October	65.717	66.191
November	60.196	60.656
December	81.438	81.856

4.4.4 Performance results of the 240 MW wind farm

Tables 4.19 and 4.20 show the 50% system specifications' performance results on direct drive and single stage-low speed generators for the 240 MW wind farm. This wind farm generated annual energy, system energy losses and capacity factor shown in Table 4.19. It also produced the monthly energy indicated in Table 4.20. On the other side, Table 4.12 presents the average daily minimum and maximum air temperature, wind speed, pressure and wind direction for the wind farm.

Table 4.19 Annual energy, capacity factor and energy losses for 240 MW wind farm.

Performance metrics (year 1)	Single stage-low speed generator	Direct drive
Annual gross energy (GWh)	1616.620	1616.620
Annual energy after losses (GWh)	1340.186	1340.186
Capacity factor (%)	63.7	63.7
System energy losses (GWh)		
Availability losses	88.914	88.914
Electrical losses	32.332	32.332
Environmental losses	38.799	38.799
Operational losses	45.265	45.265
Turbine losses	63.857	63.857
Wake losses	30.069	30.069
Curtailment losses	00.000	00.000

Table 4.20 Monthly energy production of the 240 MW wind farm.

Month	Monthly energy production (MWh)	
	Single stage-low speed generator	Direct drive
January	120.474	120.474
February	96.4859	96.4859
March	114.992	114.992
April	102.670	102.670
May	111.354	111.354
June	121.584	121.584
July	117.554	117.554
August	113.512	113.512
September	101.956	101.956
October	107.686	107.686
November	108.809	108.809
December	123.108	123.108

4.5 RESULTS FOR BASELINE WIND TURBINE AND WIND FARM

The baseline results for the Vestas 8 MW wind turbine and Vestas 160 MW wind farm are presented in this section. They are the reference points for the performance of UD wind turbines and wind farms. Like UD results, their performance is equally given as annual gross energy, annual energy, system energy losses, power curve and monthly energy production. Tables 4.22, 4.23 and Figure 4.6 shows these results. In addition, the prevailing weather conditions for the results are discussed in Table 4.21. The capacity factor, system energy losses and annual energy production are shown in Table 4.22. On the other part, Table 4.23 presents the monthly energy production, while Figure 4.6 shows the Vestas 8 MW wind turbine's power curve.

Table 4.21 Weather conditions for baseline wind turbine and wind farm.

Weather conditions	Average daily minimum values		Average daily maximum values	
	December	Annual	December	Annual
Wind direction (^{o})	64.645	92.660	299.645	328.118
Air temperature (^{o}C)	8.628	9.848	11.302	12.700
Wind speed (m/s)	5.438	4.655	14.824	12.522
Pressure (atm)	0.982	0.985	0.993	0.992

Table 4.22 Baseline results for annual energy, capacity factor and energy losses.

Performance metrics (year 1)	Vestas 8 MW turbine	Vestas 160 MW wind farm
Annual gross energy (GWh)	32.450	648.997
Annual energy after losses (GWh)	27.078	537.471
Capacity factor (%)	38.6	38.3
System energy losses (GWh)		
Availability losses	1.785	35.695
Electrical losses	0.649	12.980
Environmental losses	0.779	15.576
Operational losses	0.909	18.172
Turbine losses	1.282	25.635
Wake losses	0.604	12.071
Curtailment losses	0.000	00.000

Table 4.23 Monthly energy production for baseline wind turbine and wind farm.

Month	Energy production (GWh)	
	Vestas 8 MW turbine	Vestas 160 MW wind farm
January	2.481	49.260
February	1.894	37.561
March	2.474	49.140
April	1.981	39.313
May	2.023	40.058
June	2.737	54.300
July	2.373	47.129
August	2.291	45.399
September	1.843	36.622
October	2.163	42.950
November	2.031	40.362
December	2.786	55.378

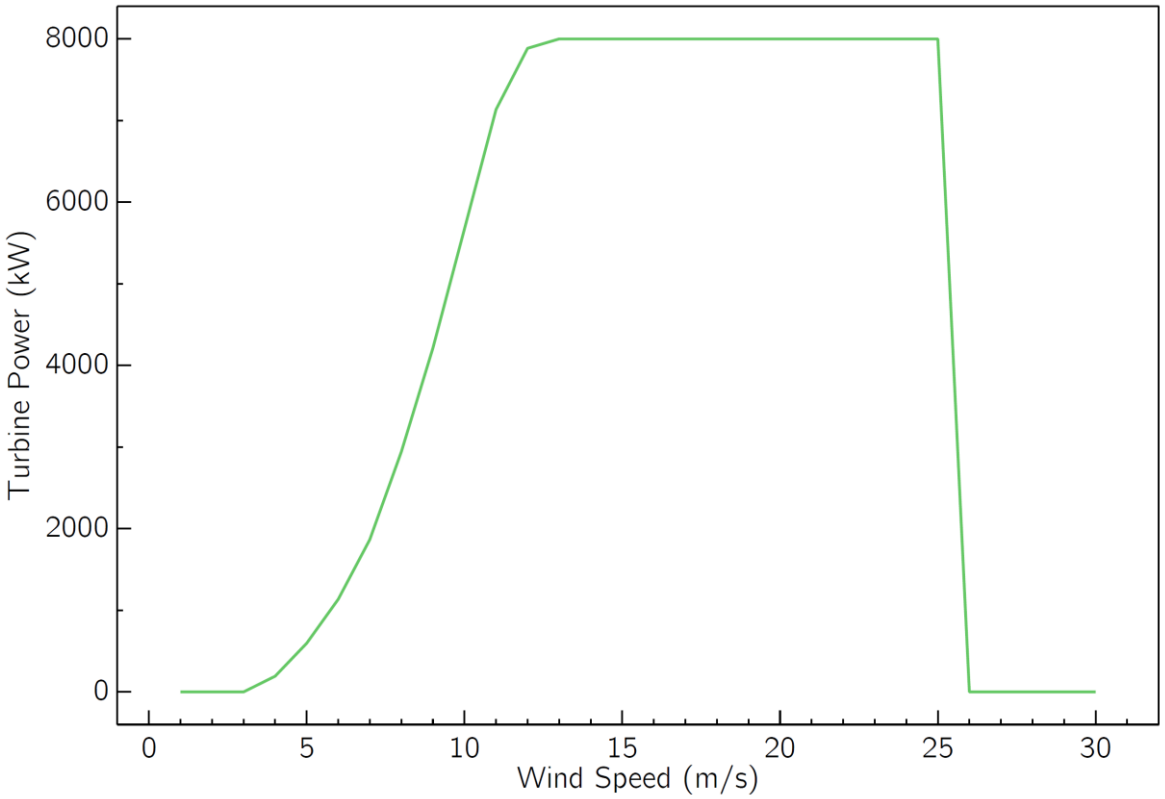

Figure 4.6. The power curve of the Vestas 8 MW wind turbine.

4.6 RESULTS FOR PARAMETRIC SIMULATIONS

The graphical results for parametric simulations of input and output variables of the equation $U = 0.125Wn + W$ are given in Figures 4.7, 4.8, 4.9, and 4.10. Figure 4.7 shows the graphical effects of input variables on annual gross energy, whereas Figure 4.8 illustrates how these variables affect the annual energy after losses. Similarly, Figures 4.9 and 4.10 show how the input variables affect the capacity factor and monthly energy production.

4.6.1 Graphical results for annual gross energy

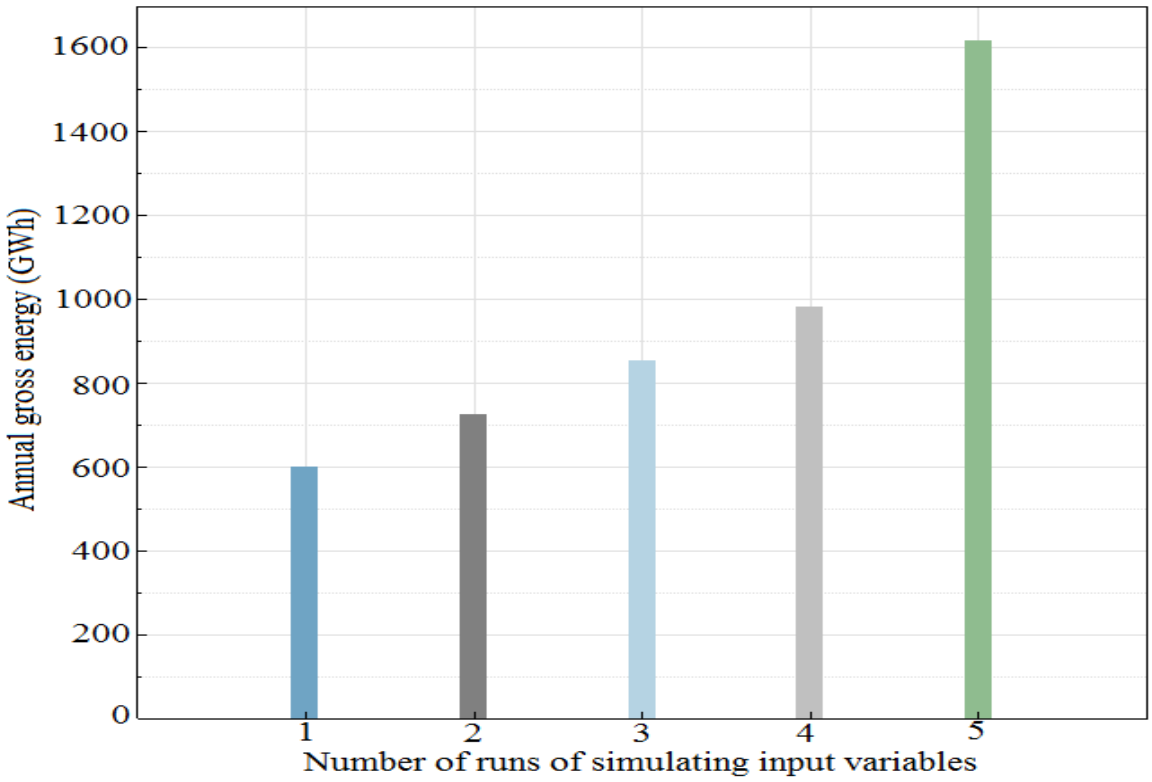

Figure 4.7. Graphical relationship of annual gross energy with input variables.

4.6.2 Graphical results for annual energy

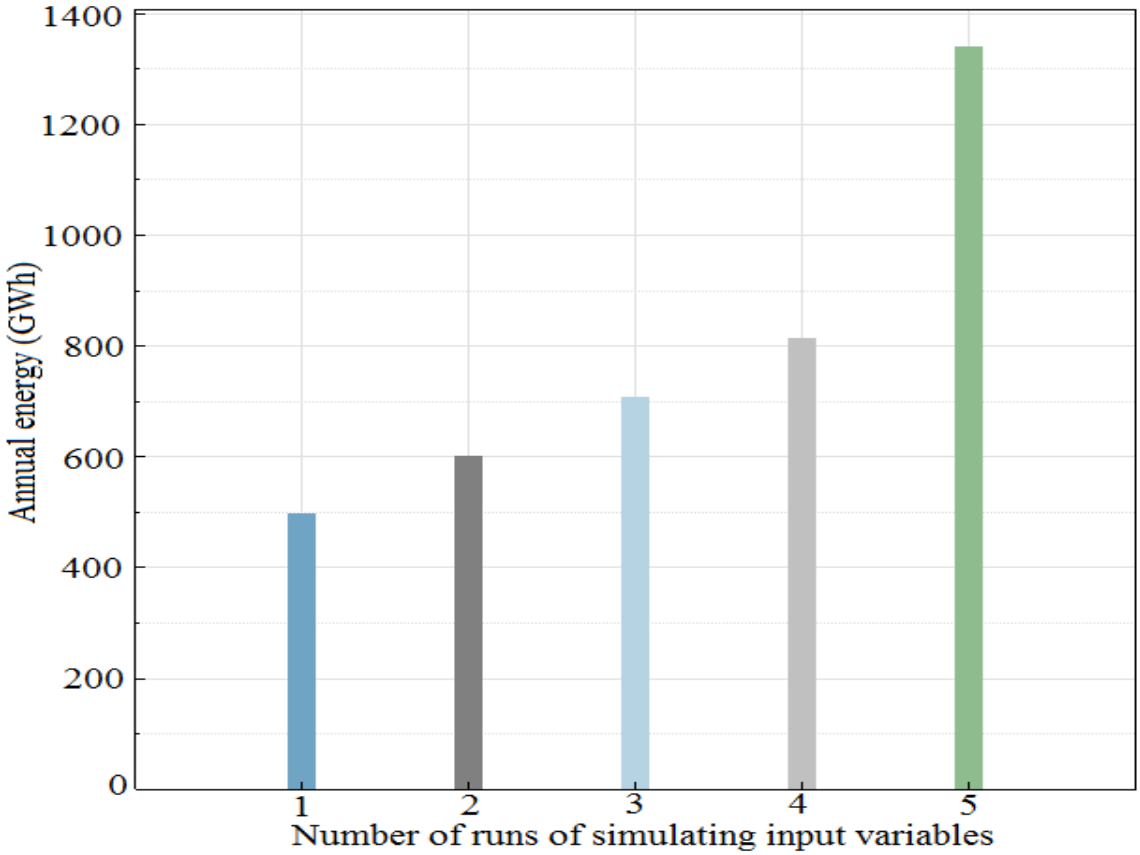

Figure 4.8. Graphical relationship of annual energy with input variables.

4.6.3 Graphical results for capacity factor

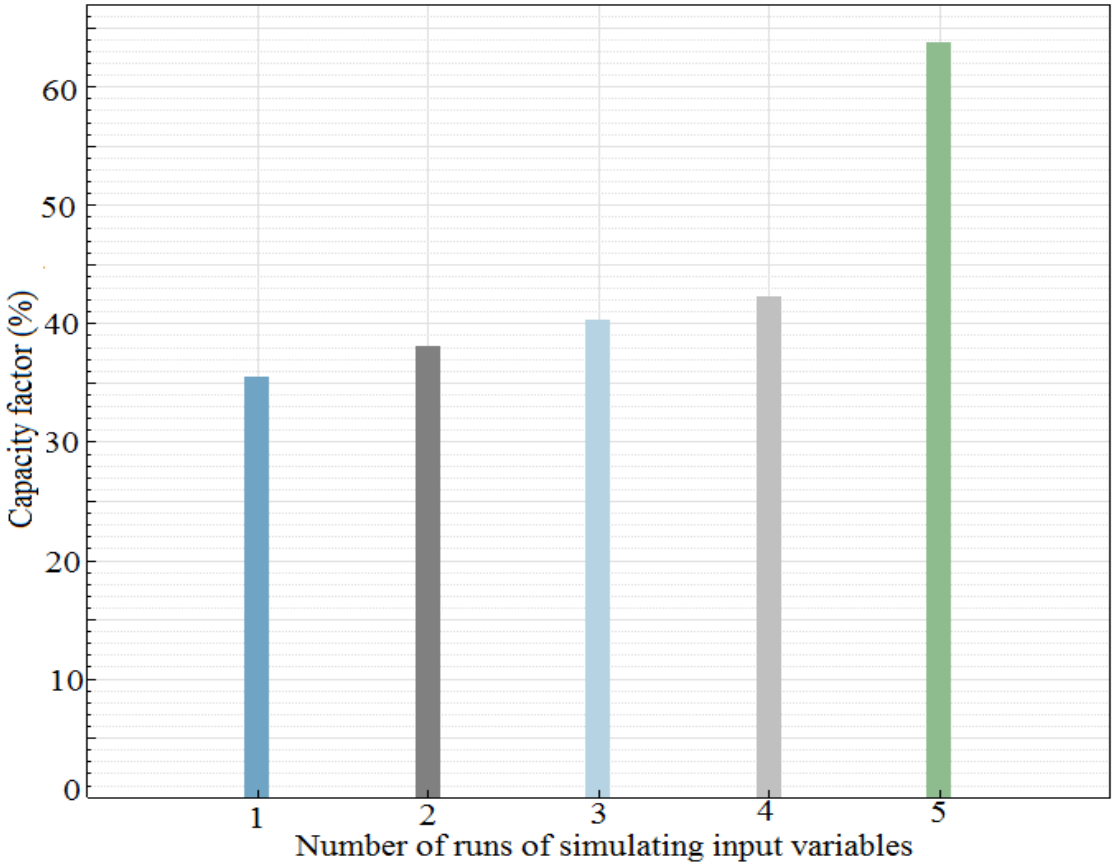

Figure 4.9. Graphical relationship of the capacity factor with input variables.

4.6.4 Graphical results for monthly energy

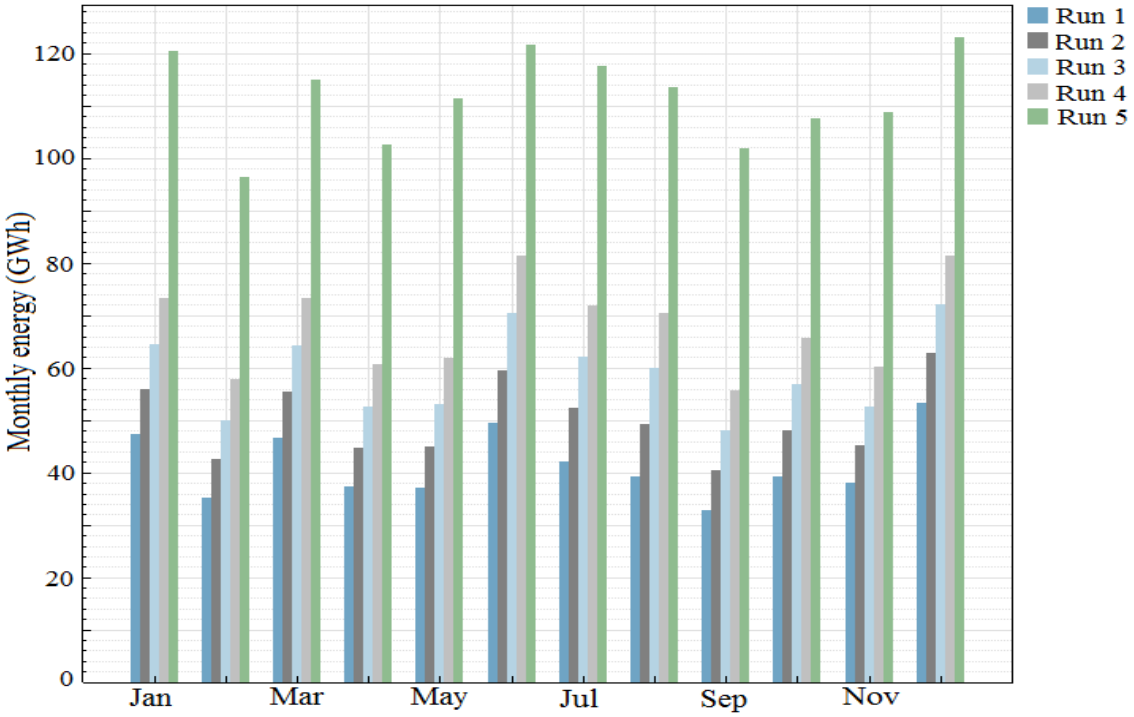

Figure 4.10. Graphical relationship of monthly energy with input variables.

4.7 SUMMARY

In this chapter, the practical outcome of the implementation of SSTM in the SAM simulator is shown using tables and figures. There are three types of results that arise from this application. The first results are for UD wind turbines and wind farms, whose system specifications are derived from the equation $\mathrm{U} = 0.125Wn + W$. These results are for the performance of the direct-drive and single stage-low speed generators on the 9 MW, 10 MW, 11 MW and 12 MW wind turbines. At the same time, the performance of these generators on the 180 MW, 200 MW, 220 MW and 240 MW wind farms is also given. On the other part, the Vestas 8 MW wind turbine and Vestas 160 MW wind farm's performance is also stated. These baseline results are the reference points to which UD wind turbines and wind farms' performance are compared. The measure of performance between UD and the

baseline wind turbines include power curves, capacity factor, annual gross energy, monthly energy, system energy losses, and annual energy after losses. System energy losses consist of availability, electrical, environmental, operational, turbine, wake, and curtailment losses. On another note, the last portion of the results are for parametric simulations, and they illustrate the dependence of output metrics on input variables. The pattern of these results graphically depicts how input variables (rated power output, rotor diameter, maximum tip speed, hub height) affect annual gross energy, monthly energy, capacity factor and annual energy after losses.

CHAPTER 5 THE ENERGY POTENTIAL OF LARGE WIND TURBINES AND WIND FARMS

5.1 CHAPTER OVERVIEW

The improvement in capacity factor and energy production that comes with increasing the size of four system specifications of the Vestas 8 MW wind turbine is examined in this chapter. For the most part, the focus of the discussion is on how 12.5%, 25%, 37.5% and 50% system specifications improve the energy production of large wind turbines. This energy production is on direct-drive and single stage-low speed generators of four large offshore wind turbines and wind farms. With reference to a baseline wind turbine and wind farm, points of comparison for this performance include power curves, capacity factor, system energy losses, monthly and annual energy production. In addition, the chapter also discusses the weather conditions under which the wind turbines and wind farms operated.

5.2 INTRODUCTION

Given the current global wind energy demand, large wind turbines are vital in accelerating the growth pace for wind energy investments and wind power installations. For this reason, the findings of this study are essential to the growth and development of large wind turbines. Electrical engineers can use this knowledge to assess the performance of these wind turbines during the initial design phase. Thus, this chapter discusses the energy potential that comes with developing large offshore wind turbines. The main interest is in the performance of large offshore wind turbines with a rated capacity of 9 MW, 10 MW, 11 MW, 12 MW and

their respective wind farms. System specifications of these wind turbines and wind farms are a modification of the Vestas 8 MW wind turbine. The four parameters that have been modified are rated power output, rotor diameter, hub height and maximum tip speed. Each of these parameters has been increased in size four times in the turbine system of SSTM using the linear equation $U = 0.125Wn + W$. As a result of this increase, 12.5%, 25%, 37.5% and 50% system specifications of large offshore wind turbines have been designed. The impact of these newly designed specifications on energy production is tested on the direct drive and single stage-low speed generators.

A baseline system for assessing these specifications' viability is the Vestas 8 MW wind turbine and Vestas 160 MW wind farm. This reference system uses specifications from the turbine library of SAM, which have been tried and tested by NREL and are currently operational. Thus, this system is a good benchmark for determining the practicability of system specifications derived from SSTM. The basis of comparison involves capacity factor, energy production, system energy losses and power curves. In addition, weather conditions under which the wind turbines and wind farms operated are also discussed. In terms of presentation, the discussion first compares the performance of the 9 MW, 10 MW, 11 MW and 12 MW wind turbines to that of the Vestas 8 MW wind turbine. This discussion is followed by a performance comparison of the 180 MW, 200 MW, 220 MW and 240 MW wind farms to the Vestas 160 MW wind farm. Lastly, at the end of the chapter, the discussion also examines the dependence and relationship of output metrics on UD input variables of the turbine system.

5.3 PERFORMANCE ANALYSIS OF SINGLE WIND TURBINES

The performance of direct drive and single stage-low speed generators on single wind turbines are compared to the Vestas 8 MW wind turbine using Tables 4.21, 4.22, 4.23 and Figure 4.6. Table 4.21 shows the weather conditions responsible for this baseline wind turbine's annual and highest monthly energy production. Likewise, Table 4.22 shows the capacity factor, system energy losses, and annual energy production for this wind turbine. Finally, its monthly energy production is given in Table 4.23, and the power curve is shown

in Figure 4.6. With reference to these tables, the energy potential of the 9 MW, 10 MW, 11 MW, and 12 MW wind turbines is assessed by calculating the percentage increase in energy production and capacity factor.

5.3.1 Performance analysis of the 9 MW wind turbine

The 12.5% system specifications consist of a rated power output of 9 MW, rotor diameter of 184.5 m, a hub height of 118.125 m, and a maximum tip speed of 117 m/s. These specifications give rise to the annual energy, capacity factor and system energy losses shown in Table 4.1 under the weather conditions of Table 4.3. One of the critical weather conditions for these results is an annual average daily minimum and maximum wind speed of 4.58 m/s and 12.21 m/s. This wind speed generated 30.26 GWh on a single stage-low speed generator and 30.54 GWh on the direct drive as annual energy. Thus, the single stage-low speed generator capacity factor is 38.4%, while the direct-drive generator has 38.7%. Furthermore, December's average daily minimum and maximum wind speed of 5.35 m/s and 14.5 m/s produced the highest energy production on both generator systems. As a result, 3155.99 MWh of energy is produced on a single stage-low speed generator and 3176.49 MW on the direct drive for this month.

In comparison to the Vestas 8 MW wind turbine's performance shown in Tables 4.22 and 4.23, the 9 MW wind turbine improvements are shown in Tables 5.1 and 5.2. Percentage increase in annual energy production, system energy losses, and capacity factor is shown in Table 5.1. It can be seen from this table that the 9 MW wind turbine increased the annual energy by 11.76% on a single stage-low speed generator and 12.78% on the direct drive. Although the single stage-low speed generator's capacity factor decreased by 0.52%, it increased by 0.26% on the direct-drive generator. Similarly, the annual average increase of system energy losses for a single stage-low speed generator is 10.04%, while the direct-drive generator is 10.94%. Other than that, Table 5.2 shows that the average increase in monthly energy production is 11.77% on single stage-low speed generator and 12.82% on the direct drive. Thus, the direct-drive generator's performance is better than the single stage-low speed generator for all the results. In the other part, the power curve of the 9 MW wind

turbine of Figure 4.2 is compared to the one for the Vestas 8 MW wind turbine of Figure 4.6. The similarity in these power curves' shape shows that the 9 MW wind turbine results are viable and can be obtained even on actual wind turbines. Furthermore, an annual average minimum and maximum wind speed of 4.58 m/s and 12.21 m/s is also feasible. Therefore, similar weather conditions shown in Tables 4.3 and 4.21 can be considered when selecting appropriate sites for real-life projects.

Table 5.1 Improvements in annual energy and capacity factor for 9 MW turbine.

Performance metrics	Increase in annual energy, capacity factor and energy losses	
	Single stage-low speed generator	Direct drive generator
Annual gross energy	11.757%	12.783%
Annual energy after losses	11.755%	12.782%
Capacity factor	-0.518%	0.259%
System energy losses		
Availability losses	11.765%	12.773%
Electrical losses	11.710%	12.789%
Environmental losses	11.682%	12.709%
Operational losses	11.661%	12.761%
Turbine losses	11.701%	12.793%
Wake losses	11.755%	12.748%
Curtailment losses	00.000%	00.000%

Table 5.2 Improvements in monthly energy production for 9 MW turbine.

Month	Percentage increase in monthly energy production	
	Single stage-low speed generator	Direct drive generator
January	13.255%	14.123%
February	13.039%	14.263%
March	12.589%	13.433%
April	13.849%	15.040%
May	11.929%	13.138%
June	9.631%	10.486%
July	11.001%	12.123%
August	8.633%	9.848%
September	10.341%	11.514%
October	11.732%	12.863%
November	11.972%	12.960%
December	13.297%	14.033%

Overall, the 9 MW wind turbine results for power curves, system energy losses, capacity factor, monthly and annual energy production have been compared to the Vestas 8 MW wind turbine. Also, the weather conditions under which these results are obtained have been examined. These results show that increasing the rotor diameter, hub height, rated power output, and maximum tip speed of the Vestas 8 MW by 12.5% is worthwhile. This increase leads to 3.183 GWh of more annual energy on a single stage-low speed generator and 3.461 GWh on the direct drive in the first year of wind turbine operation. Additionally, more monthly energy is produced on the direct drive than on a single stage-low speed generator. The highest production is in December. During this period, the single stage-low speed generator increased energy production by 13.30%, whereas the increase on the direct drive is 14.03%. Based upon these findings, a 9 MW wind turbine with a rotor diameter of 184.5 m, hub height of 118.125 m and a maximum tip speed of 117 m/s is practically attainable.

5.3.2 Performance analysis of the 10 MW wind turbine

This wind turbine has the following 25% system specifications: rated power output of 10 MW, rotor diameter of 205 m, hub height of 131.25 m, and maximum tip speed of 130 m/s. As can be noted from the performance of these specifications in Table 4.4, this wind turbine generated annual energy of 35.546 GWh on a single stage-low speed generator and 35.829 GWh on a direct-drive generator. On the other side, the Vestas 8 MW wind turbine produced annual energy of 27.078 GWh, as shown in Table 4.22. Thus, the annual energy increase is 8.468 GWh on a single stage-low speed generator and 8.751 GWh on a direct-drive generator. Moreover, unlike the 9 MW wind turbine, the 10 MW wind turbine gives rise to a higher annual capacity factor on both generator systems. It has a capacity factor of 40.6% on a single stage-low speed generator and 40.9% on a direct-drive generator.

In comparison to the Vestas 8 MW wind turbine's performance, Table 5.3 presents the level of improvement that the 10 MW wind turbine has achieved. These results show that annual energy increased by 31.27% on a single stage-low speed generator and 32.32% on a direct-drive generator. Similarly, the increase is 5.18% on a single stage-low speed generator and 5.96% on the direct-drive generator for the capacity factor. On the other hand, the average

increase in system energy losses is 26.76% on a single stage-low speed generator and 27.69% on a direct drive generator. Altogether, the annual performance of the 10 MW wind turbine is realistic and viable. Despite all the weather conditions of Table 4.6 having a part in these results, an annual average daily minimum and maximum wind speed of 4.63 m/s and 12.39 m/s has a more significant impact.

Table 5.3 Improvements in annual energy and capacity factor for 10 MW turbine.

Performance metrics	Increase in annual energy, capacity factor and energy losses	
	Single stage-low speed generator	Direct drive generator
Annual gross energy	31.276%	32.321%
Annual energy after losses	31.273%	32.318%
Capacity factor	5.181%	5.959%
System energy losses		
Availability losses	31.261%	32.325%
Electrical losses	31.279%	32.358%
Environmental losses	31.194%	32.349%
Operational losses	31.243%	32.233%
Turbine losses	31.279%	32.293%
Wake losses	31.126%	32.285%
Curtailment losses	00.000%	00.000%

In like manner, monthly energy production for the 10 MW and Vestas 8 MW wind turbines is compared in Tables 4.5 and 4.23. As can be observed from the tables, the 10 MW wind turbine produced more energy than the Vestas 8 MW wind turbine for all the months. The percentage increase in monthly energy production is shown in Table 5.4. On average, monthly energy production increased by 31.38% on a single stage-low speed generator and 32.44% on a direct-drive generator. December has the highest production of 3621.68 MWh on a single stage-low speed generator and 3642.31 MWh on the direct drive. This month, the increase in energy production is 30.02% on a single stage-low speed generator and 30.76% on the direct-drive generator.

One of the primary weather conditions of Table 4.6 that gave rise to this production is an average daily minimum and maximum wind speed of 5.41 m/s and 14.69 m/s. Thus, for real-life projects intending to have similar results shown in Table 4.5, the projects' sites should have identical weather conditions. On the other hand, a comparison of Figures 4.3 and 4.6

indicates that the 10 MW and Vestas 8 MW wind turbine's power curves are very similar. This similarity demonstrates that increasing the rotor diameter, maximum tip speed, hub height and rated power output of the Vestas 8 MW wind turbine by 25% does not negatively affect its operation. On the other part, comparing the 9 MW and 10 MW results reveals that the direct-drive generator has performed better even on the 10 MW wind turbine.

Table 5.4 Improvements in monthly energy production for 10 MW turbine.

Month	Percentage increase in monthly energy production	
	Single stage-low speed generator	Direct drive generator
January	30.664%	31.583%
February	32.852%	34.120%
March	30.531%	31.393%
April	33.566%	34.789%
May	32.447%	33.737%
June	29.626%	30.522%
July	31.861%	32.895%
August	31.838%	33.042%
September	30.933%	32.119%
October	32.263%	33.373%
November	29.947%	30.989%
December	30.015%	30.755%

For the results of one year, a comparison of capacity factor, system energy losses, power curves, annual and monthly energy production of the 10 MW and Vestas 8 MW wind turbines are made in this section. This performance shows that a 10 MW wind turbine with a hub height of 131.25 m, maximum tip speed of 130 m/s and a 205 m rotor diameter produces feasible results. Moreover, given similar weather conditions for air temperature, pressure, and wind direction in Table 4.6, these results can be generated even on actual wind turbine projects. But more importantly, an annual average daily minimum and maximum wind speed of 4.63 m/s and 12.39 m/s is necessary.

5.3.3 Performance analysis of the 11 MW wind turbine

The 37.5% system specifications point to a rated power output of 11 MW, rotor diameter of 225.5 m, hub height of 144.375 m and maximum tip speed of 143 m/s. As shown in Table 4.7, this wind turbine generated annual energy of 40.93 GWh on a single stage-low speed

generator and 41.23 GWh on the direct drive. Thus, its capacity factor is 42.5% on a single stage-low speed generator and 42.8% on a direct-drive generator. In comparison to the results of Table 4.22 for the Vestas 8 MW wind turbine, Table 5.5 presents the level of progress in the 11 MW wind turbine performance. This table reveals that annual energy increased by 51.16% on a single stage-low speed generator and 52.25% on a direct-drive generator. Additionally, the capacity factor increased by 10.1% on a single stage-low speed generator and 10.88% on the direct drive. On average, system energy losses increased by 43.79% on a single stage-low speed generator and 44.75% on a direct drive. Even if all the weather conditions of Table 4.9 are responsible for these results, an average daily minimum and maximum annual wind speed of 4.68 m/s and 12.58 m/s largely contributed to this production.

Table 5.5 Improvements in annual energy and capacity factor for 11 MW turbine.

Performance metrics	Increase in annual energy, capacity factor and energy losses	
	Single stage-low speed generator	Direct drive generator
Annual gross energy	51.159%	52.250%
Annual energy after losses	51.156%	52.249%
Capacity factor	10.104%	10.881%
System energy losses		
Availability losses	51.149%	52.213%
Electrical losses	51.156%	52.234%
Environmental losses	51.091%	52.247%
Operational losses	51.045%	52.145%
Turbine losses	51.092%	52.262%
Wake losses	50.993%	52.152%
Curtailment losses	00.000%	00.000%

Correspondingly, Table 5.6 states the improvements in the production of monthly energy. On average, the 11 MW wind turbine's monthly energy production increased by 51.38% on a single stage-low speed generator and 52.5% on the direct drive. These results indicate that the 11 MW wind turbine generated more monthly energy than the Vestas 8 MW wind turbine. Its highest energy production is in June. At this time of the year, 4103 MWh of energy is generated on a single stage-low speed generator and 4128.75 MWh on the direct-drive generator. One of the significant weather conditions of Table 4.9 that brought about this high production is an average daily minimum and maximum wind speed of 6.5 m/s and

12.96 m/s. On another note, Figures 4.4 and 4.6 depicts the power curves of the 11 MW and Vestas 8 MW wind turbines. From a comparison point of view, one can see that both power curves are similar. This similarity shows the typical and expected shape familiar to most power curves of wind turbines. Consequently, this similarity in the two power curves proves that increasing the hub height, maximum tip speed, rotor diameter and rated power output of the Vestas 8 MW wind turbine by 37.5% still make it operate normally. This increase is realistic and can be obtained even in real-life projects.

Table 5.6 Improvements in monthly energy production for 11 MW turbine.

Month	Percentage increase in monthly energy production	
	Single stage-low speed generator	Direct drive generator
January	48.640%	49.647%
February	53.697%	55.044%
March	48.789%	49.681%
April	54.040%	55.279%
May	54.016%	55.423%
June	49.907%	50.848%
July	52.177%	53.247%
August	54.867%	56.082%
September	51.766%	53.016%
October	52.764%	53.874%
November	49.041%	50.195%
December	46.858%	47.618%

To a great extent, a comparison of annual energy, capacity factor, power curves, monthly energy and system energy losses between the 11 MW and Vestas 8 MW wind turbines has been conducted in this section. After comparing these performance metrics, this study considers an offshore wind turbine with a rated power output of 11 MW, maximum tip speed of 143 m/s, rotor diameter of 225.5 m and a hub height of 144.375 m to be practically feasible. Furthermore, the percentage increase in energy production from these specifications and their respective weather conditions are realistic and attainable even for actual wind turbines. It has also been observed that the direct drive generator system performs better on these specifications than a single stage-low speed generator.

5.3.4 Performance analysis of the 12 MW wind turbine

The rated power output of 12 MW, maximum tip speed of 156 m/s, the hub height of 157.5 m and the rotor diameter of 246 m make up the 50% system specifications. According to the results of Table 4.10, this wind turbine produced annual energy of 67.45 GWh on both direct drive and single stage-low speed generators. Similarly, the capacity factor for both generator systems is 64.2%. Compared with the Vestas 8 MW wind turbine's performance, Table 5.7 shows the percentage increase in energy production and capacity factor derived from these specifications. In one year, the capacity factor increased by 66.32% on the direct drive and single stage-low speed generator.

Additionally, the annual energy increased by 149.09% on single stage-low speed generator and direct-drive generator. At the same time, there is an average increase of 127.73% in system energy losses on both generators. Given the huge percentage increase in capacity factor and annual energy production, these results are not practically possible to attain in real-life situations. Although all the weather conditions of Table 4.12 are the basis for this performance, an average daily minimum and maximum annual wind speed of 4.73 m/s and 12.73 m/s is the main contributor.

Table 5.7 Improvements in annual energy and capacity factor for 12 MW turbine.

Performance metrics	Increase in annual energy, capacity factor and energy losses	
	Single stage-low speed generator	Direct drive generator
Annual gross energy	149.094%	149.094%
Annual energy after losses	149.092%	149.092%
Capacity factor	66.321%	66.321%
System energy losses		
Availability losses	149.076%	149.076%
Electrical losses	149.153%	149.153%
Environmental losses	149.037%	149.037%
Operational losses	148.955%	148.955%
Turbine losses	149.064%	149.064%
Wake losses	148.841%	148.841%
Curtailment losses	000.000%	000.000%

On the other side, Table 5.8 presents the improvements in the 12 MW wind turbine's monthly energy production compared to the Vestas 8 MW wind turbine performance of Table 4.23. One can notice that the average percentage increase in monthly energy production is 151.35% on both direct drive and single stage-low speed generators. Furthermore, Table 4.11 shows that the highest energy production for the 12 MW wind turbine occurred in December. This month, 6193.030 MWh of energy is generated on a single stage-low speed generator and direct drive. Finally, Table 4.12 presents the average daily minimum and maximum wind speed of 5.53 m/s and 15.08 m/s responsible for this production. Despite being so impressive, an average increase of 151.35% in monthly energy production cannot be practically obtained with the current wind turbine technology.

Table 5.8 Improvements in monthly energy production for 12 MW turbine.

Month	Percentage increase in monthly energy production	
	Single stage-low speed generator	Direct drive generator
January	144.351%	144.351%
February	156.059%	156.059%
March	133.432%	133.432%
April	161.108%	161.108%
May	177.337%	177.337%
June	123.136%	123.136%
July	148.989%	148.989%
August	149.139%	149.139%
September	180.049%	180.049%
October	150.438%	150.438%
November	169.873%	169.873%
December	122.324%	122.324%

On another note, a comparison of power curves of Figures 4.5 and 4.6 for the 12 MW and Vestas 8 MW wind turbines is also undertaken. It is observed from the two figures that the power curves of these wind turbines are very different from each other in terms of shape. The shape of the 12 MW wind turbine's power curve is not a standard and typical curve for wind turbines. This power curve has 0 gradients (slope) for the cut-in and cut-out wind speeds. As a consequence, this type of power curve is not viable. Moreover, this study has discovered that increasing the maximum tip speed value beyond 143 m/s results in this unusual power curve. Similarly, increasing the rotor diameter beyond 246 m also brings

about the same effect. Therefore, compared to rated power output and hub height, maximum tip speed and rotor diameter significantly distort the slope of the cut-in and cut-out wind speeds. For the most part, it is worth noting that increasing the hub height, rotor diameter, and rated output of the Vestas 8 MW wind turbine by 50% distorts its system operations.

As a whole, the 12 MW and Vestas 8 MW wind turbines' performance metrics have been compared in this section. These metrics cover annual energy, capacity factor, monthly energy production, and system energy losses. In addition, another metric that has been analyzed is the power curves of these two wind turbines. Given the current pace of wind turbine technology, it is found that the results of the 12 MW wind turbines are too high to be generated in real-life situations. Therefore, under this study's weather conditions, an offshore wind turbine with 50% system specifications is not practically attainable for now. These specifications include a rated power output of 12 MW, a hub height of 157.5 m, a rotor diameter of 246 m, and a maximum tip speed of 156 m/s. However, with continuous advancement in wind turbine technology, they can be helpful in large offshore wind turbines' future designs.

5.4 PERFORMANCE ANALYSIS OF WIND FARMS

This section discusses the performance effect of scaling up the size of four system specifications of the Vestas 8 MW wind turbine on wind farms. Thus, unlike the analysis of single wind turbines in Section 5.3, the wind turbines on wind farms have wake effects considered in their performance metrics. However, much like the analysis for single wind turbines, wind farms' performance metrics include system energy losses, capacity factor, annual and monthly energy production. For these metrics, the performance of the 180 MW, 200 MW, 220 MW and 240 MW wind farms are compared to the Vestas 160 MW baseline wind farm using Tables 4.22 and 4.23. The performance of this wind farm comes from the weather conditions shown in Table 4.21.

5.4.1 Performance analysis of the 180 MW wind farm

The 180 MW wind farm has 20 wind turbines based on the 12.5% system specifications. Thus, each of the 20 wind turbines has a rotor diameter of 184.5 m, a hub height of 118.125 m, a rated power output of 9 MW and a maximum tip speed of 117 m/s. According to Table 4.13, this wind farm generated annual energy of 600.71 GWh on a single stage-low speed generator and 606.17 GWh on the direct drive in the first year of operation. Therefore, its annual capacity factor is 38.1% on a single stage-low speed generator and 38.4% on a direct-drive generator. When this performance is compared to the Vestas 160 MW wind farm, it is found that more annual energy is produced by the 180 MW wind farm than the Vestas 160 MW farm.

The percentage increase in annual energy and capacity factor is shown in Table 5.9. As indicated in the table, annual energy increased by 11.77% on a single stage-low speed generator and 12.78% on a direct-drive generator. During the same period, the capacity factor decreased by 0.52% on a single stage-low speed generator and increased by 0.26% on the direct drive. On average, system energy losses increased by 11.76% on a single stage-low speed generator and 12.78% on a direct drive. Taken as a whole, the annual performance metrics of the 180 MW wind farm on both generator systems are practically feasible. However, the direct-drive generator has better performance than a single stage-low speed generator. Table 4.3 describes the air temperature, wind direction, pressure, and wind speed for the annual weather conditions of the wind farm. For real-world wind farms, these conditions can be used to produce similar results. But, the most notable weather condition is wind speed. An annual average daily minimum and maximum wind speed of 4.58 m/s and 12.21 m/s is required for the sites.

Table 5.9 Improvements in annual energy and capacity factor of 180 MW wind farm.

Performance metrics	Increase in annual energy, capacity factor and energy losses	
	Single stage-low speed generator	Direct drive generator
Annual gross energy	11.757%	12.784%
Annual energy after losses	11.766%	12.782%
Capacity factor	-0.522%	0.261%
System energy losses		
Availability losses	11.755%	12.783%
Electrical losses	11.757%	12.781%
Environmental losses	11.755%	12.783%
Operational losses	11.754%	12.783%
Turbine losses	11.757%	12.787%
Wake losses	11.764%	12.791%
Curtailment losses	00.000%	00.000%

On a similar note, the 180 MW wind farm's monthly energy production is shown in Table 4.14. Compared with Table 4.23, the 180 MW wind farm produced more energy per month than the Vestas 160 MW wind farm. Table 5.10 shows the percentage increase in energy production for all the months. On average, monthly energy production increased by 11.78% on single stage-low speed generator and 12.82% on the direct drive. December has the highest monthly energy production, with 62.75 GWh on a single stage-low speed generator and 63.16 GWh on the direct drive. The weather conditions for December are given in Table 4.3. But of all the four weather conditions, an average daily minimum and maximum wind speed of 5.35 m/s and 14.5 m/s has a greater effect on the results. This study considers these weather conditions and monthly results as realistic and achievable even for real-world wind farms. Therefore, for real-life projects contemplating producing the results shown in Table 4.14, the projects should have similar weather conditions. In the light of the above performance, the annual and monthly energy production of the 180 MW wind farm is practically feasible. Thus, a 12.5% increment of the rotor diameter, hub height, rated power output, and maximum tip speed of the Vestas 8 MW wind turbine is appropriate even for the 180 MW wind farm.

Table 5.10 Improvements in monthly energy production of 180 MW wind farm.

Month	Percentage increase in monthly energy production	
	Single stage-low speed generator	Direct drive generator
January	13.287%	14.141%
February	13.053%	14.265%
March	12.566%	13.407%
April	13.901%	15.079%
May	11.993%	13.186%
June	9.654%	10.492%
July	10.961%	12.073%
August	8.591%	9.793%
September	10.346%	11.504%
October	11.709%	12.838%
November	12.016%	12.985%
December	13.312%	14.045%

5.4.2 Performance analysis of the 200 MW wind farm

A 200 MW wind farm resulting from the 25% system specifications is the subject of analysis in this section. This wind farm has the following system specifications for each of its 20 wind turbines: rated power output is 10 MW, rotor diameter is 205 m, hub height is 131.25 m, and maximum tip speed is 130 m/s. Table 4.15 shows that these specifications made the 200 MW wind farm generate 706.072 GWh of annual energy on a single-stage-low speed generator and 711.627 GWh on the direct drive. This wind farm's capacity factor is 40.3% on a single stage-low speed generator and 40.6% on the direct drive. Compared to the Vestas 160 MW wind farm, which produced 537.471 GWh of annual energy in year 1, the 200 MW wind farm results are better.

Table 5.11 shows the percentage increase in annual energy, capacity factor and system energy losses. The annual energy increase is 31.37% on a single stage-low speed generator and 32.4% on a direct drive. As for the capacity factor, the increase is 5.22% on a single stage-low speed generator and 6.01% on the direct drive. The average annual increase is 31.28% on a single stage-low speed generator and 32.32% on the direct drive for system energy losses. These results are practically attainable, even on real wind farms. On the

subject of annual weather conditions, the air temperature, pressure, wind direction, and wind speed that gave rise to these results are shown in Table 4.6. Although the other three weather conditions are necessary, an average daily minimum and maximum wind speed of 4.63 m/s and 12.39 m/s is considerably more critical.

Table 5.11 Improvements in annual energy and capacity factor of 200 MW wind farm.

Performance metrics	Increase in annual energy, capacity factor and energy losses	
	Single stage-low speed generator	Direct drive
Annual gross energy	31.275%	32.320%
Annual energy after losses	31.369%	32.403%
Capacity factor	5.222%	6.005%
System energy losses		
Availability losses	31.276%	32.318%
Electrical losses	31.279%	32.319%
Environmental losses	31.273%	32.319%
Operational losses	31.273%	32.319%
Turbine losses	31.278%	32.323%
Wake losses	31.282%	32.325%
Curtailment losses	00.000%	00.000%

On the other part, monthly energy production between the 200 MW wind farm and Vestas 160 MW wind farm is compared in Tables 4.16 and 4.23. Findings from these tables indicate that the 200 MW wind farm generated more energy from January to December. Its highest monthly energy production is in December, with 72.06 GWh on a single stage-low speed generator and 72.47 GWh on the direct drive. This production is achieved under the weather conditions shown in Table 4.6. However, the essential condition is the wind speed. The required wind speed is an average daily minimum of 5.41 m/s and an average daily maximum of 14.69 m/s. These conditions are relevant even for real-world offshore wind farms. The percentage increase in energy production for all the months is given in Table 5.12. On average, monthly energy production increased by 31.47% on a single stage-low speed generator and 32.53% on a direct-drive generator. This percentage increase is reasonable and can be achieved even on real offshore wind farms.

Table 5.12 Improvements in monthly energy production of 200 MW wind farm.

Month	Percentage increase in monthly energy production	
	Single stage-low speed generator	Direct drive generator
January	30.735%	31.636%
February	32.949%	34.206%
March	30.647%	31.504%
April	33.663%	34.882%
May	32.575%	33.846%
June	29.680%	30.567%
July	31.972%	32.997%
August	31.950%	33.146%
September	30.998%	32.167%
October	32.375%	33.479%
November	30.018%	31.044%
December	30.117%	30.855%

5.4.3 Performance analysis of the 220 MW wind farm

The performance metrics of the 220 MW and Vestas 160 MW wind farms are compared in this section. These metrics include annual energy, capacity factor, system energy losses and monthly energy production. In terms of design, each of the 20 wind turbines on the 220 MW wind farm has the following 37.5% system specifications: rotor diameter of 225.5m, a rated power output of 11 MW, the hub height of 144.375 m, and a maximum tip speed of 143 m/s. As shown in Table 4.17, the 220 MW wind farm generated 813.40 GWh of annual energy on a single stage-low speed generator and 819.24 GWh on the direct drive. Its annual capacity factor is 42.2% on a single stage-low speed generator and 42.5% on a direct drive.

Table 5.13 presents the percentage increase in annual energy, capacity factor and system energy losses. It can be seen from this table that the 220 MW wind farm increased the annual energy production of the Vestas 160 MW by 51.34% on a single stage-low speed generator and 52.43% on the direct drive. In addition, the capacity factor increased by 10.18% on a single stage-low speed generator and 10.97% on the direct drive. Similarly, the average increase in system energy losses is 51.16% on a single stage-low speed generator and 52.25% on the direct drive. These annual performance results are very realistic and can be achieved even on real wind farms. A description of the weather conditions for these results is given in

Table 4.9. Even though the given air temperature, pressure, and wind direction contributed to the wind farms' good performance, wind speed proved more significant. Hence, an annual average daily minimum and maximum wind speed of 4.68 m/s and 12.58 m/s has a more significant impact on energy production.

Table 5.13 Improvements in annual energy and capacity factor of 220 MW wind farm.

Performance metrics	Increase in annual energy, capacity factor and energy losses	
	Single stage-low speed generator	Direct drive generator
Annual gross energy	51.158%	52.252%
Annual energy after losses	51.338%	52.425%
Capacity factor	10.183%	10.966%
System energy losses		
Availability losses	51.158%	52.251%
Electrical losses	51.156%	52.250%
Environmental losses	51.156%	52.254%
Operational losses	51.156%	52.251%
Turbine losses	51.161%	52.253%
Wake losses	51.164%	52.258%
Curtailment losses	00.000%	00.000%

On the other hand, Tables 4.18 and 4.23 compare the 220 MW and Vestas 160 MW wind farms' monthly energy production. These results show that the 220 MW wind farm's energy production is higher than the Vestas 160 MW wind farm. A percentage increase in monthly energy production is given in Table 5.14. It is observed from this table that the average increase in energy production is 51.56% on a single stage-low speed generator and 52.67% on a direct drive. The highest production of energy for these generators is in June. At this time of the year, the wind farm generated 81.47 GWh of energy on a single stage-low speed generator and 81.97 GWh on the direct drive. The prevailing weather conditions for June is shown in Table 4.9. This table shows that suitable air temperature, pressure, wind direction, and wind speed are required for wind farms' flawless operation. However, an average daily minimum wind speed of 6.5 m/s and an average daily maximum wind speed of 12.96 m/s is more critical if these weather conditions are to produce similar results on real wind farms. Given the above percentage increase in monthly energy production, the results of Table 4.18 are viable and practically possible to obtain.

Table 5.14 Improvements in monthly energy production of 220 MW wind farm.

Month	Percentage increase in monthly energy production	
	Single stage-low speed generator	Direct drive generator
January	48.713%	49.706%
February	53.864%	55.212%
March	49.009%	49.896%
April	54.282%	55.524%
May	54.172%	55.567%
June	50.033%	50.963%
July	52.405%	53.464%
August	55.149%	56.369%
September	51.911%	53.148%
October	53.008%	54.112%
November	49.140%	50.280%
December	47.058%	47.813%

5.4.4 Performance analysis of the 240 MW wind farm

The performance of the 240 MW wind farm is discussed in this section. All the 20 wind turbines on this wind farm have 50% system specifications. Thus, each wind turbine has a rotor diameter of 246 m, a rated power output of 12 MW, a maximum tip speed of 156 m/s, and a hub height of 157.5 m. Compared to the Vestas 160 MW wind farm, the performance of these specifications is discussed in terms of annual energy, system energy losses, capacity factor, and monthly energy production. As shown in Table 4.19, in the first year of operation, the 240 MW wind farm generated annual energy of 1616.620 GWh on a single stage-low speed generator and direct drive. The wind farm's capacity factor is 63.7% on both single stage-low speed and direct drive generators.

Percentage increase in annual energy, capacity factor and system energy losses is shown in Table 5.15. As can be noted from this table, the 240 MW wind farm increased the Vestas 160 MW wind farm's annual energy by 149.35% on both generators. Similarly, the capacity factor for this wind farm is increased by 66.32%. The average increase in system energy losses is 149.10%. Although there is a considerable increase in all the three annual performance metrics of the 240 MW wind farm, obtaining these results with the existing wind turbine technology is not practically possible. Hence, for now, these results are not

feasible for real wind farm projects. However, given the current pace at which wind turbine technology evolves, it may be possible to generate these results in future offshore wind farms. Even though these results cannot be attained on real wind farms, the weather conditions under which they were obtained are viable, as shown in Table 4.12.

Table 5.15 Improvements in annual energy and capacity factor of 240 MW wind farm.

Performance metrics	Increase in annual energy, capacity factor and energy losses	
	Single stage-low speed generator	Direct drive generator
Annual gross energy	149.095%	149.095%
Annual energy after losses	149.350%	149.35%
Capacity factor	66.319%	66.319%
System energy losses		
Availability losses	149.094%	149.094%
Electrical losses	149.091%	149.091%
Environmental losses	149.095%	149.095%
Operational losses	149.092%	149.092%
Turbine losses	149.101%	149.101%
Wake losses	149.101%	149.101%
Curtailment losses	000.000%	000.000%

Performance assessment of monthly energy production between the 240 MW wind farm and the Vestas 160 MW wind farm is done using Tables 4.20 and 4.23. It is found that the energy generated by the 240 MW wind farm is higher than that of the Vestas 160 MW wind farm. The highest production for the 240 MW wind farm is 123.108 GWh in December. For the other months, Table 5.16 presents the percentage increase in their energy production. It can be seen from this table that the average increase in monthly energy production is 151.58% on single stage-low speed generator and direct drive. However, just like the results for the annual performance metrics of Table 5.15, this increase is also too high compared to the Vestas 160 MW wind farm results. Therefore, the monthly results of the 240 MW wind farm are also not viable and practical. Despite these infeasible results, the weather conditions for the highest monthly energy production are shown in Table 4.12. Although these conditions can be used for real offshore wind farms, the 50% system specifications are not feasible for this purpose. Wind power's intermittency nature makes these specifications too high for the prevailing wind turbine technology.

Table 5.16 Improvements in monthly energy production of 240 MW wind farm.

Month	Percentage increase in monthly energy production	
	Single stage-low speed generator	Direct drive generator
January	144.568%	144.568%
February	156.878%	156.878%
March	134.009%	134.009%
April	161.160%	161.160%
May	177.982%	177.982%
June	123.912%	123.912%
July	149.430%	149.430%
August	150.032%	150.032%
September	178.401%	178.401%
October	150.724%	150.724%
November	169.583%	169.583%
December	122.305%	122.305%

5.5 ANALYSIS OF PARAMETRIC RESULTS

The graphical relationship between input variables (rotor diameter, maximum tip speed, hub height) and output performance metrics (capacity factor, annual gross energy, monthly and annual energy) is given by Figures 4.7, 4.8, 4.9 and 4.10. It can be deduced from these figures that it is possible to increase the rotor diameter, rated power output, maximum tip speed and hub height simultaneously by the same increment factor. Consequently, this gives rise to higher capacity factor, monthly and annual energy production. Furthermore, these graphical results show a linear relationship between the input variables and the output performance metrics. This relationship is mathematically expressed, as shown in (5.1), (5.2), and (5.3).

$$Annual\,energy = F\left(hK + h, pK + p, dK + d, mK + m\right) \tag{5.1}$$

$$Monthly\,energy = F\left(hK + h, pK + p, dK + d, mK + m\right) \tag{5.2}$$

$$Capacity\ factor = F\left(hK + h, pK + p, dK + d, mK + m\right) \tag{5.3}$$

where K is the percentage increment factor of each input variable (12.5%), d is rotor diameter in metres, p is the rated power output in kW, m is maximum tip speed in m/s, h is hub height in metres, and F is SAM algorithm for parametric simulations. All three

equations contributed to higher results for each input variable's capacity factor, monthly and annual energy production.

5.6 THE SOCIAL AND ECONOMIC IMPACT OF THE DESIGNED WIND TURBINES AND WIND FARMS

The wind energy explored from the 9 MW, 10 MW, 11 MW and their respective wind farms have many economic and social benefits to local communities of many countries. This section explains some of the benefits of installing these wind turbines and wind farms.

5.6.1 Employment for rural communities

There would be many employment opportunities for the community during the construction, manufacturing and transportation of wind turbines for wind farms. In addition, these activities can provide a large amount of induced financial impacts (increased spending in local shops, restaurants and hotels) and indirect economic impacts such as supply chain and manufacturing of goods and services. Moreover, many full-time permanent jobs would be created for the community when the wind farms are operational.

5.6.2 Benefits of land lease payments and local tax revenue

These wind farm projects can significantly benefit rural landowners and farmers through land lease agreements. The value of these payments would be substantial given that these wind farms would require much land for the giant wind turbines. In addition, these wind farm projects would also enable the community to have the much-needed revenue through property tax payments and other municipal revenues. This revenue can build new community infrastructures such as bridges, hospitals, schools and roads.

5.6.3 Source of attraction for tourism

In places where tourism is an essential part of the community's economy, the 180 MW, 200

MW and 220 MW wind farms would significantly enhance local tourism. For those interested in wind turbine technology, these wind farms would be a beautiful spectacle to behold. In addition, the size of these wind farms and their engineering design and operation would surely impress thousands of tourists. Thus, these wind farms would boost tourism and open many financial opportunities to the country's local communities.

5.6.4 Environmental community benefits

Unlike fossil fuel power sources, energy generated from wind turbines is clean and renewable. It does not emit any carbon emissions that can pollute the air or water around the communities. Thus, clean energy means a reduction in environmental and health costs related to water or air pollutions. Furthermore, because wind energy does not involve transportation of fuels, mining or drilling, it does not pose any extensive risks to contamination of the community environment.

5.6.5 Reduced costs and energy independence

Using wind energy generated from the 180 MW, 200 MW, and 220 MW wind farms is a better way of saving money on electrical bills for community members. This observation stems from the fact that this energy can meet most of the domestic needs of the community. Thus, the community would depend less on hydro and thermal power, which is susceptible to changing weather conditions and high production costs.

5.7 SUMMARY

The energy potential and capacity factor of the 12.5%, 25%, 37.5% and 50% system specifications of wind turbines and wind farms have been analyzed in this chapter. Compared with the Vestas 8 MW wind turbine and Vestas 160 MW wind farm's baseline specifications, there is much improvement in energy production from these four system specifications. For example, the 12.5% specifications for the 9 MW wind turbine and 180

MW wind farm increased the annual energy by 11.76% on a single stage-low speed generator and 12.78% on the direct drive. As for monthly energy production, the average increase is 11.77% on a single stage-low speed generator and 12.82% on a direct-drive generator. Similarly, the 25% specifications of the 10 MW wind turbine and 200 MW wind farm improved the annual energy by 31.27% on a single stage-low speed generator and 32.32% on the direct drive. Likewise, monthly energy production increased by an average of 31.38% on a single stage-low speed generator and 32.44% on a direct-drive generator. On the other side, the 37.5% specifications of the 11 MW wind turbine and 220 MW wind farm has the annual energy increased by 51.16% on single stage-low speed generator and 52.25% on the direct-drive generator. Additionally, the average increase of monthly energy production is 51.38% on single stage-low speed generator and 52.5% on a direct drive. It should be noted that the percentage increase in energy production from the system specifications of the 9 MW, 10 MW, 11 MW wind turbines and their respective wind farms are realistic and viable. This performance is possible even for actual wind turbines and wind farms as well.

On a different note, the 50% specifications of the 12 MW wind turbine and 240 MW wind farm increased the annual energy by 149.09% on both generators. Adding to this performance is an average increase in monthly energy production of 151.35%. However, unlike the 12.5%, 25% and 37.5% system specifications, the results for the 50% specifications of the 12 MW wind turbine and 240 MW wind farm are not feasible for actual wind turbines. Moreover, contrary to the baseline wind turbine, the 12 MW wind turbine's power curve is different and is not a typical power curve for wind turbines. It has been observed that increasing the maximum tip speed value beyond 143 m/s results in this unique power curve. In an equal manner, increasing the rotor diameter beyond 246 m also brings about the same effect. On the other hand, it is also apparent that an average daily minimum and maximum wind speed of 4.58 m/s and 15.08 m/s has a more significant impact on energy production and capacity factor for large offshore wind turbines and wind farms. But more significantly, under this wind speed range, the direct drive generator's performance is better than a single stage-low speed generator on large offshore wind turbines and wind farms.

CHAPTER 6 CONCLUSION

This study successfully designed an SSTM for increasing the size of maximum tip speed, hub height, rated power output and a rotor diameter of HAWT. The model is a suitable testbed for assessing energy production and capacity factor that comes with upgrading the above four system specifications. Despite using the SAM simulator to implement this model, any other suitable simulator that supports all its systems may be used. Furthermore, this model can be tested on any generator system of wind turbines. However, for this study, direct-drive and single stage-low speed generators are used to test the model's performance. It is found that for large offshore wind turbines with a rated capacity of 9 MW, 10 MW and 11 MW, a direct-drive generator system produces more energy and a better capacity factor than a single stage-low speed generator. For instance, the lowest annual energy produced by these wind turbines on a single stage-low speed generator is 30.26 GWh, and the highest is 40.93 GWh. In contrast, the direct-drive generator produced 30.54 GWh as its lowest annual energy and 41.23 GWh as its highest. Thus, for large offshore wind turbines, the direct-drive generator system is a better option.

Another notable finding for these two generator systems is that the percentage increase or decrease in capacity factor, system energy losses, monthly and annual energy is the same on single wind turbines and wind farms. That is why a direct-drive generator on large offshore wind farms also resulted in higher annual energy production than single stage-low speed generator. However, both generators' performance is subject to the following typical specifications: cut-in wind speed of 4 m/s, cut-out wind speed of 25 m/s, maximum power coefficient of 0.45, shear coefficient of 0.14 and a maximum tip speed ratio of 8. If these values are changed, some difference in their performance may be noticed. Furthermore, the performance of the two generators is also dependent on the weather conditions used in the

study. Nonetheless, even though the weather conditions for the study are for Northern California of the United States, these conditions are typical and representative of most regions in the world. That being the case, any other weather conditions will still produce similar results. Moreover, given that actual weather conditions of air temperature, wind direction, pressure, and wind speed are used, the results of this study are close to reality. Hence, they can be a basis for choosing suitable generator systems for large offshore wind turbines. Additionally, although all the four weather conditions have a place in the two generators' excellent performance, an average daily minimum and maximum wind speed of 4.58 m/s and 15.08 m/s has a significant bearing on their energy production and capacity factor. On a different note, wind farms results demonstrate that wind turbine clusters significantly impact high energy production and better capacity factor. With that said, every wind farm parameter such as number of wind turbines per row, number of rows, the shape of the farm, wind turbine spacing, row spacing, row orientation, offset for rows and offset type should be carefully designed. Given the direct-drive generator's impressive performance, clusters of 20 wind turbines for large offshore wind farms are suggested.

On the other hand, this study has shown that higher system specifications do not always produce viable results despite favourable weather conditions for wind turbine sites. Therefore, for good results in wind turbines and wind farms' performance, a limit for increasing the size of system specifications should be carefully considered. For this study's weather conditions, it is possible to scale up the rated power output, rotor diameter, hub height, and maximum tip speed of the 8 MW wind turbine by 12.5%, 25%, 37.5% and 50%. However, only 12.5%, 25% and 37.5% system specifications give realistic and attainable results that can be used in real-life situations. The viability of these specifications has been confirmed by graphs of the power curves and achievable energy production. As for system energy losses, they increased in direct proportion to the wind turbines' energy production. In the light of this realistic performance of the three percentages, it is possible to design commercial offshore wind turbines with the following system specifications:

- The rated power output of 9 MW, rotor diameter of 184.5 m, hub height of 118.125 m, and a maximum tip speed of 117 m/s.
- The rated power output of 10 MW, rotor diameter of 205 m, hub height 131.25 m,

and a maximum tip speed of 130 m/s.

- The rated power output of 11 MW, rotor diameter of 225.5 m, hub height of 144.375 m, and a maximum tip speed of 143 m/s.

On the contrary, the 50% system specifications, which involve a rated power output of 12 MW, rotor diameter of 246 m, hub height of 157.5 m and a maximum tip speed of 156 m/s, did not give practical results. These specifications are too high for the current wind turbine technology. Moreover, the shape of the power curve from these specifications is not a standard and typical curve for wind turbines. Based on the weather conditions used on these specifications, it has been discovered that increasing the rotor diameter beyond 246 m and maximum tip speed value beyond 143 m/s results in an unusual power curve.

The energy that single wind turbines and wind farms have generated in this study has many potential applications. Among other things, it can be used as a more reliable and cleaner backup source of renewable energy for hydro and solar power. It is further observed that findings in this study specifically help understand how the size of system specifications affect energy production, energy losses and the capacity factor of large wind turbines. Besides, these findings are also fundamental and significant in optimizing the design of large offshore wind turbines. These wind turbines can help speed up the growth of wind power installation and wind energy investments. Thus, to encourage this investment, this study has contributed a model for increasing the size of four system specifications of HAWT and testing their performance. Although the study is conducted on a simulator, the results have financial implications. On this ground, future work on this study should involve assessing the system costs that come with these upgrades. It is, therefore, necessary to consider the following financial parameters for the wind turbines: capital, maintenance and operational costs, LCOE, net present value and internal rate of return, power purchase agreement, payback period and total electricity savings. Furthermore, under similar system specifications and weather conditions, a study that models the physical stress and electrical transients of the 9 MW, 10 MW, 11 MW and 12 MW wind turbine components is equally welcome. In like manner, a stability and protection study and realistic hybrid system model of wind-solar for these wind turbines is recommended.

REFERENCES

[1] SADC energy monitor. “Baseline study of the SADC energy sector.” https://www.sadc.int/files/1514/7496/8401/SADC-energy-monitor-2016 (accessed July, 2018).

[2] B. Schreiner, and H. Baleta, “Broadening the lens: A regional perspective on water, food and energy integration in SADC,” *Aquat. Procedia*, vol. 5, pp. 90-103, Oct. 2015.

[3] S. J. Mwale, and I. Davidson, “SADC power grid reliability – A steady-state contingency analysis and strategic HVDC interconnections using the N-1 criterion,” *In Proc. 2nd Int. Symp. Energy Chall. Mech.*, Scotland, UK, Aug. 2014, pp. 1-5.

[4] Y. Kumar, J. Ringenberg, S. S. Depuru, V. K. Devabhaktuni, J. W. Lee, E. Nikolaidis, B. Andersen, and A. Afjeh, "Wind energy: Trends and enabling technologies," *Renew. Sust. Energ. Rev.*, vol. 53, pp. 209-224, Jan. 2016.

[5] J. C. Nkomo, “Energy use, poverty and development in the SADC,” J. *Energy South. Afr.*, vol.18, no.3, pp.1-8, Aug. 2007.

[6] Africa energy outlook. “Africa’s energy future matters for the world.” https:// www.iea.org/news/africas-energy-future-matters-for-the-world (accessed Nov.7, 2019).

[7] J. Caboz. “The five biggest green energy projects in South Africa - all wind farms.” https://www.businessinsider.co.za/5-massive-new-renewable-energy-projects-that-transformed-south-africas-landscape-2018-4 (accessed Apr. 6, 2018).

[8] Africa's Power Journal, ESI Africa. “The state of wind energy in Africa.” https:// www.esi-africa.com/top-stories/the-state-of-wind-energy-in-Africa (accessed Mar. 14, 2018).

[9] Wikipedia, the free encyclopedia. “Simulation.” https://en.wikipedia.org/wiki/ simulation (accessed Apr. 18, 2019).

[10] M. Moness, and A. M. Moustafa, “A survey of cyber-physical advances and challenges of wind energy conversion systems: prospects for the internet of energy." *IEEE Internet Things J.*, vol. 3, no. 2, pp. 134-145, Mar. 2016.

[11] J. F. Manwell, A. L. Rogers and J.G McGowan, “Wind turbine materials and components,” in *Wind energy explained, theory, design and applications*, 2nd ed. Washington, USA, Wiley, 2009, ch.6, pp. 270-273.

[12] G.M Masters, “Wind power systems,” in *Renewable and efficient electric power systems*, 2nd ed. New Jersey, USA: Wiley, 2013, pp. 424-436.

[13] C. Seceleanu, M. Johansson, J. Suryadevara, G. Sapienza, T. Seceleanu, S. Ellevseth, and P. Pettersson, "Analyzing a wind turbine system: From simulation to formal verification," *Sci. Comput. Program*, vol. 133, pp. 216-242, Jan. 2017.

[14] T. Ashuri, M. B. Zaaijer, J. R. Martins, and J. Zhang, "Multidisciplinary design optimization of large wind turbines-technical, economic, and design challenges," *Energy Convers. Manag.*, vol.123, pp. 56-70, Sept. 2016.

[15] Office of energy efficiency and renewable energy. “The inside of a wind turbine.” https://www.energy.gov/eere/wind/inside-wind-turbine (accessed Aug. 2, 2019).

[16] J. Dai, X. Yang, W. Hu, L. Wen, and Y. Tan, "Effect investigation of yaw on wind turbine performance based on SCADA data," *Energy J.*, vol.149, pp. 684-696, Apr. 2018.

[17] D. J. Willis, C. Niezrecki, D. Kuchma, E. Hines, S. R. Arwade, R. J. Barthelmie, M. DiPaola et al. "Wind energy research: State-of-the-art and future research directions," *Renew. Energy*, vol. 125, pp. 133-154, Sept. 2018.

[18] T. Bagherpoor, and L. Xuemin, "Structural optimization design of 2MW composite wind turbine blade," *Energy Procedia*, vol. 105, pp. 1226-1233, May 2017.

[19] S. F. Hosseini, and B. Moetakef-Imani, "Innovative approach to computer-aided design of horizontal axis wind turbine blades," *J. Comput. Des. Eng*, vol. 4, no. 2, pp. 98-105, Apr. 2017.

[20] X. Tang, X. Huang, R. Peng, and X. Liu, "A direct approach of design optimization for small horizontal axis wind turbine blades," *Procedia CIRP,* vol. 36, pp. 12-16, Aug. 2015.

[21] S. A. Abdulqadir, H. Iacovides, and A. Nasser, "The physical modelling and aerodynamics of turbulent flows around horizontal axis wind turbines," *Energy J.*, vol. 119, pp. 767-799, Jan. 2017.

[22] I. Guenoune, F. Plestan, A. Chermitti, and C. Evangelista, "Modeling and robust control of a twin wind turbines structure," *Control Eng. Pract.*, vol. 69, pp. 23-35, Dec. 2017.

[23] L. Dai, Q. Zhou, Y. Zhang, S. Yao, S. Kang, and X. Wang, "Analysis of wind turbine blades aeroelastic performance under yaw conditions," *J. Wind. Eng. Ind. Aerodyn.*, vol. 171, pp. 273-287, Dec. 2017.

[24] J.M O'Brien, T. M. Young, D. C. O'Mahoney, and P. C. Griffin, "Horizontal axis wind turbine research: A review of commercial CFD, FE codes and experimental practices," *Prog. Aerosp. Sci.*, vol. 92, pp. 1-24, July 2017.

[25] M. Sessarego, N. Ramos-García, H. Yang, and W. Z. Shen, "Aerodynamic wind-turbine rotor design using surrogate modelling and three-dimensional viscous–inviscid interaction technique," *Renew. Energy*, vol. 93, pp. 620-635, Aug. 2016.

[26] W. Liu, "Design and kinetic analysis of wind turbine blade-hub-tower coupled system," *Renew. Energy*, vol. 94, pp. 547-557, Aug. 2016.

[27] G. M. Ibrahim, K. Pope, and Y. S. Muzychka, "Effects of blade design on ice accretion for horizontal axis wind turbines," *J. Wind. Eng. Ind. Aerodyn.,* vol. 173, pp. 39-52, Feb. 2018.

[28] A. Albanesi, V. Fachinotti, I. Peralta, B. Storti, and C. Gebhardt, "Application of the inverse finite element method to design wind turbine blades," *Compos. Struct.,* vol. 161, pp. 160-172, Feb. 2017.

[29] M. Lee, Y. C. Shiah, and C. Bai, "Experiments and numerical simulations of the rotor-blade performance for a small-scale horizontal axis wind turbine," *J. Wind. Eng. Ind. Aerodyn.,* vol. 149, pp. 17-29, Feb. 2016.

[30] M. Tahani, G. Kavari, M. Masdari, and M. Mirhosseini, "Aerodynamic design of horizontal axis wind turbine with innovative local linearization of chord and twist distributions," *Energy J.*, vol.131, pp. 78-91, July 2017.

[31] M. Sessarego, N. Ramos-García, H. Yang, and W. Z. Shen, "Aerodynamic wind-turbine rotor design using surrogate modelling and three-dimensional viscous–inviscid interaction technique," *Renew. Energy*, vol. 93, pp. 620-635, Aug. 2016.

[32] T. Bagherpoor, and L. Xuemin, "Structural optimization design of 2MW composite wind turbine Blade," *Energy Procedia,* vol. 105, pp. 1226-1233, May 2017.

[33] A. Pourrajabian, P. A. Afshar, M. Ahmadizadeh, and D. Wood, "Aero-structural design and optimization of a small wind turbine blade," *Renew. Energy,* vol. 87, pp. 837-848, Mar. 2016.

[34] L. Wang, X. Liu, and A. Kolios, "State of the art in the aeroelasticity of wind turbine blades: Aeroelastic modelling," *Renew. Sust. Energ*, vol. 64, pp. 195-210, Oct. 2016.

[35] P. A. Costa, J. W. Araujo, R. J. Lima, M.E. Silva, D. Albiero, C. F. de Andrade, and F. O. Carneiro, "The Effects of blade pitch angle on the performance of small-scale

wind turbine in urban environments," *Energy J.*, vol. 148, no. 1, pp.169-178, Apr. 2018.

[36] F. Grasso, "ECN-G1-21 Airfoil: Design and wind-tunnel testing," *J. Aircraft*, vol. 53, no. 5, pp. 1478-1484, Jan. 2016.

[37] J. Chen, Q. Wang, S. Zhang, P. Eecen, and F. Grasso, "A new direct design method of wind turbine airfoils and wind tunnel experiment," *Appl. Math. Model*, vol. 40, no. 3, pp., 2002 - 2014, Feb. 2016.

[38] Q. Wang, J. Wang, J. Sun, J. Ren, and Q. Wei, "Optimal design of wind turbine airfoils based on functional integral and curvature smooth continuous theory," *Aerosp. Sci. Technol*, vol. 55, pp. 34-42, Aug. 2016.

[39] R. Pereira, W. A. Timmer, G. D. Oliveira, and G. J. W. Bussel, "Design of HAWT airfoils tailored for active flow control," *Wind Energy*, vol. 20, no. 9, pp. 1569-1583, May 2017.

[40] S. D. Nikhade, S. C. Kongare, and S. A. Kale, "Design of an airfoil for low wind horizontal axis micro wind turbine," *In Proc. 2nd IEEE Converg. Technol. Conf.*, Mumbai, India, Apr. 2017, pp. 850-853.

[41] W. J. Zhu, W. Z. Shen, and J. N. Sørensen, "Integrated airfoil and blade design method for large wind turbines," *Renew. Energy*, vol. 70, pp.172-183, Oct. 2014.

[42] M. Ge, D. Tian, and Y. Deng, "Reynolds number effect on the optimization of a wind turbine blade for maximum aerodynamic efficiency," *J. Energy Eng.*, vol. 142, no. 1 pp. 1-12, Mar. 2014.

[43] F. Grasso, D. P. Coiro, N. Bizzarrini, and G. Calise, "Design of advanced airfoil for stall-regulated wind turbines," *J. Phys. Conf. Ser*., vol. 753, no. 2, pp. 403-412, July 2017.

[44] Q. Wang, J. Chen, X. Pang, S. Li, and X. Guo, "A new direct design method for the

medium thickness wind turbine airfoil," *J. Fluid Struct.,* vol. 43, pp. 287-301, Nov. 2013.

[45] T. Segev, T. Roberts, K. Dieppa, and J. Scherrer, "Improved energy generation with insect-inspired wind turbine designs: Towards more durable and efficient turbines," *In Proc. IEEE Undergrad. Res. Technol. Conf.,* Cambridge, MA, USA, Feb. 2018, pp. 1-4.

[46] C. Pavese, T. Kim, and J. P. Murcia, "Design of a wind turbine swept blade through extensive load analysis," *Renew. Energy*, vol. 102, pp. 21-34, Mar. 2017.

[47] I. Bayati, M. Belloli, L. Bernini, H. Giberti, and A. Zasso, "Scale model technology for floating offshore wind turbines," *IET Renew. Power Gener.*, vol. 11, no. 9, pp., 1120-1126, Sept. 2017.

[48] W. Chong, K. Wong, C. Wang, M. Gwani, Y. Chu, W. Chia, and S. Poh, "Cross-axis-wind-turbine: A complementary design to push the limit of wind turbine technology," *Energy Procedia*, vol.105, pp. 973-979, May 2017.

[49] W. Chong, W. K. Muzammil, K. Wong, C. Wang, M. Gwani, Y. Chu, and S. Poh, "Cross axis wind turbine: Pushing the limit of wind turbine technology with complementary design," *Appl. Energy*, vol. 207, pp. 78-95, Dec. 2017.

[50] L. Thomas, and M. Ramachandra, "Advanced materials for wind turbine blade-a review," *Mater. Today: Proc,* vol. 5, no. 1, pp. 2635-2640, Aug. 2018.

[51] L. Scappatici, N. Bartolini, F. Castellani, D. Astolfi, A. Garinei, and M. Pennicchi, "Optimizing the design of horizontal-axis small wind turbines: From the laboratory to market," *J. Wind. Eng. Ind. Aerodyn.* vol. 154, pp. 58-68, July 2016.

[52] IEEE spectrum. "The troubled quest for the superconducting wind turbine." https: // spectrum.ieee.org/green-tech/wind/the-troubled-quest-for-the-super conducting wind-turbine (accessed Feb. 5, 2019).

[53] X. Jin, W. Qiao, Y. Peng, F. Cheng, and L. Qu, "Quantitative evaluation of wind turbine faults under variable operational conditions," *IEEE Trans. Ind. Appl.*, vol. 52, no.3, pp. 2061-2069, Jan. 2016.

[54] S. K. Raju, and G. N. Pillai, "Design and implementation of a type-2 fuzzy logic controller for DFIG-based wind energy systems in distribution networks," *IEEE Trans. Sustain. Energy*, vol. 7, no.1, pp. 345-353, Jan. 2016.

[55] H. Torkaman, and A. Keyhani, "A review of design consideration for doubly fed induction generator based wind energy system," *Electr. Power Syst. Res.*, vol. 160, pp. 128-141, July 2018.

[56] L. J. Cai, I. Erlich, U. Karaagac, and J. Mahseredjian, "Stable operation of a doubly-fed induction generator in weak grids," *In Proc. IEEE Pow. Ener. Soc. Ge.*, Denver, CO, USA, July 2015, pp. 1-5.

[57] G. Gao, and W. Chen, "Design challenges of wind turbine generators," *In Proc. IEEE Electr. Insul. Conf.*, July 2009, Montreal, Canada, pp. 146-152.

[58] T. D. Strous, H. Polinder, and J. A. Ferreira, "Brushless doubly-fed induction machines for wind turbines: developments and research challenges," *IET Electr. Power Appl.*, vol. 11, no. 6, pp. 991-1000, July 2017.

[59] S. Abdi, A. Grace, E. Abdi, and R. McMahon, "A new optimized rotor design for brushless doubly-fed machines," *In Proc. 20th Int. Conf. Electr. Mach.* Sydney, Australia, Aug. 2017, pp. 1-6.

[60] D. Wang, X. Gao, K. Meng, J. Qiu, L. L. Lai, and S. Gao, "Utilization of kinetic energy from wind turbine for grid connections: A review paper," *IET Renew. Power Gener.*, vol.12, no. 6, pp. 615-624, Apr. 2018.

[61] M. Cheng, and Y. Zhu, "The state of the art of wind energy conversion systems and technologies: A review." *Energy Convers. Manag.*, vol. 88, pp. 332-347, Dec. 2014.

[62] J. Jeong, D. An, J. Hong, H. Kim, and Y. Jo, "Design of a 10-MW-class high-temperature superconductor homopolar generator for wind turbines," *IEEE Trans. Appl. Supercond.* , vol. 27, no. 4, pp. 1-4, June 2017.

[63] B. Go, H. Sung, M. Park, and I. Yu, "Structural design of a module coil for a 12-MW class HTS generator for a wind turbine," *IEEE Trans. Appl. Supercond.*, vol. 27, no. 4, pp. 1-5, June 2017.

[64] R. Shafaie, F. Amirkhanloo, and M. Kalantar, "Toward an optimum design of large-scale high-temperature superconducting synchronous generator for wind turbine applications," *IEEE Trans. Appl. Supercond.*, vol. 26, no. 2, pp. 1-8, Mar. 2016.

[65] T. Hoang, L. Queval, C. Berriaud, and L. Vido, "Design of a 20-MW fully superconducting wind turbine generator to minimize the levelized cost of energy," *IEEE Trans. Appl. Supercond.*, vol. 28, no. 4, pp. 1-5, June 2018.

[66] M. Saruwatari, K. Yun, M. Iwakuma, K. Tamura, Y. Hase, Y. Sasamori, and T. Izumi, "Design study of 15-MW fully superconducting generators for an offshore wind turbine," *IEEE Trans. Appl. Supercond.*, vol. 26, no. 4, pp. 1-5, June 2016.

[67] M. Tajdinian, A. R. Seifi, and M. Allahbakhshi, "Sensitivity-based approach for real-time evaluation of transient stability of wind turbines interconnected to power grids," *IET Renew. Power Gener.*, vol. 12, no. 6, pp. 668-679, Apr. 2018.

[68] M. M. Hossain, and M. H. Ali, "Future research directions for the wind turbine generator system." *Renew. Sust. Energ. Rev.*, vol. 49, pp. 481-489, Sept. 2015.

[69] J. Mohammadi, S. Afsharnia, S. Vaez-Zadeh, and S. Farhangi, "Improved fault ride-through strategy for doubly fed induction generator based wind turbines under both symmetrical and asymmetrical grid faults," *IET Renew. Power Gener.*, vol. 10, no. 8, pp. 1114-1122, Sept. 2016.

[70] C. Park, and G. Jang, "Voltage quality assessment considering low voltage ride-through requirement for wind turbines," *IET Gener. Transm. Distrib.*, vol.10, no. 16,

pp. 4205-4212, Dec. 2016.

[71] D. M. Yehia, D. A. Mansour, and W. Yuan, "Fault ride-through enhancement of PMSG wind turbines with DC microgrids using resistive-type SFCL," *IEEE Trans. Appl. Supercond.*, vol. 28, no. 4, pp.1-5, June 2018.

[72] C. Seceleanu, M. Johansson, J. Suryadevara, G. Sapienza, T. Seceleanu, S. Ellevseth, and P. Pettersson, "Analyzing a wind turbine system: From simulation to formal verification," *Sci. Comput. Program.*, vol. 133, pp. 216-242, Jan. 2017.

[73] B. Zhang, M. Soltani, W. Hu, P. Hou, Q. Huang, and Z. Chen, "Optimized power dispatch in wind farms for power maximizing considering fatigue loads," *IEEE Trans. Sustain. Energy*, vol. 9, no. 2, pp. 862-871, Apr. 2018.

[74] H. D. Azevedo, A. M. Araújo, and N. Bouchonneau, "A review of wind turbine bearing condition monitoring: State of the art and challenges," *Renew. Sust. Energ. Rev.*, vol. 56, pp. 368-379, Apr 2016.

[75] J. G. Njiri, and D. Söffker, "State-of-the-art in wind turbine control: Trends and challenges," *Renew. Sust. Energ. Rev.*, vol. 60, pp. 377-393, July 2016.

[76] W. Lin, Z. Lu, and W. Wei, "Asymptotic tracking control for wind turbines in variable speed mode," *IEEE/CAA J. Automatica Sin.*, vol. 4, no. 3, pp. 569-576, July 2017.

[77] G. P. Prajapat, N. Senroy, and I. N. Kar, "Wind turbine structural modelling consideration for dynamic studies of DFIG based system," *IEEE Trans. Sustain. Energy*, vol. 8, no. 4, pp. 1463-1472, Oct. 2017.

[78] D. Li, W. Cai, P. Li, S. Xue, Y. Song, and H. Chen, "Dynamic modelling and controller design for a novel front-end speed regulation (FESR) wind turbine," *IEEE Trans. Power Electron.*, vol. 33, no. 5, pp. 4073-4087, May 2018.

[79] Y. Ma, W. Cao, L. Yang, F. F. Wang, and L. M. Tolbert, "Virtual synchronous

generator control of full converter wind turbines with short-term energy storage." *IEEE Trans. Ind. Electron.* vol. 64, no. 11, pp. 8821-8831, Nov. 2017.

[80] S. G. Iordanov, M. Collu, and Y. Cao, "Can a wind turbine learn to operate itself? Evaluation of the potential of a heuristic, data-driven self-optimizing control system for a 5MW offshore wind turbine," *Energy Procedia,* vol. 137, pp. 26-37, Oct 2017.

[81] V. Petrović, and C. L. Bottasso, "Wind turbine envelope protection control over the full wind speed range," *Renew. Energy,* vol. 111, pp. 836-848, Oct. 2017.

[82] D. Palejiya, and D. Chen, "Performance improvements of switching control for wind turbines," *IEEE Trans. Sustain. Energy,* vol. 7, no. 2, pp. 526-534, Apr. 2016.

[83] E. N. Menezes, A. M. Araújo, and N. S. Silva, "A review on wind turbine control and its associated methods," *J. Clean. Prod.,* vol. 174, pp. 945-953, Feb. 2018.

[84] R. S Carbajo, E. S Carbajo, B. Basu, and C. M. Goldrick, "Routing in wireless sensor networks for wind turbine monitoring," *Pervasive Mob. Comput.*, vol. 39, pp. 1-35, Aug. 2017.

[85] Wind power monthly. "Ten of the biggest wind turbines." https://www.windpowermonthly.com/10-biggest-turbines (accessed Sept. 20, 2019).

[86] J. H. Koh, and E. Y. K. Ng, "Downwind offshore wind turbines: Opportunities, trends and technical challenges," *Renew. Sust. Energ. Rev.*, vol. 54, pp. 797-808, Feb. 2016.

[87] Solar Feeds. "Top ten largest offshore wind farms in the world." https://solarfeeds.com/largest-offshore-wind-farms-in-the-world/ (accessed Oct. 22, 2019).

[88] Proceedings of the IEEE. "Wind energy systems." https://twitter.com/IEA/status/576850361190748160 (accessed Feb.24, 2019).

[89] Kikomaza. “Wind offshore turbines: Battle of the giants.” https://www.kikomaza.com/en/category/product/ (accessed Jan. 16, 2020).

[90] R. McKenna, P. Ostman, V. D. Leye, and W. Fichtner, "Key challenges and prospects for large wind turbines," *Renew. Sust. Energ. Rev.*, vol. 53, pp. 1212-1221, Jan. 2016.

[91] N. Sedaghatizadeh, M. Arjomandi, R. Kelso, B. Cazzolato, and M. H. Ghayesh. "Modelling of wind turbine wake using large eddy simulation," *Renew. Energy, vol.* 115, pp. 1166-1176, Jan. 2018.

[92] A. Cerveira, A. Sousa, E. J. Pires, and J. Baptista, "Optimal cable design of wind farms: The infrastructure and losses cost minimization case," *IEEE Trans. Power Syst.,* vol. 31, no. 6, pp. 4319-4329, Nov. 2016.

[93] A. McDonald, and G. Jimmy, "Parallel wind turbine powertrains and their design for high availability," *IEEE Trans. Sustain. Energy*, vol. 8, no. 2, pp. 880-890, Apr. 2017.

[94] P. Liu, Z. Li, Y. Zhuo, X. Lin, S. Ding, M. S. Khalid, and O. S. Adio, "Design of wind turbine dynamic trip-off risk alarming mechanism for large-scale wind farms," *IEEE Trans. Sustain. Energy*, vol. 8, no. 4, pp. 1668-1678, Oct. 2017.

[95] M. Zheng, Z. J. Yang, S. Yang, and B. Still, "Modeling and mitigation of excessive dynamic responses of wind turbines founded in warm permafrost," *Eng. Struct,* vol. 148, pp. 36-46, Oct. 2017.

[96] M. Moness, and A. M. Moustafa, "A survey of cyber-physical advances and challenges of wind energy conversion systems: Prospects for the internet of energy," *IEEE Internet Things J.*, vol. 3, no. 2, pp. 134-145, Sept. 2016.

[97] Y. Guan, Z. Q. Zhu, G. Li, Z. Azar, A. S. Thomas, F. Vedreño-Santos, and M. Odavic, "Influence of pole number and stator outer diameter on volume, weight, and cost of superconducting generators with iron-cored rotor topology for wind

turbines," *IEEE Trans. Appl. Supercond.* vol. 27, no. 6, pp.1-9, June 2017.

[98] P. Hou, W. Hu, M. Soltani, C. Chen, B. Zhang, and Z. Chen, "Offshore wind farm layout design considering optimized power dispatch strategy," *IEEE Trans. Sustain. Energy*, vol. 8, no. 2, pp. 638-647, Apr. 2017.

[99] D. J. Willis, C. Niezrecki, D. Kuchma, E. Hines, S. R. Arwade, R. J. Barthelmie, M. DiPaola et al. "Wind energy research: State-of-the-art and future research directions," *Renew. Energy*, vol. 125, pp. 133-154, Sept. 2018.

[100] S.N. Akour, M. Al-Heymari, T. Ahmed, and K. A. Khalil, "Experimental and theoretical investigation of a micro wind turbine for low wind speed regions," *Renew. Energy*, vol. 116, pp. 215-223, Feb. 2018.

[101] L. Hirth, and S. Müller, "System-friendly wind power: How advanced wind turbine design can increase the economic value of electricity generated through wind power," *Energy Econ.*, vol. 56, pp. 51-63, May 2016.

[102] M. Zheng, Z. J. Yang, S. Yang, and B. Still, "Modeling and mitigation of excessive dynamic responses of wind turbines founded in warm permafrost," *Eng. Struct*, vol. 148, pp. 36-46, Oct. 2017.

[103] The National Renewable Energy Laboratory. "The system advisor model." https://sam.nrel.gov/ (accessed Jan. 15, 2018).

[104] Wind turbine models manufacturers. "MHI Vestas offshore V164-8.0 MW." https://en.wind-turbine-models.com/turbines/1419-mhi-vestas-offshore-v164-8.0-mw (accessed Feb. 14, 2018).

[105] P. Gilman, T. Ferguson, J. Freeman and J. Jorgenson. *Reference manual for the system advisor model's wind power performance model* (2014). Accessed: Apr. 16, 2018. [Online]. Available: https://www.nrel.gov/docs/fy14osti/60570.pdf.

ADDENDUM A SYSTEM SPECIFICATIONS FOR VESTAS 8 MW WIND TURBINE

Shown below are the system specifications for the Vestas 8MW wind turbine [101].

A.1 SPECIFICATIONS FOR POWER

Rated power:	8,000.0 kW
Cut-in wind speed:	4.0 m/s
Rated wind speed:	13.0 m/s
Cut-out wind speed:	25.0 m/s
Survival wind speed:	50.0 m/s

A.2 SPECIFICATIONS FOR THE ROTOR

Diameter:	164.0 m
Swept area:	21,164.0 m²
Number of blades:	3
Rotor speed, max:	12.1 U/min
Tip speed:	104 m/s
Type:	80m
Manufacturer:	Vestas
Power density 1:	378.0 W/m²

Power density 2:	2.6 kW/m²

A.3 SPECIFICATIONS FOR THE GENERATOR

Type:	Synchronous permanent
Voltage:	30,000.0 V
Grid connection:	IGBT
Grid frequency:	50/60 Hz
Number:	1
Speed, max:	500.0 U/min

A.4 OTHER SYSTEM SPECIFICATIONS

Offshore:	Yes
Onshore:	Yes
Gearbox:	planetary
Manufacturer:	Winergy
Weight	
Single blade:	35.0 t
Nacelle:	375.0 t
Tower	
Hub height:	105/140 m
Type:	steel tube
Shape:	conical
Corrosion protection:	painted
Installation:	2015

ADDENDUM B INPUT SYSTEMS FOR SAM

B.1 INPUT SYSTEM FOR WIND RESOURCE FILE

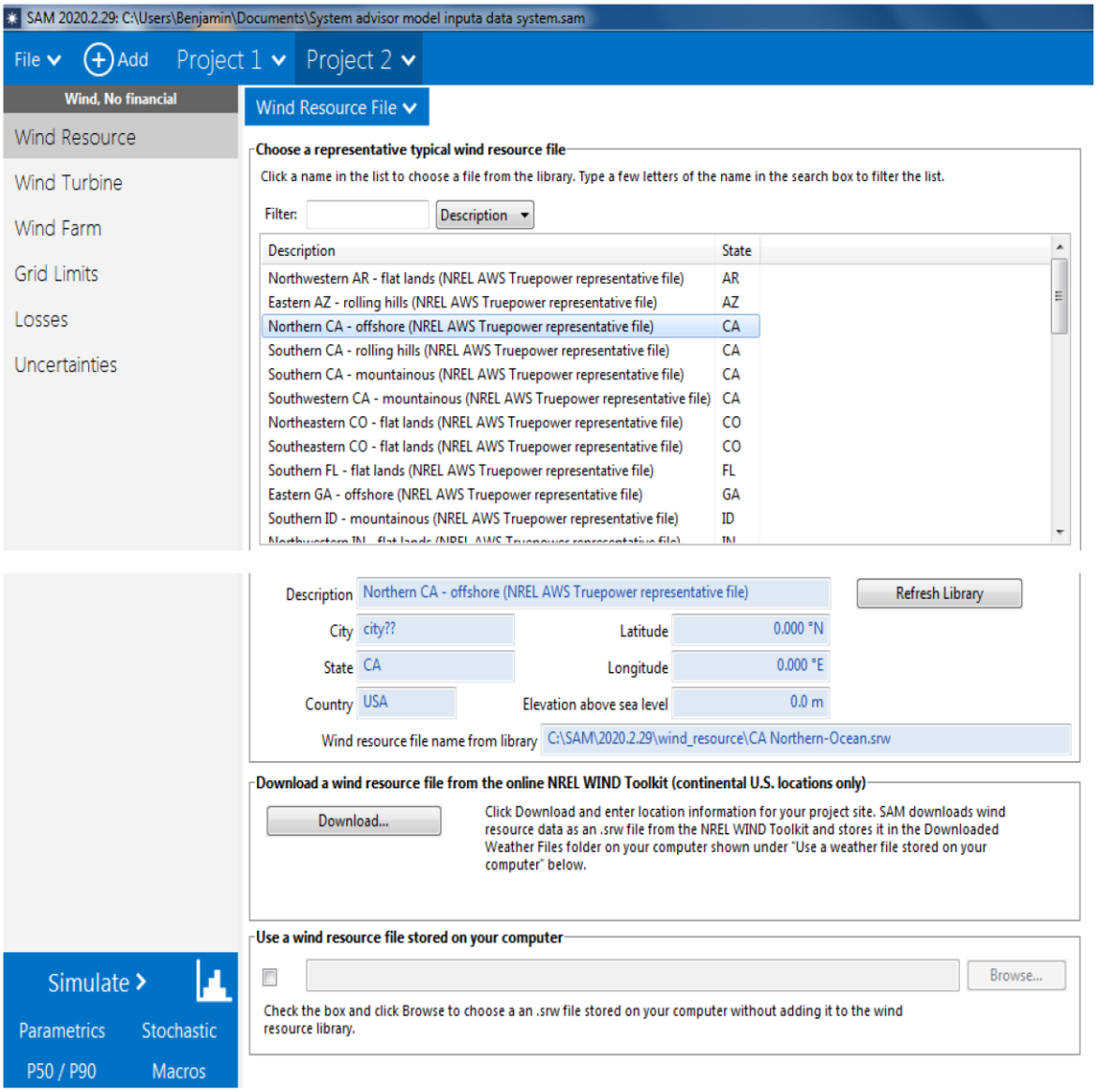

B.2 INPUT SYSTEM FOR WIND TURBINE SPECIFICATIONS

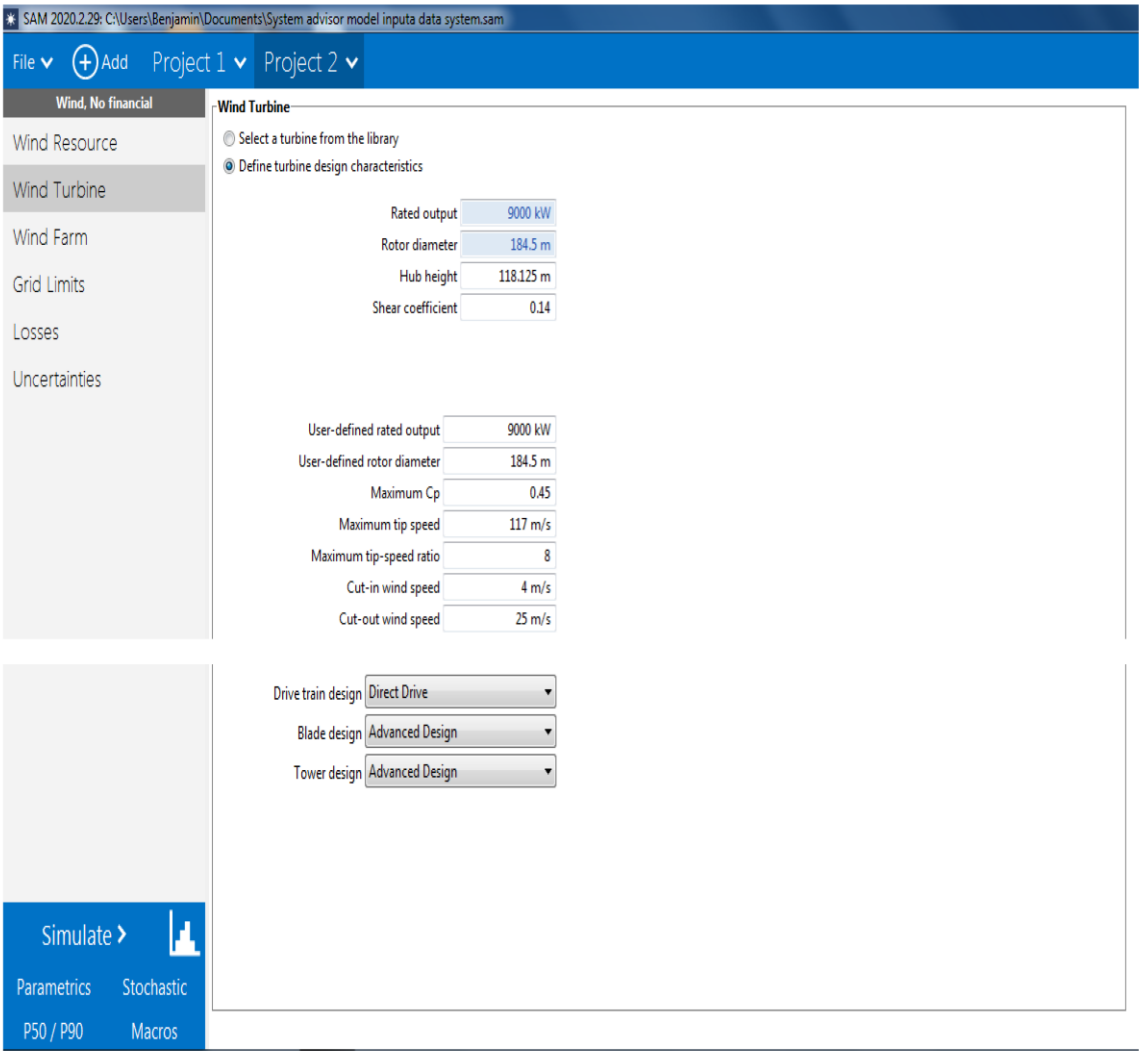

B.3 INPUT SYSTEM FOR WIND FARM SPECIFICATIONS

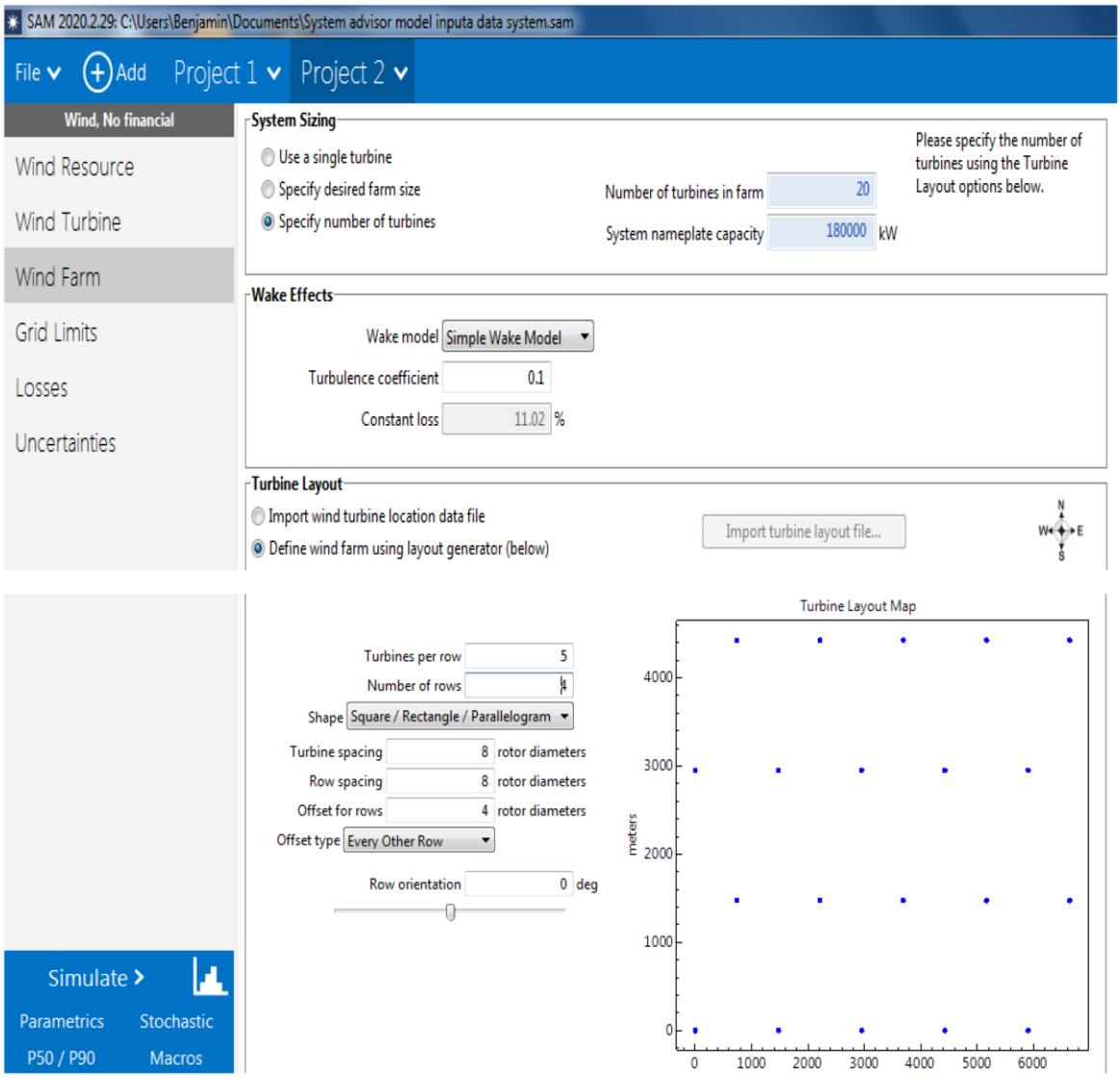

B.4 INPUT SYSTEM FOR SPECIFICATIONS OF ENERGY LOSSES

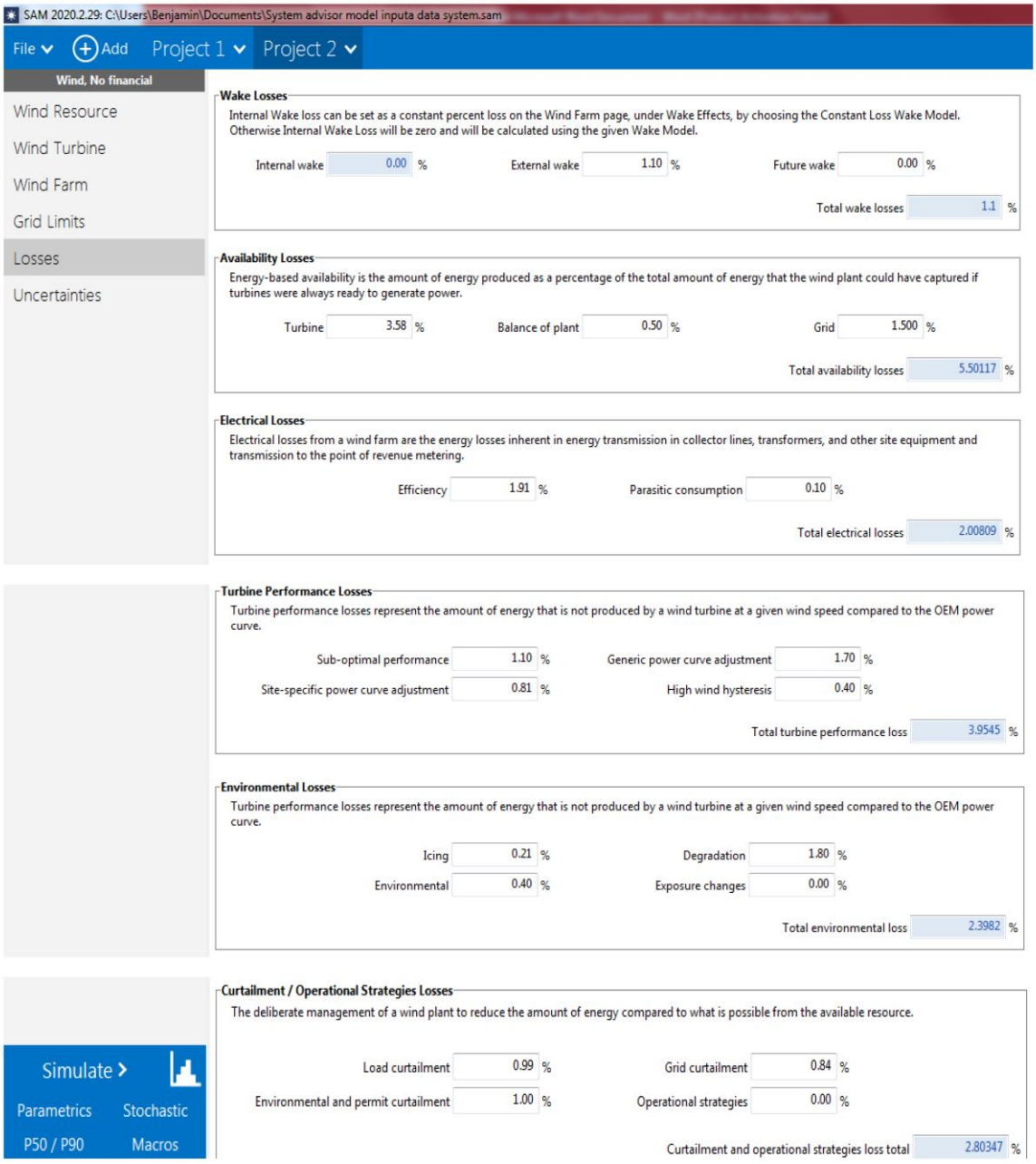

B.5 INPUT SYSTEM FOR PARAMETRIC SPECIFICATIONS